RUNX3 PROTECTS GASTRIC EPITHELIAL CELLS AGAINST EPITHELIAL-MESENCHYMAL TRANSITION-INDUCED CELLULAR PLASTICITY AND TUMORIGENICITY

WANG HUAJING

B. SC. (HONS), NUS

A THESIS SUBMITTED

IN PARTIAL FULFILLMENT OF THE REQUIREMENTS

FOR THE DEGREE OF DOCTOR OF PHILOSOPHY

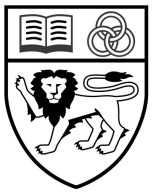

FACULTY OF MEDICINE

YONG LOO LIN SCHOOL OF MEDICINE

NATIONAL UNIVERSITY OF SINGAPORE

SINGAPORE

November 2012

Acknowledgement

I would like to express my sincere gratitude towards the people who walked through the four years of journey with me. They are:

Prof Yoshiaki ITO, my supervisor who gave me the opportunity to work on this exciting and challenging project. He fosters collaborations between us and the experts with the relevant skills and tools who impart depth to my study. I thank him for providing the generous funding for this work. His magnanimous personality touched me as he always keeps his group's interest in mind.

Dr Dominic VOON being my co-supervisor, is also the primary person who leads me into the field of research. I thank him for his unreserved and continuous guidance and encouragement on a daily basis. I also thank him for the intellectual and stimulating discussions and critical reading of my thesis. On the personal level, he often offers valuable advice and assistance when circumstances arise.

Dr Jason KOO who is my senior and close labmate is very patient and helpful in teaching me. He contributed to this project in areas such as gene expression profiling and immuno-fluorescent staining. I also thank him for the meticulous reading of this thesis and the discussions involved.

Yit Teng HOR being my junior and close co-worker is always supportive and considerate. She contributed to the gene expression profiling of this study and the

critical editing of my thesis. We shared a lot of joyous, down moments and hobbies together.

Tu Anh PHAM NGUYEN laid the groundwork for this project including establishment of Hoechst 33342 staining and the survey of cell surface markers in GIF-14 cells.

Lekshmi D/O MANOBAR was our lab biologist who worked closely with me during the last year of my PhD study. I enjoyed training her and I thank her for her efforts and companionship.

Juin Hsien CHAI contributed to the revision of our manuscript to Stem cells.

Dr Shing Leng CHAN, Eileen TENG had generously shared their expertise in nude mice transplantations, sphere-forming assays and kindly provided us some of the reagents. Hui Shan Chong from their team also provided strong support for fluorescence-activated cell sorting (FACS).

Prof Jean-Paul THIERY and Dr Yeh-Shiu CHU were actively involved in the time-lapse videomicroscopy experiments and provided reagents for immuno-fluorescent staining.

Dr Motomi OSATO and Lynettee CHAN provided strong technical support for FACS required for this project.

Dr Carol Stocking (Heinrich-Pette-Institut, Germany) had kindly provided the iG2 lentiviral transfer vector.

Dr Vinay TERGANONAR had kindly assisted in lentivirus production and provided the pBOBI lentiviral vector.

Wen Min LAU for her careful proofreading of this thesis.

Chelsia WANG for her assistance in editing the bibliography.

Xu PENG for his kind assistance in assembling and formatting the figures.

Members of the RUNX group who helped and stimulated me in one way or another during the course of my PhD study.

The department of Medicine, Yong Loo Lin School of Medicine, National University of Singapore for providing the NUS research scholarship throughout my PhD study.

My friends from NUS Dance Synergy who always stand by me throughout these years. We shared the greatest dance moments together which strongly motivates me to push myself to excellence.

Lastly, I would like to express my deepest appreciation to my parents, my family and other friends who dedicate endless encouragement and support especially during the tough periods in my life.

Declaration

I hereby declare that the research and work described in this dissertation is my original work and that, to the best of my knowledge and belief, it contains no material previously published or written by another person, except where due acknowledgement has been made in the text. Some of the work described in Chapter 3 and Chapter 4 were performed by Dr Jason KOO and Yit Teng HOR and I assess my overall contribution to the work described in that chapter to be 80%. Dr Dominic VOON performed the cloning of *RUNX3* and *RUNX3*^{R178Q} into lentiviral vectors

WANG HUAJING

HT070055U

November 2012

Table of Contents

List of figures

List of tables

List of abbreviations and symbols

AGM	aorta-gonad-mesonephros
APC	adenomatous polyposis coli
ATCC	American Type Culture Collection
ATP	adenosine triphosphate
bFGF	basic fibroblast growth factor
BMP	bone morphogenetic protein
BP	band-pass
BSA	bovine serum albumin
CBC	crypt base columnar
CBFβ	core-binding factor beta
CBP	CREB-binding protein
cDNA	complementary deoxyribonucleic acid
ChIP	chromatin immuno-precipitation
Cm	conditioned medium
CMV	cytomegalovirus
CSC	cancer stem cell
Cy	cyanine
DIC	differential interference contrast
DMEM	Dulbecco's modified eagle medium
DNA	deoxyribonucleic acid
ECM	extracellular matrix
EGF	epidermal growth factor
EGFP	enhanced green fluorescent protein
EMT	epithelial-mesenchymal transition
EpCAM	epithelial cell adhesion molecule
E-cad	E-cadherin
F	forward
FACS	fluorescence activated cell sorting
FBS	fetal bovine serum
FGF	fibroblast growth factor
Fn1	fibronectin 1
GSK3β	glycogen synthase kinase beta
HBSS	Hanks' balanced saline solution
HEPES	4-(2-hydroxyethyl)-1-piperazineethanesulfonic acid
HGF	hepatocyte growth factor
HMGA2	high mobility group A2
HSC	hematopoietic stem cell
IM	intestinal metaplasia
IgCα	immunoglobulin constant alpha
iPS	induced pluoripotent stem
IRES	internal ribosome entry site
LB	Luria-Bertani
LEF	lymphoid enhancer-binding factor
Lgr5	leucine-rich repeat-containing G-protein coupled receptor 5
LP	long-pass
MEF	murine embryonic fibroblast

MET	mesenchymal-epithelial transition
MMP	matrix metalloprotease
MNU	*N*-methyl-*N*-nitrosourea
MPO	myeloperoxidase
N-cad	N-cadherin
PCR	polymerase chain reaction
PBS	phosphate buffered saline
PE	phycoerythrin
PEBP2	polyomavirus enhancer-binding protein 2
PI	propidium iodide
qRT-PCR	quantitative reverse transcription-polymerase chain reaction
P/CAF	p300/CBP-associating factor
R	reverse
RNA	ribonucleic acid
RT	reverse transcription
SEM	standard error mean
SMAD	small mothers against decapentaplegic
SP	side population
SPEM	spasmolytic polypeptide-expressing metaplasia
SFFV	spleen focus-forming virus
TCF	T-cell factor
TGF-β	transforming growth factor-beta
TIC	tumour-initiating cell
TLE	transducin-like enhancer
UV	ultraviolet
Vim	vimentin
ZO	zonula occludens

cm	centimeter
CO_2	carbon dioxide
h	hour
H_2O	water
L	liter
$MgSO_4$	magnesium sulphate
µg	microgram
µl	microlitre
µM	micromolar
µm	micrometer
min	minute
ml	millilitre
mM	millimolar
mm	millimeter
ng	nanogram
nm	nanometer
pmol	picomole
rpm	revolutions per minute
s	second
U	units

^{o}C	degree Celsius

Abstract

The Runt domain transcription factor RUNX3 is a prominent tumour suppressor in the gastrointestinal tract where it is required for proper proliferation and differentiation of gastric epithelial cells. These functions are partly elicited by mediating the tumour suppressive TGF-β/SMAD signaling and antagonising the oncogenic Wnt pathway. Consistent with these, immoralised *Runx3*$^{-/-}$ gastric epithelial cells (GIF lines) are refractory to TGF-β1-induced apoptosis and are tumorigenic in nude mice, but not their *Runx3*$^{+/+}$ equivalents. In this study, we observed the spontaneous emergence of a tumorigenic and stem-cell like subpopulation, P2 through Epithelial-Mesenchymal Transition (EMT) in *Runx3*$^{-/-}$ GIF-14 cells. Paradoxically, EMT was driven by aberrantly activated TGF-β signaling, suggesting that the loss of Runx3 render cells sensitised to the EMT-promoting functions of TGF-β. Interestingly, the P2 subpopulation expressed markedly higher levels of *Lgr5*, a canonical Wnt target gene that is exclusively expressed in the pyloric gastric stem cells. Moreover, TGF-β1-induced EMT reactivates *Lgr5* which acts synergistically with Wnt3a to cause amplified activation of *Lgr5*. This observation was largely absent in *Runx3*$^{+/+}$ GIF-13 cells. Finally, the re-introduction of RUNX3 in GIF-14 cells strongly abrogated Wnt3a-induced *Lgr5*, reduced the P2 subpopulation and TGF-β1-activated EMT- and stemness-related genes such as *Hmga2*, *Snai1* and *Lgr5*, confirming the negative roles of RUNX3 on EMT and stemness. Taken together, our data revealed that Runx3 maintains gastric epithelial cell integrity and its absence causes sensitisation to Wnt and EMT-activating properties of TGF-β, resulting in increased cellular plasticity and the emergence of a tumorigenic, stem cell-like subpopulation.

CHAPTER 1

Introduction

1.1 The RUNX family of transcription factors

The RUNX family of transcription factors plays pivotal roles in mammalian developmental processes (Ito, 1999). The RUNX family is evolutionarily conserved from the nematode worm *Caenorhabditis elegans* to fruitfly *Drosophila melanogaster* and in mammals, indicating that RUNX proteins have pivotal functions even in the most primitive metazoan and unicellular holozoan (Sullivan *et al.*, 2008; Sebe-Pedros *et al.*, 2011). RUNX was initially discovered by independent groups to be a nuclear protein that binds to the enhancer elements of polyomavirus and Moloney murine leukemia viruses (Kamachi *et al.*, 1990; Speck *et al.*, 1990). It was found that the RUNX genes encoded the DNA-binding α-subunits of the heterodimeric transcription factor, known as polyomavirus enhancer-binding protein 2 or core-binding factor (PEBP2/CBF) (Ito, 2004). The founding member of the RUNX gene family is *Runt*, a *Drosophila* pair-rule gene that controls the segmentation in embryos and is required for neurogenesis and sex determination (Kania *et al.*, 1990; Duffy *et al.*, 1991; Duffy and Gergen, 1991; Ingham and Gergen, 1998). To date, three mammalian *runt*-related genes *RUNX1, RUNX2* and *RUNX3* have been characterised which play distinct biological roles during development and diseases.

The RUNX family members share a high degree of sequence and structural homology where they contain a highly conserved 128-amino-acid Runt domain and a 5- amino-acid VWRPY domain (Ito, 1999). The high level of sequence conservation reflects a crucial importance of these domains to the function of RUNX proteins. The Runt domain is critical for RUNX proteins to function as transcription factors as it confers sequence-specific DNA binding and dimerisation with their non DNA-binding partner, core-binding factor β (CBFβ) (Kamachi *et al.*, 1990). Although the

Runt domain can bind DNA independently, its binding affinity and hence transcriptional activity is greatly enhanced when dimerised with CBFβ (Ogawa *et al.*,1993; Ogawa *et al.*, 1993). The VWRPY motif located at the carboxyl-terminal modulates the transcriptional activity of RUNX proteins by recruiting co-repressors such as the transducin-like enhancer (TLE)/Groucho (Levanon *et al.*, 1994; Aronson *et al.*, 1997).

Studies in both *Drosophila* and mammalian systems suggest that RUNX proteins act as context-dependent transcription regulators, which either activate or repress gene expression by cooperating with different transcription factors or cofactors in specific cell or tissue types (Wheelers *et al.*, 2000). A classic example of synergistic interaction between RUNX proteins and other transcription factors is the cooperative DNA binding and transcriptional activation of T cell receptor and Moloney murine leukemia virus enhancer elements by RUNX1 and Est-1 (Wotton *et al.*, 1994; Sun *et al.*, 1995; Kim *et al.*, 1999). RUNX1 also cooperates with Myb, PU.1 and C/EBPα transcription factors to transactivate various promoters and enhancers of the hematopoietic genes (Hernandez-Munain and Krangel, 1994; Zaiman and Lenz, 1996; Zhang *et al.*, 1996; Britos-Bray and Friedman, 1997; Petrovick *et al.*, 1998). In other cases, RUNX proteins recruit co-repressors such as TLE/Groucho to transcriptionally repress hematopoietic and osteoblastic genes (Imai *et al.*, 1998; Javed *et al.*, 2000). Besides associating with co-repressors, RUNX1 interacts with p300/CREB-binding proteins (CBP) to recruit histone acetyltransferase, p300/CBP-associating factor (P/CAF), resulting in epigenetic derepression of *myeloperoxidase* (*MPO*) during myeloid differentiation (Kitabayashi and Yokoyama *et al.*, 1998). Being intricately involved in cell fate determination during development as prominent

regulators of gene expression, it is not surprising that the dysregulation of the Runt domain-containing genes are often associated with oncogenesis.

1.2 Important roles of RUNX genes in development and human cancers

1.2.1 RUNX1 in hematopoiesis and human leukemia

Amongst the most studied *RUNX* genes is *Runx1*, often regarded as the master regulator of adult hematopoiesis in vertebrates. Homozygous deletion of *Runx1* in mice resulted in complete lack of fetal liver hematopoiesis suggesting that *Runx1* is absolutely required for definitive hematopoiesis (Okuda *et al.*, 1996; Wang *et al.*, 1996). In this context, Runx1 is indispensible for the emergence of the first hematopoietic stem cells (HSCs) from hematogenic endothelial clusters in the embryonic aorta-gonad-mesonephros (AGM) region (North *et al.*, 1999; Yokomizo *et al.*, 2001). Conditional targeting of *Runx1* in adult mice led to an initial expansion of short term HSCs with limited self-renewal capacity, which was followed by stem cell exhaustion at a later stage (Ichikawa *et al.*, 2004; Motoda *et al.*, 2008; Jacob *et al.*, 2010). This is thought to be the result of compromised HSC-niche interactions (Jacob *et al.*, 2010). HSCs exhibiting long term self-renewal activity would exit quiescence due to disrupted HSC-niche associations to become short term HSCs, eventually leading to stem cell exhaustion (Wang *et al.*, 2010). These evidences indicate a role of Runx1 in maintaining HSCs in quiescence through a niche-related mechanism. These data also suggest that Runx1 deficiency triggers a pre-leukemic state by increasing the number of short term HSCs as a cell pool for further oncogenic alterations, leading to leukemia development (Growney *et al.*, 2005; Putz *et al.*, 2006). In further support of these observations, *Runx1*-deficient mice developed myelodysplastic syndrome and thymic lymphoma, indicating a precancerous condition (Putz *et al.*, 2006). Apart from its function in adult HSCs, Runx1 is also essential for terminal differentiation of hematopoietic progenitors of the megakaryocytic and lymphocytic lineages (Ichikawa *et al.*, 2004). During the development of T lymphocytes, Runx1 is required for active

repression of *CD4* in $CD4^{-}CD8^{-}$ double negative immature thymocytes through direct binding to two Runx-binding motifs in the *CD4* silencer (Taniuchi *et al.*, 2002). It is apparent that Runx1 is involved in multiple levels of adult hematopoiesis from the maintenance of quiescent HSCs to defining proper differentiation programs towards the full range of hematopoietic lineages.

Given its pivotal roles in mammalian hematopoiesis, *RUNX1* is one of the most frequently disrupted genes in human leukemias (Look *et al.*, 1997). Loss of RUNX1's function due to chromosomal translocations and point mutations is featured strongly in various types of leukemias such as acute myelogenous leukemia, myelodysplastic syndrome, chronic myelogenous leukemia and childhood acute lymphoblastic leukemia (Nucifora *et al.*, 1993; Mitani *et al.*, 1994; Golub *et al.*, 1995). Inactivation of RUNX1 predisposes patients to the development of leukemias upon further genetic mutations. Therefore, RUNX1 is a key regulator of embryonic and adult hematopoiesis where its disruption is strongly linked to leukemogenesis.

1.2.2 RUNX2 regulates bone development

RUNX2 is a major transcription factor required for bone formation in mammals. Genetic ablation of *Runx2* resulted in impaired osteoblasts maturation and osteogenesis, leading to complete lack of bone formation. Therefore, $Runx2^{-/-}$ mice die soon after birth from severe respiratory defects possibly caused by the absence of a rib cage (Komori *et al.*, 1997; Otto *et al.*, 1997). Consistent with this phenotype, Runx2 regulates bone-specific genes such as *osteocalcin* and *alkaline phosphatase* during osteoblast differentiation from mesenchymal precursor cells (Ducy *et al.*, 1999). *Runx2* heterozygous mice displayed skeletal abnormalities resembling that of the

human congenital skeletal disorder, cleidocranial dysplasia. Importantly, loss-of-function mutations in *RUNX2* were found in patients suffering from this disease (Otto *et al.*, 2002; Tessa *et al.*, 2003; Xuan *et al.*, 2008). In the context of cancer, RUNX2 was reported to promote breast and prostate tumour growth, and their metastasis to the bone (Javed *et al.*, 2005; Pratap *et al.*, 2008; Das *et al.*, 2009; Akech *et al.*, 2010; Lim *et al.*, 2010). Moreover, *Runx2* cooperated strongly with *c-myc* to induce T-cell lymphoma in transgenic mouse models (Stewart *et al.*, 1997).

1.2.3 RUNX3 regulates neuron and lymphocyte development

Compared to its other mammalian members, Runx3 is expressed in a relatively diverse cell types including the dorsal root ganglion neurons, hematopoietic cells and various epithelial organs including the lung, liver and the gastrointestinal tract. As a result, *Runx3*$^{-/-}$ mice displayed abnormalities in these tissues such as motor discoordination, disrupted cytotoxic T lymphocyte function and hyperplasia in the gastrointestinal epithelium (Inoue *et al.*, 2002; Levanon *et al.*, 2002; Li *et al.*, 2002; Taniuchi *et al.*, 2002; Woolf *et al.*, 2003; Ito *et al.*, 2008). Runx3 controls the axonal projection of proprioceptive dorsal root ganglion neurons, and thus the deletion of *Runx3* led to the loss of these cells and ataxia (Inoue *et al.*, 2002; Levanon *et al.*, 2002). Distinct from the active repression of *CD4* in $CD4^-CD8^-$ double negative immature thymocytes by Runx1, Runx3 is necessary for epigenetic silencing of *CD4* in $CD4^-CD8^+$ mature cytotoxic thymocytes (Taniuchi *et al.*, 2002; Woolf *et al.*, 2003). *Runx3*-null $CD4^-CD8^+$ T cells, but not helper $CD4^+CD8^-$ T cells failed to proliferate and displayed defective cytotoxic activity, suggesting that Runx3 has critical functions in lineage specification and homeostasis of $CD4^-CD8^+$ lineage T lymphocytes (Taniuchi *et al.*, 2002).

1.2.4 RUNX3 is a gastrointestinal tumour suppressor

A function of Runx3 in the gastrointestinal epithelium was first implicated by the pronounced hyperplastic gastric epithelium of the *Runx3*-knockout mice. Further analysis revealed that the glandular stomach displayed excessive cell proliferation and inhibition of apoptosis in these epithelial cells (Li *et al.*, 2002; Ito *et al.*, 2008). The dysregulated proliferation and apoptosis experienced by gastric epithelial cells following the loss of Runx3 are consistent with its role as a tumour suppressor in this tissue type. However, the neonatal death of *Runx3*-deficient mice in C57BL/6 genetic background has hampered the detailed analysis of their phenotypes. To overcome this, a series of immortalised mouse gastric epithelial cell lines, termed GIF lines, were established from the entire stomach epithelia of $Runx3^{+/+}$ and $Runx3^{-/-}$ E16.5 fetuses in a $p53^{-/-}$ background (Li *et al.*, 2002). Concordant with the tumour suppressive properties of Runx3, $Runx3^{-/-}.p53^{-/-}$ embryonic GIF cell lines but not their $Runx3^{+/+}.p53^{-/-}$ equivalents formed tumours when transplanted in immuno-compromised nude mice (Li *et al.*, 2002).

More recently, $Runx3^{-/-}$ mice in BALB/c genetic background that survived up to one year were generated. Analysis of these mice revealed that spasmolytic polypeptide-expressing metaplasia (SPEM), a precancerous metaplasia developed in the gastric mucosa due to altered differentiation of the gastric epithelial cells (Ito *et al.*, 2011). As Runx3 is prominently expressed in pepsinogen-positive chief cells and Muc5AC-positive surface mucous cells, it may be involved in the differentiation of these lineages. Indeed, $Runx3^{-/-}$ mice exhibited loss of chief cells and antralisation of the fundic stomach. This was likely consequent to a block in chief cell differentiation or trans-differentiation of chief cells into SPEM cells (Ito *et al.*, 2011). Remarkably,

the induction of an intestinal phenotype with ectopic expression of the intestinal-specific transcription factor Cdx2 was observed in the gastric mucosa of *Runx3*$^{-/-}$ adult mice (Ito *et al.*, 2011). These observations suggest that *Runx3*$^{-/-}$ gastric epithelial cells possess a disrupted gastric epithelial identity and their differentiation *in vivo* is easily altered by extracellular morphogenetic cues. More importantly, *Runx3*$^{-/-}$ SPEM was readily transformed into adenocarcinomas in the stomach by exposure to the carcinogen, *N*-methyl-*N*-nitrosourea (MNU), indicating that loss of Runx3 induces a pre-neoplastic condition in the stomach (Ito *et al.*, 2011).

Consistent with the disrupted differentiation in adult BALB/c *Runx3*$^{-/-}$ mice, *Runx3*$^{-/-}$*.p53*$^{-/-}$ embryonic GIF cell lines displayed impaired cell-cell adhesion, epithelial cell polarity and altered differentiation *in vitro*. When cultured between collagen sheets, *Runx3*$^{+/+}$*.p53*$^{-/-}$ GIF lines readily formed simple columnar epithelia with glandular structures exhibiting intact cell-cell adhesion and apical-basal polarity (Fukamachi *et al.*, 2004). In contrast, *Runx3*$^{-/-}$*.p53*$^{-/-}$ GIF lines under similar culturing conditions displayed altered differentiation as reflected in the inability to form glandular structures (Fukamachi *et al.*, 2004). These phenotypes were attributed in part to the significantly reduced expression of tight junction proteins critical for cell-cell adhesion, such as Claudin-1 which was discovered to be a positive target of RUNX3 in gastric epithelial cells (Chang *et al.*, 2010). These data suggests that Runx3 is crucial for the proper differentiation into glandular epithelial sheet with established cell-cell adhesion and polarity in collagen cultures. As *Runx3*$^{-/-}$*.p53*$^{-/-}$ GIF cell lines formed tumours in nude mice, these tumours were analysed for their differentiation capacity. Akin to intestinalisation observed in adult BALB/c *Runx3*$^{-/-}$ mouse stomachs, analysis of the tumours derived from nude mice and *in vitro* culture

in three dimensional matrigel revealed that *Runx3*$^{-/-}$ GIF cell lines could trans-differentiate into intestinal-type cells (Fukamachi *et al.*, 2004). These observations indicate that *Runx3*$^{-/-}$ gastric epithelial cells display cellular plasticity as they are prone to the influences of extracellular stimuli.

The tumour suppressive activities of Runx3 revealed in the analysis of *Runx3*$^{-/-}$ mice are firmly supported by human clinical data. In human, loss of RUNX3 expression is strongly correlated to the genesis and progression of gastric cancer. Silencing of *RUNX3* was observed in more than 80% of primary gastric tumours and gastric cancer cell lines due to hemizygous deletions, promoter hypermethylation and protein mislocalisation in the cytoplasm (Li *et al.*, 2002; Ito *et al.*, 2005). Moreover, RUNX3 inactivation was also prevalent in human colorectal carcinomas in which *RUNX3* was silenced in 40% of primary colorectal tumours and 60% of colorectal cancer cell lines (Ito *et al.*, 2008). In addition, downregulation of RUNX3 was frequently observed in intestinal metaplasia (IM) which is often regarded as a precancerous state in gastric cancer (Li *et al.*, 2002). Similarly, inactivation of RUNX3 induced intestinal adenomas in both human and mice, which provided favourable conditions for the progression of these adenomas to malignant adenocarcinomas (Ito *et al.*, 2008). Together, these mouse and human data strongly argue that RUNX3 functions as a tumour suppressor in the gastrointestinal tract, where its disruption appears to be a key event in early gastrointestinal carcinogenesis.

1.3 The involvement of RUNXs in major signaling pathways

1.3.1 RUNXs are integral components of the TGF-β/SMAD signaling cascade

Transforming growth factor-β (TGF-β) is a family of multifunctional cytokines that regulate growth, differentiation, apoptosis, matrix accumulation and motility of many cell types (Blobe *et al.*, 2000). TGF-β acts as a potent inhibitor of cell growth in hematopoietic cells, endothelial cells and epithelial cells, whereas it stimulates the growth of mesenchymal cells (Derynck *et al.*, 2001). Members of the TGF-β superfamily consist mainly of TGF-βs, activins and bone morphogenetic proteins (BMPs). The binding of these TGF-β ligands results in the formation of type I and type II receptor heterodimeric complex which leads to the activation of downstream effectors of the SMAD family. The receptor-activated SMADs (R-SMADs) become phosphorylated and associate with SMAD4 (Co-SMAD) and translocate to the nucleus to regulate transcription of target genes together with other transcription factors (Feng and Derynck, 2005; Massague *et al.*, 2005). SMAD2 and SMAD3 serve as R-SMADs transducing the TGF-β/activin-like signals while SMADs 1, 5 and 8 act as R-SMADs mediating BMP-like signals (Miyazono *et al.*, 2004). The roles of TGF-β family members in carcinogenesis are complex as they demonstrate both tumor suppressive and oncogenic potentials. In the current paradigm, the tumour suppressive function of TGF-β dominate in normal tissues and in early stages of cancer, but in advanced cancers, changes in TGF-β expression and cellular responses tip the balance in favor of its oncogenic activities (Derynck *et al.*, 2001). These are supported by the implication that activated TGF-β signaling promotes cancer progression and metastasis via epithelial-mesenchymal transition (EMT), angiogenesis and immuno-suppression (Wakefield and Roberts, 2002).

Interestingly, some of the biological functions of the TGF-β cytokines are similar to those of RUNX proteins. Indeed, all three RUNXs have been shown to physically interact with R-SMADs (Hanai *et al.*, 1999). For instance, RUNX3 interacted with Smad2 and Smad3 to cooperatively activate *germline immunoglobulin constant α* (*IgCα*) promoter to direct class switching to IgA in B lymphocytes (Hanai *et al.*, 1999; Pardali *et al.*, 2000). During BMP-induced osteoblastic differentiation, the physical interaction between Runx2 and BMP-specific Smad1 and Smad5 synergistically activated osteoblast-specific gene expression in pluripotent mesenchymal precursor cells (Lee *et al.*, 2000). Importantly, impaired RUNX2-SMAD interaction due to mutations in RUNX2 may contribute to the pathogenesis of cleidocranial dysplasia (Zhang *et al.*, 2000). In contrast to the synergy between RUNXs and SMADs on their target genes, the association of Runx2 and TGF-β-specific Smad3 led to transcriptional repression of *osteoclacin*, and thus inhibited osteoblast differentiation (Alliston *et al.*, 2001). Based on these evidences, RUNX proteins act as nuclear effectors of the TGF-β signaling pathway through the formation of complexes with specific R-SMADs to control transcription in a context dependent manner.

TGF-β/SMAD signaling cascade is one of the central pathways that controls the growth and differentiation of gut epithelial cells (Mishra *et al.*, 2005). The role of TGF-β signaling as a tumour suppressor pathway in the gastrointestinal tract is best illustrated by the prevalent inactivating mutations in several components of the TGF-β signaling cascade such as the type II TGF-β receptor and SMAD4 in gastrointestinal cancers (Park *et al.*, 1994; Markowitz *et al.*, 1995; Lu *et al.*, 1996; Howe *et al.*, 1998; Xu *et al.*, 2000). In gastric epithelial cells, RUNX3 mediates the tumour suppressive

effect of TGF-β by cooperating with R-SMADs to activate the transcription of the negative regulator of cell cycle, *p21*$^{WAF/Cip1}$ and proapoptotic gene, *BIM* (Chi *et al.*, 2005; Yano *et al.*, 2006; Ito, 2008). Concordant with this, *Runx3*$^{-/-}$.*p53*$^{-/-}$ GIF cells were resistant to TGF-β1-induced growth arrest and apoptosis (Li *et al.*, 2002). Therefore, it appears that an important part of the tumour suppressor function of RUNX3 is achieved through the modulation of the TGF-β pathway.

1.3.2 RUNX3 attenuates the oncogenic Wnt signaling pathway

In mammals, the canonical Wnt pathway is critical in cell fate determination in embryogenesis and orchestrates self-renewal in various tissues (Clevers, 2006). Wnt signaling promotes the stabilisation of cytoplasmic β-catenin through functional deactivation of glycogen synthase kinase-β (GSK3β) which phosphorylates β-catenin. As a result, unphosphorylated β-catenin is translocated to the nucleus to stimulate the transcription of Wnt target genes by interacting with the T-cell factor (TCF) or lymphoid enhancer-binding factor (LEF) transcription factors (Bienz and Clevers, 2000). The critical role of Wnt/TCF4/β-catenin signaling in intestinal homeostasis is best demonstrated by the phenotype of homozygous *Tcf-4* knockout mice. Strikingly, the proliferative stem cell compartment was entirely absent in the small intestines of *Tcf-4*$^{-/-}$ neonatal mice, suggesting that Wnt/TCF4/β-catenin pathway is necessary for the maintenance of crypt stem/progenitor cells in intestinal epithelium (Korinek *et al*, 1998). Recently, a new pool of intestinal stem cells, the crypt base columnar (CBC) cells marked by the Wnt target gene, *leucine-rich repeat-containing G-protein coupled receptor 5* (*Lgr5*) has been characterised (Barker *et al.*, 2007). Lineage tracing experiments using *Lgr5-EGFP-IRES-creERT2.Rosa26-lacZ* compound mice

revealed that Lgr5-positive cells gave rise to all lineages of the intestinal epithelium and maintained the epithelia self-renewal over a long period of time (Barker *et al.*, 2007). Subsequently, Lgr5 was reported to demarcate an analogous stem cell compartment in the pyloric stomach (Barker *et al.*, 2010). This was supported by the ability of single Lgr5-positive cells to form intestinal/gastric three-dimensional organoid structures, resembling those of normal gastrointestinal epithelium (Sato *et al.*, 2009; Barker *et al.*, 2010).

As a major growth factor pathway, the dysregulation of Wnt signaling is strongly implicated in gastrointestinal cancers (Clevers, 2006). Constitutive activation of the Wnt pathway, either through the inactivation of the adenomatous polyposis coli (APC) complex or gain of oncogenic mutations in β-catenin results in the aberrant stabilisation and nuclear accumulation of β-catenin (Kinzler and Vogelstein, 1996; Bienz and Clevers, 2000). In mouse, this phenomenon is readily reproduced and studied in the $Apc^{min/+}$ transgenic mouse model, which carries a heterozygous mutation at codon 850 of the *Apc* tumour suppressor gene (Moser *et al.*, 1992). The $Apc^{min/+}$ mice developed intestinal adenomas spontaneously, which bears close resemblance to the phenotype of aged BALB/c $Runx3^{+/-}$ mice (Moser *et al.*, 1992, Ito *et al.*, 2008). RUNX3 functions as an attenuator of the Wnt pathway and this was reflected in the increased intestinal tumour incidence and mass in $Runx3^{+/-}.Apc^{min/+}$ compound mutant mice (Ito *et al.*, 2008). Consistent with this, increased Wnt signaling activity was observed in BALB/c $Runx3^{-/-}$ gastrointestinal epithelium as reflected in the upregulation of Wnt target genes such as c-*Myc, cyclinD1, EphB2* and *CD44* (He *et al.*, 1998; Tetsu and McCormick, 1999; Batlle *et al.*, 2002; van de Wetering *et al.*, 2002). Due to aberrant activated Wnt signaling in the intestinal

epithelium, paneth cells were mislocated from their normal positions at the base of the crypt, indicative of profound disruptions to intestinal differentiation (Ito *et al.*, 2008). The molecular mechanism underlies the antagonist effects of RUNX3 on Wnt signaling is through a direct interaction with the TCF4/β-catenin complex, thus revealing a new aspect to its role as a gastrointestinal tumour suppressor.

1.4 Understanding the interplay between RUNX3, TGF-β and Wnt

It is known that the disruption of key regulators of cell proliferation, apoptosis and differentiation would lead to the development of gastrointestinal cancers. The transcription factor RUNX3 appears to be one such important player which intersects multiple key signaling pathways to regulate gene expression. Earlier studies have shown that the inactivation of Runx3 in mice would result in defective cell proliferation, apoptosis and differentiation in the gastrointestinal epithelium, due to the dysregulation of TGF-β and Wnt signaling pathways, rendering them precancerous conditions (Li *et al.*, 2002; Ito *et al.*, 2008; Ito *et al.*, 2010). Despite these findings, the precise changes in the cell biology of gastric epithelial cells due the loss of RUNX3 and how they contribute to tumorigenicity are not fully understood. To investigate this, the *Runx3*$^{+/+}$*.p53*$^{-/-}$ and *Runx3*$^{-/-}$*.p53*$^{-/-}$ gastric epithelial cell lines, which have been partially characterised in earlier studies can be used (Li *et al*., 2002; Fukamachi *et al*., 2004). An important feature of the *Runx3*$^{-/-}$ GIF lines is that they are weakly tumorigenic when transplanted into nude mice, unlike their *Runx3*$^{+/+}$ counterparts which do not produce tumours. However, individual GIF cell lines were each established from a whole fetal stomach epithelia that consisted a mixture of cell types and had not gone through clonal selection. Therefore, they are heterogeneous in nature. This heterogeneity is compounded by additional genetic and epigenetic changes gained during extended *in vitro* culture in the absence of p53. As such, distinct subpopulations exist within individual *Runx3*$^{-/-}$ GIF cell lines and the observed tumorigenicity may be restricted to specific subpopulations. This study aims to identify the tumour-initiating cells within these *Runx3*$^{-/-}$ GIF cells. This will be followed by a thorough interrogation of the identified tumorigenic cell population to

generate novel insights into the molecular basis of their tumorigenicity and its relationship with Runx3.

1.5 Experimental aims

1. To identify the tumorigenic subpopulation within the *Runx3*$^{-/-}$.*p53*$^{-/-}$ GIF-14 gastric epithelial cells.

2. To investigate the cause of the appearance of this subpopulation and the involvement of TGF-β and Wnt signaling pathways.

3. To demonstrate the negative role of Runx3 in the emergence of the tumorigenic subpopulation.

CHAPTER2

Materials and methods

2.1 Cell culture and growth factor treatments

Murine gastric epithelial cell lines GIF-5, GIF-9, GIF-13, and GIF-14 were previously established from E16.5 *Runx3*$^{+/+}$.*p53*$^{-/-}$ and *Runx3*$^{-/-}$.*p53*$^{-/-}$ embryonic stomachs by Fukamachi (Fukamachi *et al.*, 2004). They were maintained in Dulbecco's Modified Eagle Medium (DMEM) (Invitrogen, CA, USA) supplemented with 4500mg/L glucose, 10% fetal bovine serum (FBS), 100 U/ml penicillin and 100µg/ml streptomycin antibiotics (Hyclone, UT, USA). The cells were sub-cultured in 10-cm or 6-cm tissue culture dishes at 1:10 (Nunc A/S, Roskilde, Denmark), and maintained at 37^{o}C in a humidified atmosphere containing 5% CO_2. To activate TGF-β pathway, cells were treated with 2.5ng/ml of human recombinant TGF-β1 (R & D systems, MN, USA) for the indicated periods prior to Hoechst 33342 staining, antibody staining and/or quantitative RT-PCR. TGF-β signaling was inhibited using 10µM of small molecule TGF-β inhibitor, SB431542 (Sigma-Aldrich, MO, USA). To activate Wnt pathway, cells were treated with control- or Wnt3a-conditioned medium (Cm) for 15h prior to analysis. To study the contribution of various growth factors, cells were treated with 10ng/ml of murine recombinant epidermal growth factor (EGF), 10ng/ml of human recombinant EGF, 10ng/ml of human recombinant basic fibroblast growth factor (bFGF) and 10ng/ml of human recombinant FGF10 purchased from PeproTech (NJ, USA) and 10ng/ml of human recombinant hepatocyte growth factor (HGF) purchased from Merck Biosciences-Calbiochem (NH, UK) prior measurement of transcriptional changes by quantitative RT-PCR.

2.2 Production of Wnt3a-conditioned medium

Wnt3a- and control-conditioned media (Cm) were prepared following protocol described in Willert *et al.*, 2003. Mouse L-cells producing secreted Wnt3a ligand and the parent L-cells were obtained from American Type Culture Collection (ATCC). They were cultured in DMEM supplemented with 4500mg/L glucose, 10% FBS, 100 U/ml penicillin and 100µg/ml streptomycin antibiotics (Hyclone, UT, USA). Cells were passaged 1:10 in 15-cm tissue culture dishes and grown to confluency for 4 days. The first harvest of conditioned media was collected, and cells were washed with phosphate buffered saline (PBS) prior to addition of 15ml of fresh culture media. The second harvest of conditioned media was collected three days later, and mixed with media from the first harvest, prior to filter-sterilisation with a 0.45µm filter. Conditioned media was kept in -80°C for long term storage.

2.3 Hoechst 33342 and surface antigen staining

Cells were stained with Hoechst 33342 (Sigma-Aldrich, MO, USA) according to Goodell *et al.*, 1996. Briefly, GIF cell lines were trypsinised and resuspended in DMEM supplemented with 4500mg/L glucose, 2% FBS, 10mM 4-(2-hydroxyethyl)-1-piperazineethanesulfonic acid (HEPES; Invitrogen, CA, USA) and 10µg/ml Hoechst 33342 in the presence or absence of 0.2mM verapamil (Sigma-Aldrich, MO, USA) at 10^6 cells/ml. Cells were incubated at 37^{o}C for 90min with regular mixing. Cells were then resuspended in pre-chilled Hanks' balanced saline solution (HBSS; Invitrogen, CA, USA) containing 2% FBS and 10mM HEPES and subjected to flow cytometry analysis. For experiments involving co-staining of surface antigens, cells were stained by Hoechst 33342 prior to immunostaining with fluorochrome-conjugated antibodies against various surface antigens, primarily EpCAM and CD133. Cells were incubated

with anti-EpCAM-phycoerythrin-cyanine (PE-Cy7) (Biolegend, CA, USA; catalogue number: 118215) and anti-CD133-phycoerythrin (PE) (Miltenyi Biotec, CA, USA; catalogue number: 130-092-334) mouse monoclonal antibodies at 1:100 dilution on ice for 10min in dark. The staining procedure was carried out in 50ul and the binding reaction was quenched with 1ml of PBS.

2.4 Flow cytometry analysis and fluorescence-activated cell sorting (FACS)

Cells stained by Hoechst 33342 and/or flurochrome-conjugated antibodies were counterstained with 1μg/ml of propidium iodide (PI) before analysis and/or FACS enrichment on FACSVantage^{TM} cell sorter (BD Biosciences, CA, USA) or FACSAria Special Order cell sorter (BD Biosciences, CA, USA) or LSRII Special Order (BD Biosciences, CA, USA). Hoechst 33342 dye was excited by 350nm UV laser and its fluorescence was measured at two wavelengths using 450/20nm band-pass (BP; Hoechst blue) and 675nm long-pass (LP; Hoechst red) optical filters. Fluorescence signals of EpCAM-PE-Cy7 and CD133-PE were measured by 785/50nm and 585/42nm detectors on FACSVantage^{TM} or LSRII Special Order. The same machines were used to enrich or analyse lentivirus-infected cells that express enhanced green fluorescent protein (EGFP), measured by 530/30nm detector. Flow cytometry data were analysed using the FlowJo computer software (Tree Star, OR, USA).

2.5 Purification of RNA

Cells were washed with PBS and resuspended in 350µl of RLT lysis buffer containing 1% β-mercaptoethanol. RNA extraction was performed using RNeasy Mini Kit and RNase-free DNase Set (QIAGEN, Hilden, Germany) following manufacturer's protocol. Briefly, cell lysates were homogenised by vortexing for 1 minute, followed by addition of 70% ethanol and transferred to RNeasy spin column. On column digestion of genomic DNA was carried out using 80µl of DNase I incubation mix. The spin column was then washed with buffers RW1 and RPE, followed by a final spin to remove residual ethanol. RNA was subsequently eluted in 30-50µl of RNase-free water and quantified by NanoDrop 1000 Spectrophotometer (Thermo Fisher Scientific, MA, USA).

2.6 Quantitative reverse transcription-polymerase chain reaction (qRT-PCR)

Complementary DNA (cDNA) was synthesized from 0.1-1.0µg of total RNA using Omniscript reverse transcription (RT) kit (QIAGEN, Hilden, Germany) in a T3 Thermocycler (Biometra, DE UK). The reaction mixtures were incubated at 37^{o}C for 70min and the Omniscript reverse transcriptase was inactivated at 95^{o}C for 5min. Quantitative PCR was performed in 7500 Real-time PCR system using 1µl of cDNA and TaqMan Universal PCR Master Mix or Power SYBR Green Master Mix (Applied Biosystems, CA, USA). TaqMan gene expression probes for *Lgr5* and *Gapdh* are Mm00438890_m1 and Mm99999915_g1 respectively. The list of gene-specific oligonucleotide primers used for SYBR Green-based measurements are shown below.

SYBR Green primers			
Gene	Forward primer (5' – 3')	Reverse primer (5' – 3')	Final primer concentration [nM]
Cd44	CACATATTGCTTCAATGCCTCAG	CCATCACGGTTGACAATAGTTATG	100
E-Cad	GAGCGTGCCCCAGTATCG	CTGCCTTCAGGTTTTCATCGA	50
EpCAM	ACGGAGAGCCGCTCGAT	GGGTGCCTTTTCATCAACGT	100
Fn1	CATGCCTCGGGAATGGAA	TGCCACTGTTCTCCTACATGGT	100
Hmga2	AGCTTGTTTGGTTTTCAGTGTCTTT	GTATGGACAAGAGGAATTACAGGAAGAG	50
N-Cad	GCCATCATCGCTATCCTTCTG	CGCCGTTTCATCCATACCA	50
Nanog	TGGAAGCCACTAGGGAAAGC	TGGAGTCACAGAGTAGTTCAGGAATAA	100
Oct4	GGAGTCTGGAGACCATGTTTCTG	GAACCATACTCGAACCACATCCTT	50
Snai2	ACACAGTTATTATTTCCCCATATCTCTATGA	CCGACGATGTCCATACAGTAATAGG	100
Snai1	CTGCAACCGTGCTTTTGCT	CACATCCGAGTGGGTTTGG	100
Sox9	CGAGCACTCTGGGCAATCTC	ATCAACTTTGCCAGCTTGCA	100
Twist	AGAATTGGGAAGATGGTTTTATGC	CCCACCAGCAGCCTCACTT	100
Vim	CCTGAGAGAAACTAACCTGGAGTCA	CATCTCTGGTCTCAACCGTCTTAA	100

Table 2.1. List of SYBR Green primers for qRT-PCR.

2.7 Nude mice transplantation assay

BALB/c female nude mice were purchased from Biopolis Resource Centre (BRC; A*STAR, Singapore) and all procedures performed were in accordance with BRC Institutional Animal Care and Use Committee guidelines. GIF-14 clonal lines or FACS-purified cells were resuspended in 200µl of PBS and were injected subcutaneously into 7-8 weeks or 12-13 weeks old immuno-compromised nude mice. Tumour development was monitored weekly and the tumour sizes were scored. The diameters of the tumours were determined using rulers and the tumour volumes were calculated by the formula $4/3\pi r^3$ where r represents the radius of tumour. Animals were culled when tumour sizes reached 15mm in diameter.

2.8 Soft agar colony assay

FACS-isolated cells were suspended in DMEM supplemented with 0.4% agarose and 10% FBS, and seeded at clonogenic densities over a basement layer of 0.6% agarose. The experiments were set up in 6-well plates at 200,000 and 500,000 cells/well in triplicates. Colonies of ≥150μm in size were scored after 3 weeks of culture at 37^{o}C in a humidified atmosphere containing 5% CO_2. Photographs of representative colonies were taken using Nikon Eclipse TS100 phase-contrast microscope (Nikon Corporation, Tokyo, Japan).

2.9 Sphere-forming assay

FACS-enriched cells were seeded at clonogenic densities in 6-well ultra-low attachment plates (Sigma-Aldrich, MO, USA) at 2500 cells/well. The cells were cultured in serum-free DMEM:F12 medium (Invitrogen, CA, USA) consisting of 20ng/ml of human recombinant EGF (PeproTech, NJ, USA), 10ng/ml of human recombinant bFGF (Invitrogen, CA, USA), 1x B27 (Invitrogen, CA, USA), 1x N2 (Invitrogen, CA, USA), 1ng/ml of hydrocortisone (StemCell Technologies, CA, USA), 5μg/ml of insulin (Invitrogen, CA, USA) and 0.4% bovine serum albumin (BSA) Fraction V (Sigma-Aldrich, MO, USA). Methylcellulose (Sigma-Aldrich, MO, USA) was added to a final concentration of 0.1-1.0% to prevent cell aggregation. The number of spheres/well were counted at the indicated time after culturing. To generate secondary spheres, primary spheres were harvested by centrifugation at 500rpm for 2min and dissociated to single cells by TrypLE Express (Invitrogen, CA, USA) for 7-10min. Digestion was inactivated by DMEM supplemented with 0.4% BSA. The cells were sieved through 40μm nylon mesh (BD Biosciences, CA, USA) and seeded at 2500 cells/well in sphere medium. Images of representative spheres were captured

using Nikon Eclipse TS100 phase-contrast microscope (Nikon Corporation, Tokyo, Japan).

2.10 Time-lapse videomicroscopy

FACS-purified P1 and P2 cells were seeded at clonogenic densities on 25mm glass cover slips (Marienfeld Superior, Lauda-Koenigshofen, Germany) or low evaporation 6-well plates (BD Biosciences, CA, USA). Following colony formation, the glass cover slips were transferred to Sykes Moore (BellCoGlass, NJ, USA) chamber with complete CO_2-independent medium (Invitrogen, CA, USA), while those grown in 6-well plates were replenished with standard growth medium. Sykes-Moore microperfusion chamber or 6-well plate was placed into a culture chamber (PeCon, Erbach, Germany) and mounted on Nikon Ti Eclipse microscope (Nikon Corporation, Tokyo, Japan) and maintained at 37^{o}C and 5% CO_2 throughout the experiment. Colonies on glass slips and 6-well plates were visualised at 100x magnification by differential interference contrast (DIC) microscopy or phase contrast microscopy respectively. DIC images of P1 and P2 colonies were captured by a HQ2 CCD camera (Photometrics, AZ, USA) at 3min intervals over 18h. For samples subjected to TGF-β1 treatment, DIC and phase contrast images of P1 colonies were captured before and after 2.5ng/ml of TGF-β1 treatment at 5min intervals for the indicated timeframes. These images were processed using Metamorph (Molecular Devices, CA, USA) and VirtualDub (http://www.virtualdub.org/) softwares for the construction of time-lapse movies.

2.11 Immuno-fluoresent staining

P1 and P2 colonies were generated on coverslips by seeding cells at clonogenic densities. Once the colonies were formed, P1 colonies were pre-treated with 10μM of TGF-β inhibitor, SB431542 (TOCRIS Bioscience, Bristol, UK) for 15h prior to 48h of TGF-β1 treatment at 2.5ng/ml. Colonies were fixed using 4% paraformaldehyde and permeablised with 0.5% Triton X-100. After blocking with 1% BSA, the colonies were incubated with anti-β-catenin (Sigma-Aldrich, MO, USA; clone 6F9; catalogue number: C7082), anti-desmoplakin (Millipore, MA, USA; clone DP2.15; catalogue number: CBL173), anti-Smad2/3 (BD Transduction, CA, USA; clone 18; catalogue number: 610843), or anti-phospho-Smad2/3 (Santa Cruz, CA, USA; catalogue number: sc-11769-R) primary antibodies at 1:200 dilution for 1h at room temperature. This was followed by addition of Alexa Fluor 488-conjugated anti-mouse (Invitrogen, CA, USA; catalogue number: A-11001) or Cy3-conjugated anti-rabbit (Invitrogen, CA, USA; catalogue number: 10520) secondary antibodies at 1:500 dilution for 45min at room temperature. F-actin was visualised using phalloidin conjugated to Alexa Fluor 350 (Invitrogen, CA, USA; catalogue number: A22281) at 1:50 dilution. The stained colonies were mounted on glass slides using ProLong Gold Antifade reagent (Invitrogen, CA, USA). Images were captured using Nikon Ti Eclipse confocal microscope (Nikon Corporation, Tokyo, Japan) or Leica 6000B epifluorescence microscope (Leica, Wetzlar, Germany) and processed using MetaMorph software (Molecular Devices, CA, USA).

2.12 Cloning of *RUNX3* and *RUNX3*^{R178Q} into lentiviral vectors

2.12.1 Polymerase chain reaction (PCR) amplification

The p44 isoform of human *RUNX3* and *RUNX3*^{R178Q} cDNAs were PCR-amplified from pcDNA-FLAG-RUNX3 (Bae *et al.*, 1995) and pcDNA-FLAG-RUNX3^{R178Q} encoding the DNA-binding defective form of human RUNX3 (Inoue *et al.*, 2007). PCR amplification was performed in a 50µl reaction mixture containing 1.25U of Platinum *Pfx* DNA polymerase (Invitrogen, CA, USA), 1X *Pfx* amplification buffer, 1.5 mM $MgSO_4$, 0.3 mM of each dNTP (Finzymes, Espoo, Finland), 0.4µM of forward primer (5'-AAAAAAGAATTCATGCGTATTCCCGTA GACCCAAGCACCAGC-3') and 0.4µM of reverse primer (5'-AAAAAAGCGGCC GCTCAGTAGGGCCGCCACACGGCCTCATCC-3'). The PCR cycling parameters consisted of 35 cycles at 95^{o}C for 30s, 56^{o}C for 30s and 72^{o}C for 2min. Final extension at 72^{o}C for 15min was performed. PCR products were analysed by agarose gel electrophoresis and the bands of correct sizes were excised and recovered with the QIAquick gel extraction kit following manufacturer's protocol (QIAGEN, Hilden, Germany). The PCR products were cloned immediately upstream of *IRES-EGFP* via engineered 5' *Eco*RI and 3' *Not*I sites in the LeGO-iG2 plasmid (termed iG2), a bicistronic lentiviral vector generated by Weber *et al.*, 2008. The ligation of digested PCR products and linearised iG2 vector was performed for at least 1h at room temperature using T4 DNA ligase (NEB, MA, USA) in a 20µl reaction containing 1µl of DNA ligase. The utilisation of internal ribosome entry site (IRES) in the iG2 lentiviral vector enables co-expression of RUNX3/RUNX3^{R178Q} and EGFP in the transduced cells driven by the spleen focus-forming virus (SFFV) promoter. Similarly, wild-type *RUNX3* and *RUNX3*^{R178Q} cDNAs were cloned into a modified pBOBI lentiviral vector (a kind gift of Dr Vinay Terganonar, Institute of Molecular and Cell

Biology, A*STAR, Singapore) using 5' *Xba*I and 3' *Xho*I sites. The cloning of *RUNX3* and *RUNX3*^{R178Q} into the lentiviral vectors was performed by Dr Dominic Voon (Cancer Science Institute of Singapore, National University of Singapore, Singapore).

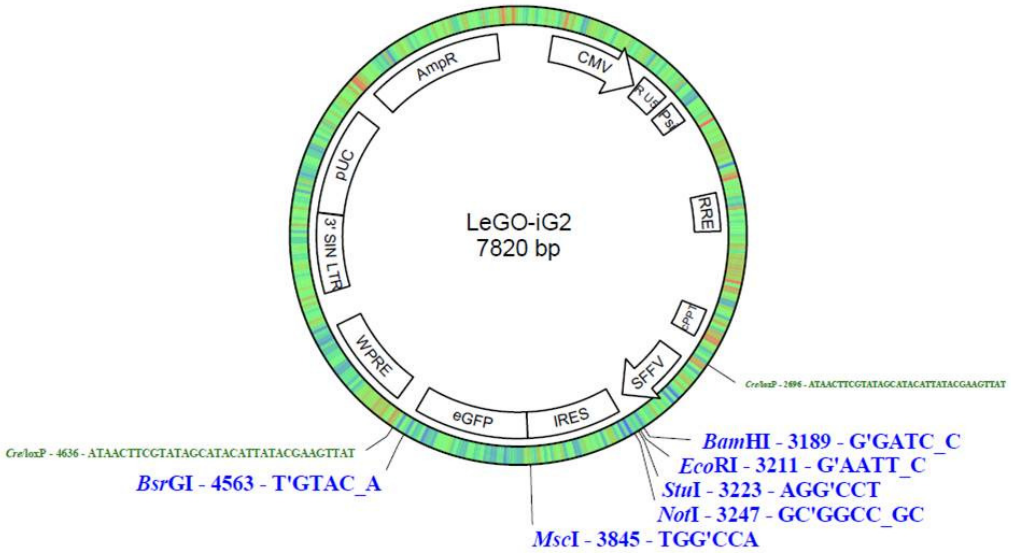

Figure 2.1. Plasmid map of the LeGO-iG2 lentiviral vector. CMV (promoter): cytomegalovirus; SFFV (promoter): spleen focus-forming virus; IRES: internal ribosome entry site; eGFP: enhanced green fluorescent protein. Unique restriction sites present in the vector are marked in blue.

2.12.2 Chemical transformation of *Escherichia coli*

Three microlitres of ligated products was transformed into 50µl of home-made chemically-competent *Escherichia coli* XL10-Gold strain originally obtained from Stratagene (CA, USA). The mixture was kept on ice for 30min prior to heat-shock at 42^{o}C for 80s. The mixture was returned to ice immediately for 5min and recovered in 200µl Luria-Bertani (LB) medium at 37^{o}C with shaking for 1h. The transformation mixture was subsequently plated onto LB agar plates containing 100µg/ml of ampicillin (Sigma-Aldrich, MO, USA) and incubated overnight at 37^{o}C for selection of successfully transformed bacterial cells.

2.12.3 Purification of plasmid DNA

DNA purification was performed at small-scale from 3ml of starter cultures with QIAprep Spin Miniprep columns (QIAGEN, Hilden, Germany) or large-scale from 50ml of overnight cultures with QIAfilter Plasmid Midi kit (QIAGEN, Hilden, Germany) according to manufacturer's protocols. The amount of DNA yielded was measured using NanoDrop 1000 Spectrophotometer (Thermo Fisher Scientific, MA, USA).

2.12.4 Sequencing of plasmid DNA

Clones of recombinant plasmid DNA were fully sequenced using BigDye Terminator version 3.1 Cycle Sequencing kit (Applied Biosystems, CA, USA). Each sequencing reaction was made up of 300ng of plasmid DNA, 3.2pmol of the forward or reverse primer (Section 2.12.1), 8µl of Terminator Ready Reaction Mix and H_2O to a final volume of 20µl. PCR was carried out in 96-well GeneAmp PCR System 9700 (Applied Biosystems, CA, USA). The PCR reaction involved an initial denaturation at 95^{o}C for 3min and 35 cycles at 95^{o}C for 30s, 52.5^{o}C for 10s and 60^{o}C for 4min. Purification and subsequent sequencing of the PCR products were carried out by the Sequencing Facility at the Institute of Molecular and Cell Biology (A*STAR, Singapore).

2.13 Lentivirus production and transduction

Lentiviruses were produced according to the protocol described in Tiscornia *et al.*, 2006 with minor modifications. Briefly, $0.7x10^6$ HEK293T cells were seeded on a 6-well plate pre-coated with 0.001% of poly L-lysine (Sigma-Aldrich, MO, USA) one day before transfection. iG2- or pBOBI-Control, -*RUNX3* or -*RUNX3*^{R178Q} transfer vectors (1µg) were co-transfected into HEK293T cells with third generation packaging plasmids containing pLP/VSVG (1µg), pLP1 gag/pol (0.66µg) and pLP2 Rev (0.33µg) (ViraPower Lentiviral Expression system; Invitrogen, CA, USA) using 10µl of FuGENE HD (Roche, Basel, Switzerland). The cells were washed with PBS 8h post-transfection and replaced with fresh DMEM supplemented with 15% FBS (HyClone Laboratories UT, USA). The supernatants containing viral particles were harvested at 24h and 48h post-transfection. For transduction with iG2-based lentiviruses, GIF-14 cells cultured in 6-well tissue culture plates at 80% confluency were incubated with virus-containing supernatants in 1:3 ratio to culture media in the presence of 5µg/ml of polybrene (Sigma-Aldrich, MO, USA) for 24h before replenishment with fresh culture medium. Infected cells were either subjected to Hoechst/antibody staining or treated with Wnt3a-Cm or TGF-β1 prior to enrichment by FACS. Transduction with pBOBI-based lentiviruses was performed in a similar manner in 48-well tissue culture plates and the cells were harvested *in situ* following 15h of Wnt3a-Cm treatment.

2.14 Protein preparation and Western blotting

Runx3$^{+/+}$ (GIF-9 and GIF-13) and *Runx3*$^{-/-}$ (GIF-5 and GIF-14) cells were seeded in 15-cm tissue culture dishes and harvested at 80% confluency for Western blot analysis. Cell pellets were lysed by urea lysis buffer (9M of urea, 2% of Triton-X-100 and 5% of β–mercaptoethanol) supplemented with 1x Complete protease inhibitor (Roche, Basel, Switzerland) and 10mM of phenylmethylsulfonyl fluoride. Transduced GIF-14 cells were lysed by RIPA buffer (50mM Tris-HCl pH 7.4, 150mM NaCl, 1% NP-40, 0.25% sodium deoxycholate and 1mM EDTA) in a similar manner. Sonication was then performed using Bioruptor (Diagenode, NJ, USA) to shear the genomic DNA to disrupt large protein-DNA complexes, allowing proteins to fully solubilise. The cell lysates were centrifuged at 10,000 rpm for 10min and the supernatants were collected into fresh microfuge tubes. The amount of protein was quantified using Bradford Assay. Briefly, 2µl of cell lysate was mixed with 1.98ml of 1X Bradford dye and incubated for 5min at room temperature prior to measurement using GeneQuant 1300 spectrophotometer (GE Healthcare, Little Chalfont, UK). After quantification, the amount of proteins was normalised against the most diluted sample before the addition of SDS-containing loading buffer. Cell lysates were heated at 37^0C for half an hour to denature the proteins. Whole cell lysates were resolved in 10% SDS-polyacrylamide gels and electrophoresed at 170V and 40mA for approximately 2.5h. Proteins were transferred onto PVDF membranes (Biorad, CA, USA) at constant 100V for 1 h 45 min prior to blocking using 5% skim milk in PBST (PBS + 0.1% Tween) (Fonterra, AU, New Zealand) for 1h. Murine Runx3 was detected using two separate anti-RUNX3 monoclonal antibodies, R3-5G4 and R3-8C9 (a kind gift of Kotaro Tada) at 1µg/ml in PBST + 1% skim milk and PBST + 2.5% skim milk, respectively. Human RUNX3 was detected using R3-5G4 antibody. Detection of the

housekeeping protein, α-tubulin was performed by incubation with anti-α-tubulin antibody (Sigma-Aldrich, MO, USA) at 1:50000 dilution for 1h. Membranes were washed for 3 times with PBST buffer before incubation with HRP-conjugated anti-mouse secondary antibody (GE Healthcare, Little Chalfont, UK) at 1:8000 dilution in PBST + 5% skim milk for 1h. After removing excess secondary antibody, chemiluminescent signals were captured using Immobilon Western Chemiluminescent HRP substrate reagents (Millipore, MA, USA).

2.15 Statistical analysis

All data performed in replicates are presented with standard error mean (SEM). When two data sets were compared, the Student's *t*-test was used and *p*-values < 0.05 and <0.01 was considered significant.

CHAPTER 3

Identification of a tumorigenic, stem/progenitor-like subpopulation within the *Runx3*$^{-/-}$ GIF-14 gastric epithelial cell line

3.1 Introduction

3.1.1 Cell immortalisation and transformation

Cancer is a multi-step process driven by the sequential accumulation of mutations in critical genes such as oncogenes and tumour suppressors. Genetic alterations of these genes lead to uncontrolled cell proliferation, resistance to apoptosis, and acquisition of other traits associated with the malignant cell phenotype (Drayton and Peters, 2002). This process usually takes a period of decades. During tumour formation, human cells need to undergo an abnormally long succession of growth-and-division cycles in order to complete the steps of tumorigenesis. In the current model of this process, the first step is the ability of cells to replicate indefinitely, termed immortalisation (Weinberg, 2007). Immortalised cells are pre-malignant but non-tumorigenic. They are susceptible to cellular transformation upon further genetic hits to become tumorigenic.

Cellular immortalisation and transformation has been intensively studied *in vitro*, most commonly in murine embryonic fibroblasts (MEFs). These studies have offered fundamental insights into the biology of carcinogenesis. Under normal culturing conditions, MEFs would rapidly cease to proliferate after several passages in response to stress (Parrinello *et al.*, 2003). Immortality could be achieved by ectopic expression of a number of oncogenes, such as the large T oncoprotein of Simian virus 40 that inactivated the function of primary negative regulators of cell cycle, p53 and pRb (Schreier and Gruber, 1990). Accordingly, mutations of either p53 or its targets $p16^{INK4a}/p19^{ARF}$ were frequently found in spontaneously immortalised NIH3T3 MEFs (Linardopoulos *et al.*, 1995). In addition, forced expression of the catalytic component of human telomerase in some cell types led to the generation of immortalised cell

lines (Bodnar *et al.*, 1998). In order for immortalised cells to become fully transformed, additional mutations are needed, typically through the introduction of an oncogene such a constitutively activate *H-Ras* mutant (Visvanathan *et al.*, 1998). Immortalisation and transformation could also be achieved through the introduction of oncogenes found in DNA tumour viruses. Middle T and large T oncogenes from polyomavirus collaborate with one another to transform rodent cells. The large T oncoprotein facilitates immortalisation while the middle T oncoprotein elicits many functions associated with the *Ras* oncogene to confer full transformation (Rassoulzadegan *et al.*, 1982). Therefore, much of the process of tumorigenesis could be revealed through these studies.

Classically, there are several experimental approaches to determine successful transformation. A particularly common benchmark used in the assessment of tumorigenicity *in vivo* is the subcutaneous transplantation of transformed cells into immuno-compromised animals such as the athymic nude mice (Flanagan, 1966). Immuno-deficient mice are incapable of mounting immune response against grafted cells. Tumorigenicity is measured by the ability of transplanted cells to form tumours in mice. As transplantation assays are typically time consuming and lengthy, rapid and quantitative *in vitro* assays have been developed to evaluate tumorigenicity. One of the key properties of transformed cells is anchorage-independent growth in which cells are able to proliferate without attachment to solid substratum (Cifone and Fidler, 1980). The soft agar colony formation assay is used to monitor anchorage-independent growth in a semi-solid agar medium. Cells that have the capability to grow as colonies under such conditions are considered tumorigenic. However, the initial set-up and final scoring of colonies can be labour-intensive. Although each of

these methodologies has its caveats and limitations, they are useful functional assays to measure tumorigenic potential.

3.1.2 Strategies for identifying tumour-initiating cells

In this study, immortalised gastric epithelial (GIF) cell lines were established from mouse embryos through genetic disruption of *p53*. As these cell lines were immortalised but not transformed, they were not expected to be tumorigenic. However, owing to the loss of the gastric tumor suppressor Runx3, *Runx3*$^{-/-}$.*p53*$^{-/-}$ GIF cell lines formed tumours when transplanted into immuno-compromised nude mice (Fukamachi *et al.*, 2004). Notably, the tumorigenic potential of *Runx3*$^{-/-}$.*p53*$^{-/-}$ GIF cell lines was inherently low as the cell number necessary for generating tumour was typically 10E4 higher than standard transformed cells (Fukamachi *et al.*, 2004). These observations indicate that Runx3 deficiency moved the cells one step closer to tumorigenesis even though full transformation did not occur. To further understand the underlying molecular mechanisms of the tumorigenicty of *Runx3*$^{-/-}$.*p53*$^{-/-}$ cells, we sought to identify and characterise the properties of these tumorigenic cells in *Runx3*$^{-/-}$.*p53*$^{-/-}$ GIF cell lines.

Recently, the hypothesis that cancer is driven and maintained by a small subpopulation of cancer cells within the tumour mass has gained attention in the tumour biology field (Lapidot *et al.*, 1994). This subpopulation is often referred to as "cancer stem cells" (CSCs). CSCs demonstrate increased resilience against conventional chemotherapy and are thought to be responsible for tumour recurrence and maintenance. There is also evidence suggesting that CSCs are involved in metastasis of solid tumours (Velasco-Velazquez *et al*., 2011). Therefore, cancer stem

cells hold promise as novel cellular targets for the treatment of malignancies (Reya *et al.*, 2001). CSCs are experimentally defined by the ability to regrow the tumour in immuno-compromised mice from which they were isolated or identified (Lapidot *et al.*, 1994). Thus, the term tumour-initiating cells (TICs) are frequently used as it more closely reflects the experimental evidence. In this chapter, TICs would be used to describe cells bearing cancer stem cell properties. The TICs in tumours are identified by the use of molecular markers expressed on the cell surface, which were first discovered to enrich for stem cells. In the hematopoietic system, purification of tissue stem/progenitor cells relies largely on cell surface markers, which can serve as either positive or negative makers for stem/progenitor cell activity (Challen and Little, 2006). Often, a combination of several cell surface markers is required to achieve high degree of enrichment of stem/progenitor cells as none of these cell surface markers is expressed exclusively on stem/progenitor cells. Although the use of cell surface markers does confer specificity to the identification and isolation of normal stem/progenitor cells and TICs, this strategy fails in the absence of known cell surface markers (Wu and Alman, 2008). Unfortunately, cell surface markers that define TICs are not well characterised in many solid tumours, including those in gastric cancers.

In the last decade, the Hoechst 33342 staining technique has gained popularity in the study of tissue stem cells as it is a versatile tool to identify, purify and characterise resident tissue stem/progenitor cells independent of cell surface markers. This method is simple and particularly useful when the stem/progenitor cells are not well characterised by cell surface markers. Based on differential staining by the Hoechst 33342 dye, this technique has facilitated the enrichment of stem/progenitor cells in a variety of normal tissues including blood, skin, lung, liver, heart, mammary

gland and skeletal muscle (Wu and Alman, 2008). Hoechst 33342 is a fluorescent dye that binds to AT-rich DNA and can be excited by ultraviolet laser. Its fluorescence is plotted at two emission wavelengths using 450/20nm band-pass (Hoechst blue) and 675nm long-pass (Hoechst red) filters on the flow cytometer. When first established in the analyses of murine bone marrow cells, it was found that cells dimly stained by the Hoechst 33342 dye were strongly enrich for long-term repopulating hematopoietic stem cells (Goodell *et al*, 1996). These cells were termed the "side population" (SP) as they resolved to the "side" of the bulk of more strongly stained cells in FACS analysis (Figure 3.1; Challen and Little, 2006). The mechanism regulating the efflux of Hoechst 33342 dye is partly conferred by the expression of ATP binding cassette protein transporters. Forced expression of these membrane-bound transporters such as *Abcg2/Bcrp1* and *Abcb1/MDR1* in murine bone marrow cells resulted in an expansion of SP *in vitro* and increased long-term repopulating hematopoietic stem cells *in vivo* (Bunting *et al*, 2000; Zhou *et al*., 2001). Therefore, when Hoechst 33342 staining was performed in the presence of an inhibitor of ATP binding cassette protein transporters, verapamil, SP cells were ablated (Figure 3.1; Challen and Little, 2006). The gate for the SP is set to demarcate the cell population specifically eliminated upon the treatment of verapamil as shown in Figure 3.1 (Challen and Little, 2006). However, a gradient of dye efflux exists within the SP in which the cells at its tip possessed the highest efflux while the cells at the top of the SP display least efflux, as reflected in the increasing Hoechst 33342 fluorescence intensity. It was found that the cells with the greatest dye efflux capability exhibited the highest long-term hematopoietic stem cell activity within the SP (Goodell *et al*., 1997). Due to the superior enrichment of stem cells, a small gate is usually applied to capture the cells at the tip of the SP for functional characterisations and comparative analyses.

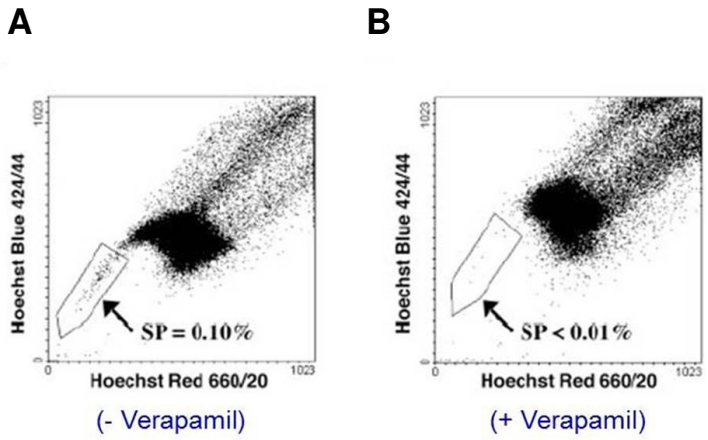

Figure 3.1. Flow cytometry profile of murine bone marrow cells after staining with Hoechst 33342. (A) The SP appeared as the Hoechst 33342 low fraction capable of pumping out the dye more efficiently than the bulk of the Hoechst 3342 high cells. (B) The SP was ablated when verapamil was added in the Hoechst 33342 incubation. This figure was taken from Challen and Little, 2006.

Subsequently, the Hoechst 33342 staining method has been utilised to identify and isolate TICs in many human cancer cell lines and primary tumours (Wu and Alman, 2008). Several studies have shown highly enriched tumour-initiating activity for the SP cells purified from hepatocellular, lung, brain, gastrointestinal and nasopharyngeal carcinoma cell lines, compared to both the bulk tumour cell population and the non-SP population (Kondo *et al.*, 2004; Chiba *et al.*, 2006; Haraguchi *et al.*, 2006; Ho *et al.*, 2007; Wang *et al.*, 2007).

It has been reported that TICs share several properties with normal stem cells, especially the capability of self-renewal (Pardal *et al.*, 2003). The sphere-forming assay is a standard *in vitro* assay frequently utilised to characterise normal tissue stem cells and TICs in the brain and mammary glands (Weiss *et al.*, 1996; Al-Hajj *et al.*, 2003; Dontu *et al.*, 2003; Kondo *et al.*, 2004). Stem cell-like properties are demonstrated by the formation of spheres on non-adherent surfaces in serum-free culture medium. The ability to generate spheres depends on the presence of

stem/progenitor cells within a cell population. Cells that form spheres, which can be serially passaged are believed to possess self-renewal properties (Dontu *et al.*, 2003).

3.1.3 Experimental approach

The experiments described in this chapter are aimed to identify and isolate the tumorigenic cells from a *Runx3*$^{-/-}$.*p53*$^{-/-}$ GIF cell line (GIF-14) by employing the Hoechst 33342 staining technique. These cells are tested for their tumorigenic potential using transplantation and soft agar colony formation assays. Furthermore, gene expression profiling for stem-cell-related markers and sphere-forming assays will be performed to assess whether these tumorigenic cells display stem cell-like characteristics.

3.2 Results

3.2.1 Hoechst 33342 staining of GIF-14 cells revealed two distinct subpopulations

Hoechst 33342 staining was performed on a *Runx3*$^{-/-}$*.p53*$^{-/-}$ GIF cell line, GIF-14, to separate the cells based on their dye exclusion capability. To obtain a reproducible Hoechst 33342 staining pattern, a series of optimisations were previously performed for various Hoechst 33342 concentrations, incubation time and verapamil concentrations. Figure 3.2 shows a typical flow cytometric profile of GIF-14 cells following staining with Hoechst 33342 under the optimised conditions. GIF-14 cells could be seen as two major subpopulations, P1 and P2 with significantly different fluorescence owing to differential dye efflux properties. The P1 subpopulation had relatively lower fluorescence as they excluded dye efficiently. This lower fluorescence was effectively blocked by verapamil as the cells were unable to efflux the dye resulting in increased intracellular Hoechst 33342 concentrations. Therefore, the P1 subpopulation was defined by the cell population that had shifted upon the treatment of verapamil, the majority of which could be analysed by marking a large gate as depicted in Figure 3.2. In contrast, the P2 subpopulation was defined by high fluorescence due to its lower dye pumping capacity, and that its staining pattern was largely unaffected by verapamil (Figure 3.2).

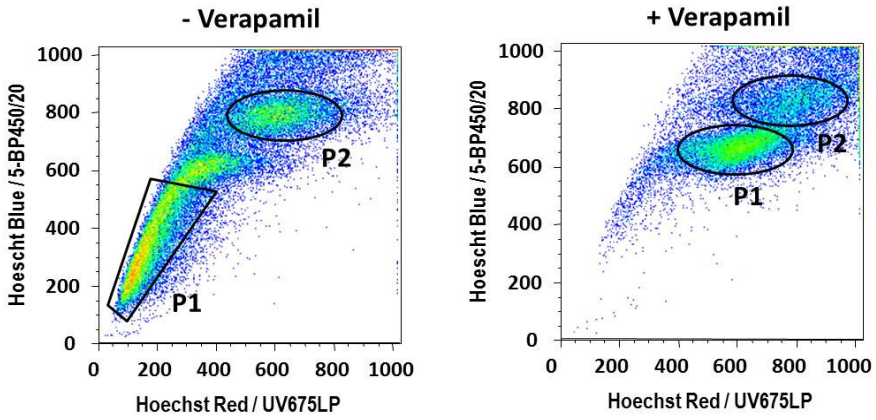

Figure 3.2. Hoechst 33342 staining of *Runx3*$^{-/-}$ GIF-14 cells revealed two distinct subpopulations. GIF-14 cells were stained by 10µg/ml of Hoechst 33342 in the absence and presence of 4µg/ml of verapamil as described Section 2.3. Hoechst fluorescence is plotted at Hoechst blue (450/20nm BP filter) and Hoechst red (675nm LP filter) on the flow cytometer. The gate for P1 is set to encompass majority of the cells which are sensitive to verapamil treatment.

3.2.2 P1 and P2 cells display differential EpCAM and CD133 expressions

To determine the relative expression of cell surface markers in P1 and P2 subpopulations, GIF-14 cells were simultaneously stained by Hoechst 33342 and antibodies against various cell surface antigens which are known to mark differentiation status in different tissues (Table 3.1). The expression levels of the tested cell surface markers in P1 and P2 subpopulations are summarised in Table 3.2. Surface marker profiling revealed that the expression of CD133, EpCAM, and CD49f were substantially higher in P1 compared with P2 (Table 3.2). However, P1 and P2 subpopulations did not show obvious difference in the expression of other cell surface markers such as Sca1, CD71, CD29, CD44 and CD24 (Table 3.2).

Cell surface markers	Functions	References
CD133 (Prominin-1)	Marker for hematopoietic and neural stem cells; also marks TICs in brain and colorectal cancers.	Yin et al., 1997; Uchida *et al.*, 2000; Salven *et al.*, 2003; Singh *et al.*, 2004
EpCAM (Epithelial cell adhesion molecule)	Used in combination with other surface markers to enrich for TICs in breast, pancreatic and liver cancers.	Al-Hajj *et al.*, 2003; Li *et al.*, 2007; Yamashita *et al.*, 2009
CD49f (Integrin α6)	Marks normal stem cells and TICs in the mammary tissue.	Stingl *et al.*, 2006; Lo *et al.*, 2011
Sca-1 (Stem cell antigen-1)	Marker for murine hematopoietic stem cells; commonly used in combination with other surface markers to enrich for stem cells.	Spangrude and Brooks, 1992
CD71 (Transferrin receptor)	Marks keratinocyte stem cells and erthyroid progenitors; $CD71^-$ cells enrich for TICs in adenosquamous carcinomas.	Lorenz *et al.*, 2008; Dong *et al.*, 2011; Ohkuma *et al.*, 2011
CD29 (Integrin β1)	Ubiqutiously expressed in many cell types; marks keratinocyte stem cells.	Lorenz et al., 2008
CD44 (Hyaluronic acid receptor)	Marks TICs in breast and colorectal cancers.	Al-Hajj *et al.*, 2003; Takaishi *et al.*, 2009
CD24	Expressed in Paneth cells, the niche for Lgr5 stem cells in intestinal crypts; marks TICs in pancreatic cancers; $CD24^-$ cells enrich for TICs in breast cancers.	Al-Hajj *et al.*, 2003; Li *et al.*, 2007; Sato *et al.*, 2011

Table 3.1. Summary of the tested cell surface markers known to mark differentiation status of cells in various tissues.

Cell Surface markers	Percentage of positivity		
	Total GIF-14	P1	P2
CD133	48.3	66.6	13.9
EpCAM	54.1	90.1	19.1
CD49f	75.5	76.5	59.9
Sca-1	68.4	71.4	78.3
CD71	25.5	25.4	30.3
CD29	98.5	99.0	99.1
CD44	92.3	97.0	96.7
CD24	91.4	94.0	94.0

Table 3.2. Summary of expression levels of cell surface antigens in P1 and P2 subpopulations. GIF-14 cells were co-stained by Hoechst 33342 and various antibodies against cell surface antigens and analysed by flow cytometry. The percentage of positivity of each surface marker in total GIF-14 cells, P1 and P2 subpopulations was tabulated.

EpCAM is expressed on the cell surface membrane of virtually all epithelial cells and hence is generally regarded as an epithelial marker (Latza *et al.*, 1990). Despite being widely expressed in many adenocarcinomas (Latza *et al.*, 1990), its expression in gastric cancer tissues is not well studied. Similar to EpCAM, the involvement of CD49f in gastric tumours is obscure. It is known that CD49f forms heterodimers with the integrin β4 subunit which acts as the receptor for laminin in all epithelial cells (Krieger *et al.*, 2004). CD133 is not only expressed in organ-specific stem cells, but also in differentiated epithelial cells in the liver, pancreas and colon (Weigmann *et al.*, 1997; Florek *et al.*, 2005, Shmelkov *et al.*, 2008). Our results revealed that these three cell surface markers, which are prominently expressed in epithelial cells, were depleted in the P2 subpopulation, suggesting that P2 cells have reduced epithelial cell characteristics compared to P1 cells. Such differences in epithelial cell differentiation status may have implications in the relative tumorigenic potential of P1 and P2 subpopulations.

Co-staining of antibodies against EpCAM and CD133 together with Hoechst 33342 in the GIF-14 cell line was performed. For flow cytometric analyses, a large P1 gate was set in order to include the majority of P1 cells to ensure the relative expressions of EpCAM and CD133 is representative of P1 cells. The results showed that the P1 subpopulation displayed $EpCAM^{high}CD133^{+}$ expression pattern while the P2 subpopulation was demarcated by $EpCAM^{low}CD133^{-}$ antigen profile (Figure 3.3 top panel). Conversely, $EpCAM^{high}CD133^{+}$ and $EpCAM^{low}CD133^{-}$ fractions enriched for P1 and P2 subpopulations, respectively (Figure 3.3 bottom panel). Therefore, the above data indicate that P1 and P2 represent distinct subpopulations of varied differentiation status within the GIF-14 cell line.

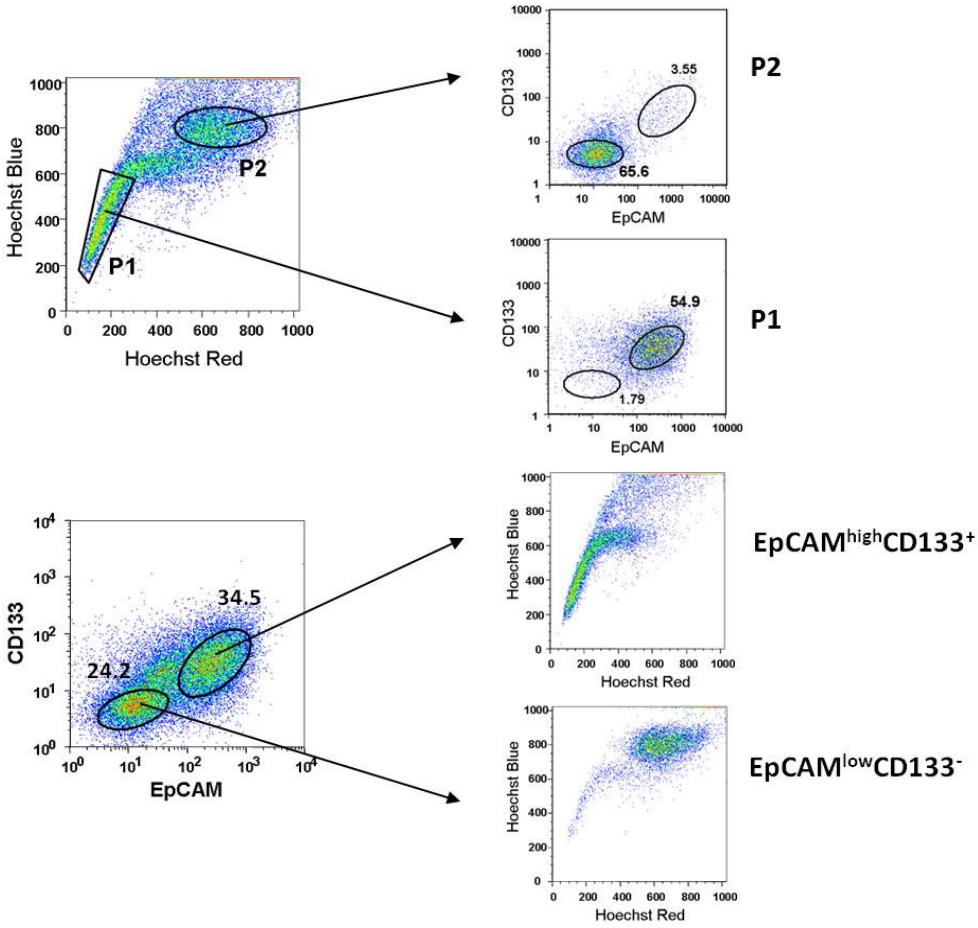

Figure 3.3. Double staining of EpCAM/CD133 with Hoechst 33342 in GIF-14 cells. Hoechst 33342-stained GIF-14 cells were co-stained by antibodies against EpCAM and CD133. Cells were then subjected to flow cytometry. The distribution of EpCAM and CD133 within P1 and P2 subpopulations (top panel) and the Hoechst 33342 profiles of $EpCAM^{high}CD133^{+}$ and $EpCAM^{low}CD133^{-}$ fractions were analysed by the Flowjo software.

3.2.3 The P2 subpopulation forms tumours more readily than the P1 subpopulation

Staining of GIF-14 cells by Hoechst 33342 enables the purification and functional characterisation of P1 and P2 subpopulations. To test their relative tumorigenicities *in vivo*, these two subpopulations were allografted into the immuno-compromised nude mice. These transplantation experiments were performed in two complementary approaches using: 1) FACS-fractionated P1 and P2 cells isolated from parental GIF-14 culture, and 2) clonal lines established from enriched P1 and P2 subpopulations. In the first experiment, P1 and P2 subpopulations were sorted from parental GIF-14 line by FACS and briefly cultured *in vitro* for recovery and expansion. Purified P1 and P2 cells were analysed by Hoechst 33342 staining to confirm that they maintained their respective staining patterns prior to transplantation into nude mice (Figure 3.4). For each tested subpopulation, cells were transplanted subcutaneously into hind flanks of each mouse. Unsorted parental GIF-14 cells were similarly injected in the neck region of the same mouse to act as a control. Two independent transplantations using 4x 10^6 and 2x 10^6 cells were performed. In both experiments, the P2 subpopulation was observed to form tumours more readily in nude mice than the P1 subpopulation. This was reflected in the higher tumour incidence and greater tumour size (Figure 3.5).

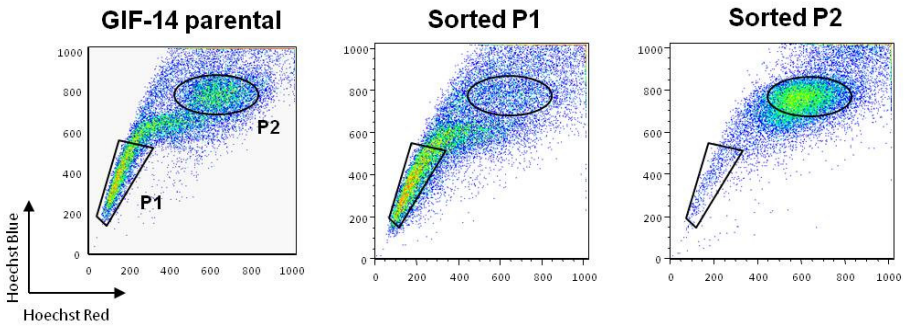

Figure 3.4. Hoechst 33342 staining profiles of sorted P1 and P2 subpopulations. P1 and P2 cells were purified by FACS and expanded in culture for about 1 week. Hoechst 33342 staining was performed on sorted cells prior to transplantation.

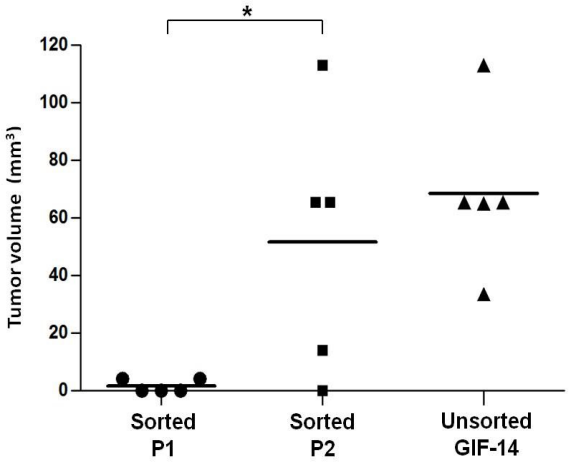

Cells	No. of mouse with tumors	Average tumor diameter (mm)
Unsorted GIF-14	5/5	5
Sorted P1	2/5	0.8
Sorted P2	4/5	3.8

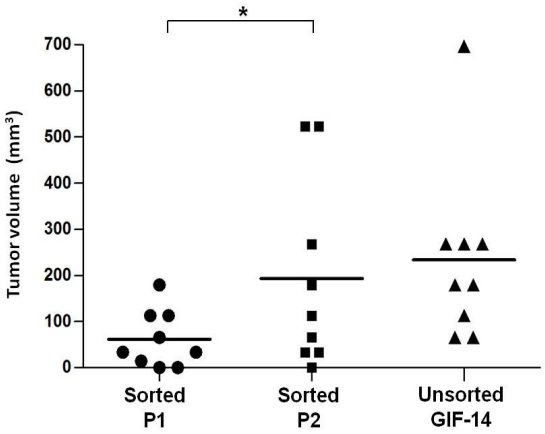

Cells	No. of mouse with tumors	Average tumor diameter (mm)	Tumour appearance
Unsorted GIF-14	9/9	7.2	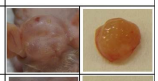
Sorted P1	7/9	3.9	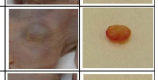
Sorted P2	8/9	6	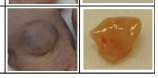

Figure 3.5. Relative tumorigenicity of FACS-enriched P1 and P2 cells in nude mice allografts. Top plot: For each mouse, 4x 10^6 of sorted P1 (left hind flank), sorted P2 (right hind flank) and unsorted (neck) cells were injected and tumour sizes were scored after 8 weeks (n=5). Age of mice was 12-13 weeks. Bottom plot: Independent but similar experiment in which 2x 10^6 cells were transplanted and the tumours were examined after 11.5 weeks (n=9). Age of mice was 7-8 weeks. Each dot on the plots represents tumour size from a single mouse. Black horizontal bars denote the mean tumour volume for each cell population. Tumour volume was calculated by the formula $4/3\pi r^3$ where r is tumour radius. Student's *t*-test was performed and single asterisk represents *p*-value <0.05. Tabulation of the number and diameter of tumours is shown in the tables on the right of the plots.

P1 and P2 clonal lines were raised from purified P1 or P2 cells through single-cell cloning in 96-well plates. Nine P1 and twelve P2 single-cell clones were obtained and three clonal lines derived from each subpopulation were analysed for the maintenance of their Hoechst 33342 staining patterns. The results for a representative clonal line derived from P1 or P2 subpopulation were shown in Figure 3.6. P1 and P2 clonal lines preserved their respective Hoechst 33342 profiles preceding transplantation in nude mice in a similar manner as described earlier. Consistent with the results from sorted pooled cells, the tested P2 clonal line was significantly more tumorigenic than the P1 clonal line both in terms of the frequency of tumour initiation and tumour size (Figure 3.7). Thus, we conclude that the tumour-initiating cells reside largely in the low dye effluxing, $EpCAM^{low}CD133^{-}$ P2 subpopulation within the GIF-14 cell line.

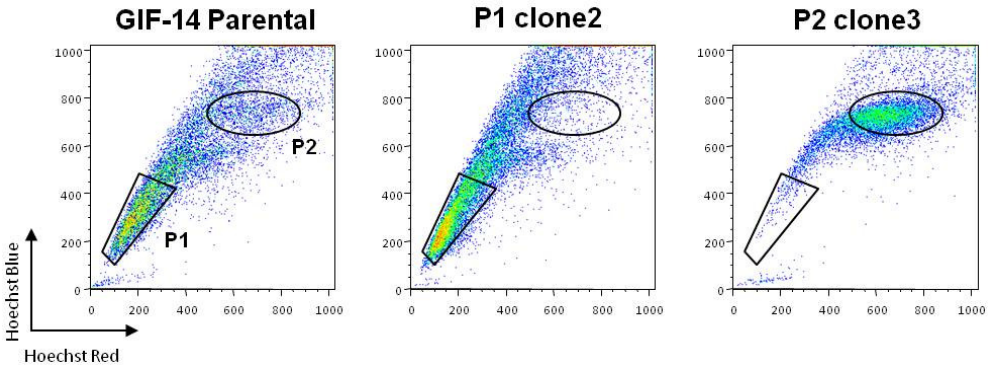

Figure 3.6. Hoechst 33342 staining of P1 and P2 clonal lines. FACS-purified P1 and P2 cells were seeded at clonagenic density in 96-well plates and colonies were raised from single P1 or P2 cells. These colonies were then expanded in culture and anlaysed for Hoechst 33342 staining patterns prior to transplantation.

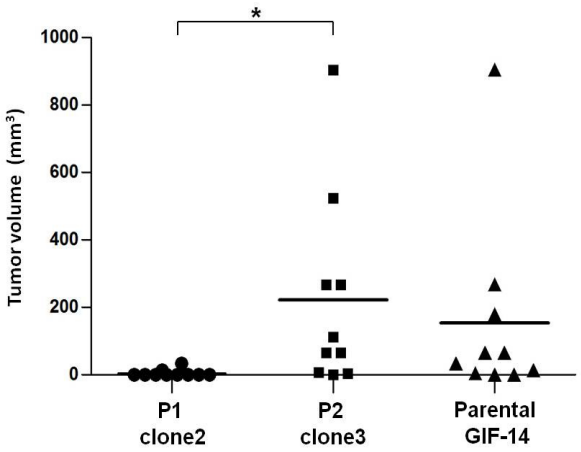

Cells	No. of mouse with tumors	Average tumor diameter (mm)	Tumour appearance
Parental GIF-14	7/9	5.1	
P1 clone2	4/9	0.8	
P2 clone3	8/9	6.5	

Figure 3.7. Comparison of the tumorigenic potential of P1 and P2 clonal lines. For each mouse, 2x 10^6 of P1 clone2 (left hind flank), P2 clone3 (right hind flank) and unsorted (neck) cells were inoculated and tumours were harvested after 14 weeks (n=10). One mouse had no tumour at all sites. Age of mice was 7-8 weeks. Each dot on the plots signifies tumour size from one mouse. Black horizontal bars represent the average tumour sizes for each cell population. Student's *t*-test was performed and single asterisk represents *p*-value <0.05. Tumour number and size are tabulated in the table next to the graph.

3.2.4 P2 cells form colonies more readily in soft agar assay

FACS-enriched P1 and P2 cells were further evaluated for their ability to exhibit anchorage-independent growth *in vitro* by soft agar assay. The isolated cell populations were suspended at clonogenic density in agar mixed with normal culture medium and colony formation was determined. Control sorted cells were all the cells collected within the FACS plot including P1 and P2 subpopulations. Consistent with the transplantation data, P2 cells formed colonies far more readily than P1 cells, reflecting greater tumorigenicity (Figure 3.8). The colonies were scored manually using a microscope as they were generally small. This reflects the low tumorigenicity of immortalised GIF-14 cells.

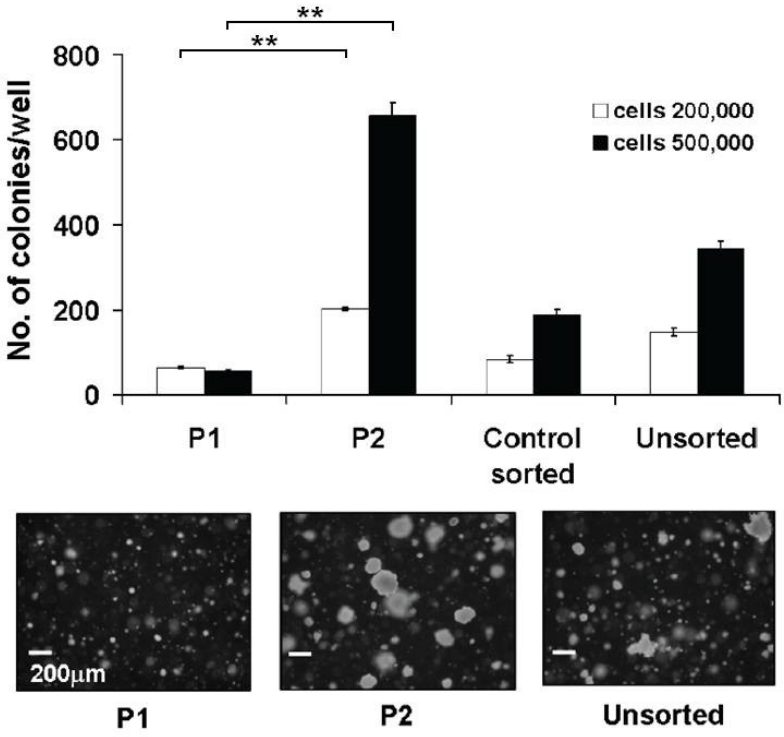

Figure 3.8. Comparison of anchorage independent growth of sorted P1 and P2 cells. FACS-fractionated P1, P2, control sorted and unsorted parental GIF-14 cells were subjected to soft agar assay to assess the relative anchorage independent growth potential. Control sorted cells represents the total population within the entire FACS plot. After 3 weeks of culture, colonies ≥150μm in size were scored and the data are represented as means ± standard error mean (SEM) (n=3). Double asterisks denotes *p*-value <0.01. Representative phase contrast images of the colonies were taken from samples with 200,000 cells/well. Scale bars, 200μm.

3.2.5 The P2 subpopulation is enriched for stem cell-related genes

To ascertain whether the tumorigenic P2 subpopulation shares attributes of stem cells, gene expression profiling was performed to measure the transcript levels of stem cell-related markers by quantitative RT-PCR (qRT-PCR). In order to perform the most effective comparison in the gene expression between P1 and P2, a small gate was applied to capture the highest dye-effluxing P1 cells as shown in Figure 3.9 left panel. This ensures that fractionated P1 and P2 cells are of high purity. Three independent preparations of P1 and P2 subpopulations were performed and the results are summarised in Figure 3.9. The expression levels of these markers are expressed as

ratios to those of control sorted cells and plotted on log scale. Our results revealed that the P2 subpopulation expressed significantly higher levels of embryonic stem cell markers *Oct4* and *Nanog* than the P1 subpopulation (Figure 3.9). Furthermore, P2 was strongly enriched for *Lgr5* to 100-fold. Lgr5 is a G protein-coupled receptor that marks a newly discovered stem cell population in the intestinal crypt and pyloric gastric glands (Barker *et al.*, 2007; Barker *et al.*, 2010) (Figure 3.9) . P2 cells also expressed elevated levels of *Sox9,* which is reported to co-localise with *Lgr5* in gastrointestinal stem cells (Barker *et al.*, 2010; Van der Flier *et al.*, 2009) (Figure 3.9). Taken together, these data indicate that the P2 subpopulation enriches for stem cell-related genes, particularly *Lgr5*.

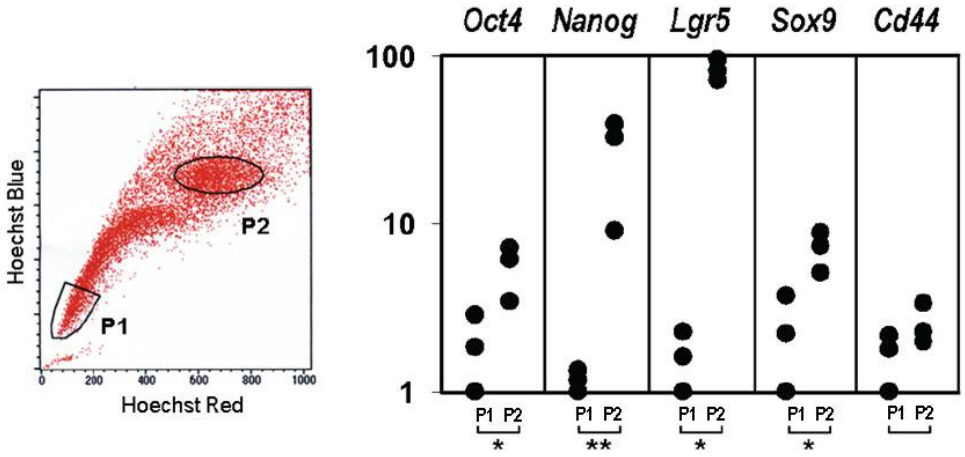

Figure 3.9. Gene expression profiling of P1 and P2 subpopulations. Left panel: Cells were sorted into P1 and P2 gates based on Hoechst 33342 staining for qRT-PCR. In this experiment, a small gate for P1 was applied to capture the highest dye effluxing-P1 cells. Right panel: Expression levels of embryonic and gastrointestinal stem cell makers are presented relative to those of control sorted cells that included the total population in the FACS plot. Three separate experiments were carried out and each dot on the plot represents a single experiment. Student's *t*-tests were performed on P1 and P2 values for various genes and the corresponding *p*-values are shown (single and double asterisks denote *p*-value <0.05 and *p*-value <0.01, respectively).

3.2.6 P2 cells display greater sphere-forming capacity than P1 cells

To assess the functional significance of elevated expression of stem cell-associated transcripts in the P2 subpopulation, *in vitro* sphere assay was performed to evaluate stem cell-like activity. Isolated P1, P2, control sorted and unsorted cells from the GIF-14 line were cultured in suspension in serum-free medium supplemented with growth factors. As sphere-forming assay measures stem cell-like activity at the single cell level, it is critical to seed cells at clonogenic density and keep them apart to yield accurate quantification of sphere-initiation. To reduce aggregation of cells, varying amount of methylcellulose was added in the sphere medium in different experiments. Under this culturing condition, P2 cells consistently displayed 5-fold greater sphere-forming capacities than P1 cells, revealing that they possessed increased stem/progenitor properties (Figure 3.10A). P2-derived spheres could be maintained for an extended period without obvious signs of differentiation. Moreover, in a preliminary experiment, these spheres could be serially passaged to generate secondary spheres readily, which is indicative of self-renewal activity (Figure 3.10B). In comparison, P1 cells were both less efficient in forming long-lived primary spheres and generating secondary spheres (Figures 3.10A and B).

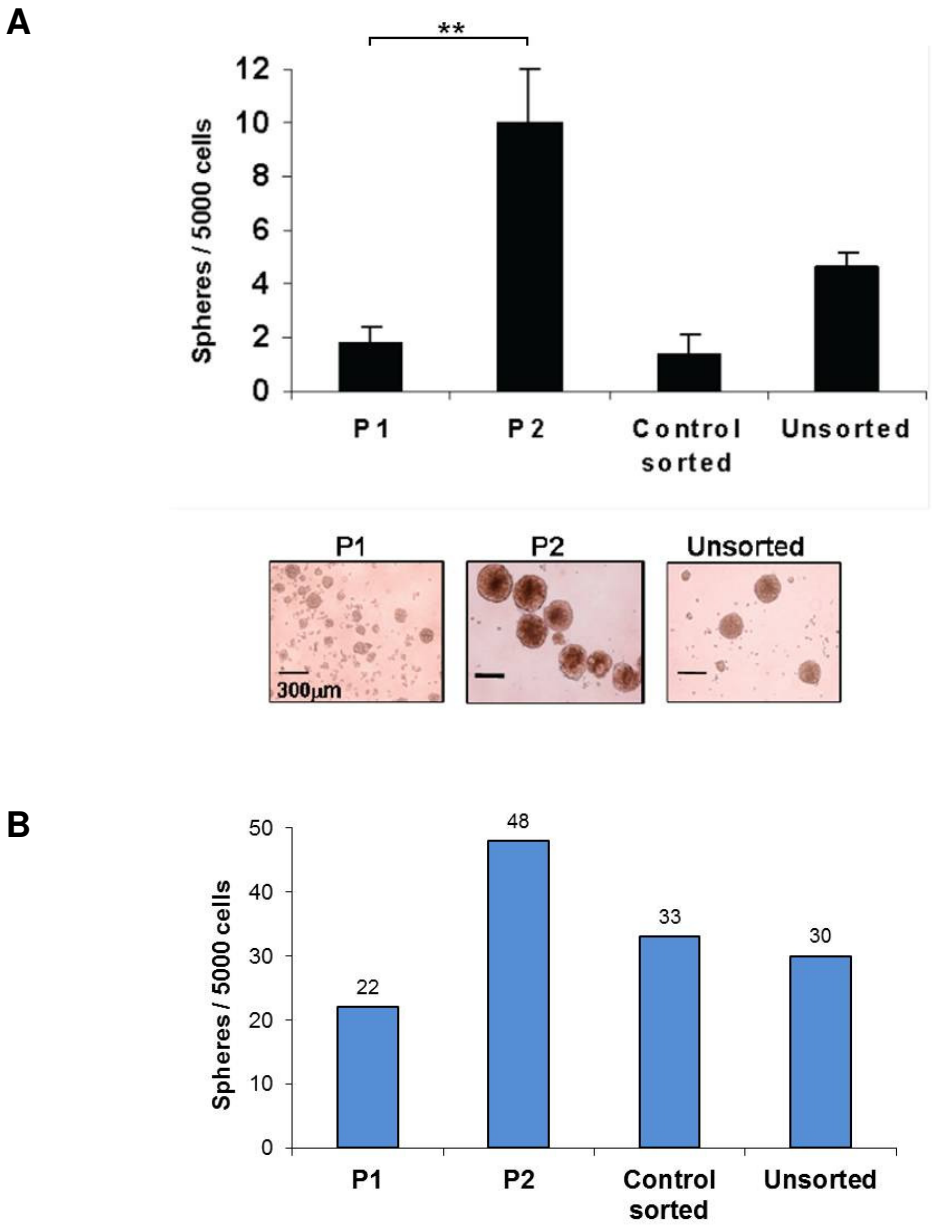

Figure 3.10. Relative sphere-initiating efficiency of P1 and P2 subpopulations. (A) FACS-isolated P1 and P2 cells were compared to control sorted (all cells on the FACS plot) and unsorted cells for sphere-forming potential. Cells were cultured in serum-free medium supplemented with various growth factors as stated in Section 2.9 and 0.1% of methylcellose was added to the culture media to reduce the formation of cell aggregates. The graph represents the number of spheres ≥300µm in size generated from 5000 cells after 30 days of culture (means ± SEM, n=5). Double asterisks denotes *p*-value <0.01. Phase contrast images of spheres are shown. Scale bars, 300µm. (B) Primary spheres were dissociated and replated to generate secondary spheres following the procedures described in Section 2.9. The graph represents the number of secondary spheres formed from each cell population after 20 days of culture in a preliminary experiment.

3.2.7 Wnt3a activates *Lgr5* expression and promotes sphere formation

It was reported that the gastrointestinal stem cell marker, *Lgr5* is a target of the canonical Wnt pathway in the intestinal epithelium (Barker *et al.*, 2007). More recently, *Lgr5* has been shown to amplify Wnt signaling through its association with R-spondin proteins (de Lau *et al.*, 2011). As the P2 subpopulation in GIF-14 cell line was found to enrich for *Lgr5*, activation of *Lgr5* by the Wnt pathway was hence tested in this cell model. To stimulate the canonical Wnt signaling, FACS-isolated P1, P2 and unsorted parental GIF-14 cells were either treated with Control- or Wnt3a-conditioned medium (Cm) for 15h prior to qRT-PCR analysis. The results revealed that *Lgr5* mRNA levels were greatly activated by Wnt3a-Cm in GIF-14 cells (Figure 3.11).

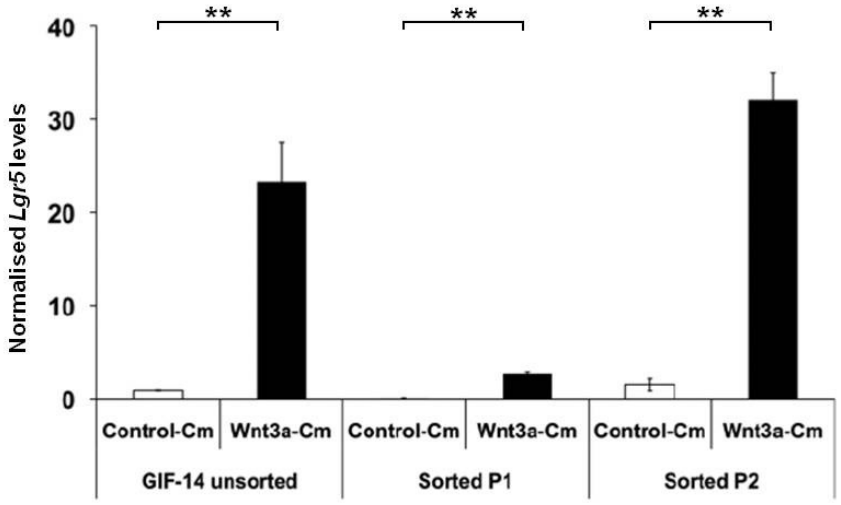

Figure 3.11. Changes in *Lgr5* mRNA expression upon Wnt3a stimulation. FACS-isolated P1, P2 and GIF-14 unsorted cells were treated with Control- or Wnt3a-Cm in 1:3 ratio to the culture medium for 15h and *Lgr5* mRNA levels were ascertained, normalised against those of *Gapdh*. Data are presented relative to Control-Cm treated GIF-14 unsorted cells. Double asterisks denotes *p*-value <0.01.

To ascertain whether Wnt3a promotes sphere formation as reflected in its induction of *Lgr5*, sphere-forming assay was carried out to examine the efficiency of sphere formation in GIF-14 cells in the presence of Wnt3a-Cm. To optimise the conditions for sphere formation using conditioned media, Control- and Wnt3a-Cm was diluted with sphere medium at various ratios of 1:20, 1:10 and 1:3. Treatment with Wnt3a-Cm led to a 2-fold increase in sphere-initiation across all dilution factors compared to Control-Cm (Figure 3.12A). As conditioned medium contained low levels of serum, which promoted the formation of cell aggregates, the amount of conditioned medium was kept minimal while maintaining good Wnt3a-reponsiveness. Thus, a dilution factor of 1:10 was chosen for the subsequent experiment. Under this condition, Wnt3-Cm treatment consistently resulted in increased sphere formation by 2-fold relative to Control-Cm (Figure 3.12B).

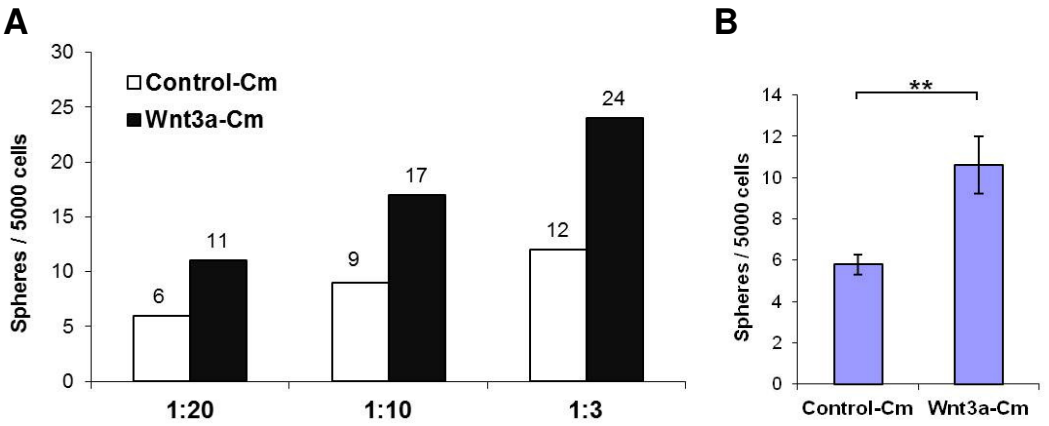

Figure 3.12. The effects of Wnt3a-Cm treatment on sphere formation. (A) Sphere-forming assay was set up at various dilutions 1: 20, 1:10 and 1:3 of Control- and Wnt3a-Cm with sphere medium using GIF-14 parental cells. Spheres ≥75µm in size were counted after 9 days of culturing and 0.5% of methylcellulose was used to keep the cells apart as low amount of serum in the conditioned media caused cell aggregation. (B) The above experiment was repeated with 1:10 Control- and Wnt3a-Cm dilution and spheres ≥100µm in size were scored after 11 days. The number of spheres are presented in means ± SEM, n=5. Double asterisks denotes *p*-value <0.01.

3.3 Discussion

To understand the basis of the tumorigenic nature of immortalised murine *Runx3*$^{-/-}$.*p53*$^{-/-}$ gastric epithelial cell lines, we set out a thorough characterisation of a *Runx3*$^{-/-}$.*p53*$^{-/-}$ line, GIF-14, with the aim of identifying and studying the tumorigenic population. Through a combination of Hoechst 33342 and cell surface marker staining, we identified a low dye-effluxing P2 subpopulation within GIF-14 that was marked by EpCAM^{low}CD133^{-} antigen profile. P2 cells were found to display significantly greater tumor-initiating activity when transplanted in nude mice.

In our study, the Hoechst 33342 staining technique was a valuable tool for isolating the subpopulations in the GIF-14 cell line. Although fractionation by FACS based on Hoechst 33342 profile is typically laborious and slow, it ensures that the enriched P1 and P2 subpopulations are of high purity. This is critical for comparing the relative tumorigenicity of these subpopulations in functional assays. It should be noted that the dye uptake kinetics are highly dynamic and the Hoechst 33342 profile of a mixed population is a function of arbitrary settings on the flow cytometer (Ibrahim *et al.*, 2007; Wu and Alman, 2008). Although the P1 subpopulation shares the common attributes of low Hoechst 33342 fluorescence and verapamil sensitivity, it is not considered analogous to a true SP. Despite being present in many cancer cell lines, the physiological relevance of the SP during *in vitro* culture remains a topic of contention. It is known that the function of normal stem cells is highly dependent on contextual signals from the surrounding niche, which also seems true for TICs (Clarke et al., 2006). The high dye efflux may improve the survival of TICs in adverse microenvironment and confer drug resistance. However, the immortalised GIF-14 cell line maintained in *in vitro* culturing conditions may possess different Hoechst 33342

efflux properties compared to cells residing in their tissue niche. Indeed, the low dye effluxing-subpopulation, P2 correlates with tumorigenicity in GIF-14 cells.

In view of these drawbacks in Hoechst 33342 staining, expression of cell surface markers in the subpopulations of GIF-14 would provide useful information about their differentiation states. The tumorigenic P2 fraction was depleted for CD133, EpCAM and CD49f cell surface markers, suggesting a link between loss of epithelial phenotype and tumorigenicty (Table 3.2). This relationship is also demonstrated in the marked reduction in the expression of Claudin-1, which is a critical component of the epithelial tight junction in tumorigenic *Runx3*$^{-/-}$.*p53*$^{-/-}$ GIF cell lines compared to *Runx3*$^{+/+}$.*p53*$^{-/-}$ cells (Chang *et al.*, 2010). In addition, *Runx3*$^{-/-}$.*p53*$^{-/-}$ GIF cell lines were prone to trans-differentiation into intestinal-like cells, indicating that they do not retain strong epithelial cell identity (Fukamachi *et al.*, 2004; Fukamachi *et al.*, 2008).

Allograft transplantation assays in nude mice revealed that the P2 subpopulation was significantly more tumorigenic than the P1 counterpart (Figures 3.5 and 3.7). It has been reported that complete tissue disruption during the retrieval of TICs from their living niche would select for cells that are more independent of their niche or better equipped for survival in mice (Vermeulen *et al.*, 2008). Thus, the increased tumorigenicity observed in the P2 subpopulation may be attributed to their greater adaptability and resistance to apoptosis in the graft niche. As P2 cells are unable to efflux Hoechst 33342, they retained high levels of the dye which can be cytotoxic. The fact that the P2 subpopulation would still initiate tumours more readily strongly suggests that P2 cells have a survival advantage over P1 cells. Alternatively, the tissue microenvironments into which the cells were transplanted might have

preferentially supported the growth of P2 cells by providing the necessary growth factors and nutrients.

In addition to the significant differences between P1 and P2, variations in the ability to form tumours by the P1 subpopulation from two independent transplantations were observed (Figures 3.5 and 3.7). These could be explained by the differences in the immune system and tumour immunity of the nude mice used in the two experiments. Differences in the age of mice and number of cells transplanted in these experiments could trigger varied immune responses. nude mice are deficient in T and B cells, but they contain natural killer cells that constitute a major part of innate immunity against foreign cells or tumour growth (Flanagan, 1966). Despite the murine origin of transplanted cell populations, immune response against these cells could still be mounted. Therefore, to eliminate the contribution of immune cells, more immune-comprised NOG (NOD/Shi-*scid*/*IL-2Rγ*^{null}) mice which lack T, B, natural killer and antigen presenting cells could be used to improve engraftment of foreign cells (Ito *et al.*, 2002).

The relationship between tumour-initiation activity and stem/progenitor phenotype has been established in many contexts. In the GIF-14 cell line, the P2 tumorigenic subpopulation was highly enriched for stem cell-related markers, especially the gastrointestinal stem cell marker *Lgr5* as revealed by gene expression profiling. Functionally, these *Lgr5*-expressing cells form long-lived spheres that could be serially passaged in serum-free cultures more readily than other cells within GIF-14. Thus, the P2 subpopulation displayed stem/progenitor features. Our results support the notion that TICs display stem/progenitor characteristics, suggesting that signaling pathways regulating self-renewal may be conserved among TICs. Although

these pathways are tightly controlled in normal stem cells, they may be constitutively activated or mis-regulated in TICs, leading to tumorigenesis (Beachy *et al.*, 2004). For instance, the canonical Wnt pathway is well known to regulate the self-renewal of crypt stem/progenitor cells in intestinal epithelium (Korinek *et al*, 1998). Aberrant activation of Wnt signaling is heavily involved in the carcinogenesis of gastrointestinal neoplasia (Clevers, 2006). In GIF-14 cells, treatment with Wnt3a-Cm which mimicked constitutive stimulation of Wnt signaling resulted in increased stem/progenitor activity, as reflected from the robust induction of *Lgr5* and greater sphere-formation (Figures 3.11 and 3.12).

The correlation between *Lgr5,* a target of the Wnt pathway with stem/progenitor characteristics and tumorigenicity has implications in the etiology of gastric cancer. During cancer development, abnormal activation of growth factor signaling such as the canonical Wnt pathway through genetic or/and epigenetic alterations may activate *Lgr5* and impart stem/progenitor properties. These *Lgr5*-expressing cells may become targets for oncogenic insults, leading to the generation of TICs that drives tumour growth. This hypothesis is supported by the recent report that *Lgr5*-positive stem cells are the cells-of-origin of intestinal adenomas in mouse model (Barker *et al.*, 2009). Therefore, it is probable that *Lgr5*-expressing P2 subpopulation within the precancerous *Runx3*$^{-/-}$*.p53*$^{-/-}$ GIF-14 cell line represents precursors of these TICs in full-blown cancer. It has been reported that *Lgr5* expression is exclusively restricted to the crypt base columnar stem cells in the intestines and is quickly silenced in their transit-amplifying daughter cells (Van der Flier *et al.*, 2009). Given its tight regulation *in vivo*, it is remarkable that a subpopulation of an immortalised cell line is enriched for *Lgr5*. The cause for the

appearance of the tumorigenic, less epithelial-like and *Lgr5*-positive P2 subpopulation will be explored in the next chapter.

CHAPTER 4:

Spontaneous EMT gives rise to the tumorigenic and stem cell-like subpopulation in the GIF-14 line

4.1 Introduction

4.1.1 Properties of epithelial cells and mesenchymal cells

The epithelium is an important tissue with unique properties and it lines most of the internal organs, covering the internal and external surfaces of the body. The epithelia are composed of epithelial cells that are tightly bound together in sheets and form barriers which protect the body from the external environment (Kolega, 1985). The epithelial cells are joined together by specialised membrane structures such as adherens junctions, tight junctions, gap junctions and desmosomes, organised as a lateral belt. These cells possess apical-basal polarity as reflected in the presence of distinct membrane proteins and outer-leaflet on the apical versus basolateral plasma membrane domains. The epithelial cells are typically polygonal in shape and their movements are restricted within the epithelial layer (Fristrom, 1988). In our study, the GIF cell lines are established from epithelial cells of the mouse stomach, which consist of simple columnar epithelial cells that are elongated and columnar.

Distinct from epithelial cells, mesenchymal cells are found most abundantly in the connective tissue and are vastly different in their properties. Unlike epithelial cells, mesenchymal cells do not form organised sheets, and consequently lack the apical-basal polarity as their epithelial counterparts, which are arrayed according to proper cell-cell junctions and actin cytoskeleton arrangement. Owing to these properties and their weaker cell-cell adhesion, mesenchymal cells possess migratory capabilities, often making transient contacts with their neighbours (Schock and Perrimon, 2002). In culture, mesenchymal cells adopt a spindle-shaped morphology and are highly motile, whereas polygonal-shaped epithelial cells grow as clusters of cells that maintain complete cell-cell adhesion with each other (Thiery and Sleeman, 2006).

4.1.2 Epithelial-Mesenchymal Transition

The epithelial-mesenchymal transition (EMT) refers to a complex cellular and molecular programme through which epithelial cells temporarily lose their characteristics, such as cell-cell adhesion and apical-basal polarity, and take on the properties of mesenchymal cells such as cell motility. This process has long been recognised as a fundamental event in morphogenesis and organogenesis during embryonic development in vertebrates and invertebrates (Hay, 1968). The epithelial cells that are converted to mesenchymal cells migrate to distant sites where they undergo a reverse process, termed mesenchymal-epithelial transition (MET) to give rise to internal organs (Nieto, 2011). Several rounds of EMTs and METs are necessary for the formation of body plan and differentiation of multiple tissues and organs (Baum *et al.*, 2008). EMT first occurs during gastrulation in which epiblast cells break away from the basement membrane to delaminate from the primitive streak to form the mesoderm germ layer (Shook and Keller, 2003). At later stage of embryogenesis, neural crest cells arising from the dorsal part of the neural tube undergo EMT and migrate to contribute to the formation of various tissues, including neurons, bones, smooth muscles and melanocytes (Lee *et al.*, 2006). Subsequently, secondary and tertiary cycles of EMTs and METs are also responsible for the development of other structures, particularly the somites, heart, secondary palate, reproductive tracts and placenta (Thiery *et al.*, 2009). Consistent with the importance of EMT in embryogenesis, mutations in genes driving EMT are often associated with congenital defects such as mesodermal malformation and neural crest emigration failure (Nieto *et al.*, 1994; Carver *et al.*, 2001).

The hallmarks of EMT are defined by the loss of cell-cell junctions, disruption of apical-basal polarity, changes in cell shape and the acquisition of cell motility (Thiery and Chopin 1999). These typically involve the dissolution of epithelial junctional structures consisting of adherens junction, tight junctions and desmosomes. Loss of E-cadherin, a major component of the adherens junction with concurrent upregulation of non-epithelial cadherins such N-cadherin has been regarded as a critical event of EMT (Llorens *et al.*, 1998). Concurrently, constituents of the core polarity complexes such as Par, Crumbs and Scribble are often downregulated or reorganised (Moreno-Bueno *et al.*, 2008). Concomitant with the loss of epithelial cell identity, epithelial cells gain mesenchymal features such as spindle-like morphology, increased cell motility and invasion (Thiery, 2002). These often involve concerted and dramatic changes in the cytoskeleton organisation and extracellular matrix (ECM) composition to allow cells to change shape and migrate. Typically, reorganisation of the actin cytoskeleton and increased production of cytoskeletal and ECM proteins such as vimentin and fibronectin occur which leads to the stimulation of the integrin signaling to facilitate cell migration and invasion (Xu *et al.*, 2009).

As EMT and MET are highly controlled and spatial-temporally regulated processes during embryonic development, they do not occur under usual circumstances. However, reactivation of the EMT trans-differentiation programme in adulthood has been implicated in the conversion of early stage tumours to invasive malignancies (Thiery, 2002). Increasing findings reveal that the acquisition of an EMT phenotype is critically linked to epithelial cancer progression and metastasis which allows tumour cells to disseminate from primary tumours to distant loci through intravasation into the blood circulation (Irie *et al.*, 2005; Chaffer *et al.*, 2006;

Aigner *et al.*, 2007; Moustakas and Heldin, 2007). Subsequently, these metastatic tumour cells with mesenchymal phenotype are believed to undergo MET to form macroscopic metastases at secondary sites that resemble the primary tumours (Kong *et al.*, 2011). Therefore, it appears that the regulatory programme that governs embryonic EMT is exploited by tumour cells to adopt metastatic traits during tumour progression (Thiery *et al.*, 2009).

4.1.3 Regulatory factors controlling EMT

EMT is regulated by a complex network of transcriptional regulators under the control of mitogenic signals. During EMT, various extracellular cues including soluble growth factors and components of the ECM activate a genetic program that leads to pronounced cellular changes in epithelial cells (Boyer *et al.*, 2000). Multiple growth factors and morphogens, such as transforming growth factor-β (TGF-β), Wnt, fibroblast growth factor (FGF), hepatocyte growth factor (HGF), epidermal growth factor (EGF), Notch and sonic hedgehog proteins are capable of inducing an EMT (Thiery and Sleeman *et al.*, 2006). The gene regulatory networks governing EMT during embryonic development have been well established in sea urchin and *Drosophila*, whereas those operating in the vertebrates are far from complete (Thiery, 2009). The key transcription factors involved in the regulatory loops include Snail, Twist, Zeb, Foxc, Goosecoid, Sox, Eomesodermin, Mesps and others, of which the Snail, Twist and Zeb families are best characterised in the mammalian system (Polyak and Weinberg, 2009; Thiery, 2009). Recently, a non-histone chromatin binding factor, the high mobility group a2 (Hmga2), has been proposed to be a potential master regulator of EMT, whereby ectopic expression of HMGA2 activated the transcription of *Snai1, Snai2* and *Twist* (Thuault *et al.*, 2006). The induction of these transcription

factors in response to extracellular signals leads to the activation or repression of several sets of genes that influence cell morphology and behaviour. These molecular targets consist of epithelial/polarity genes such as *E-cadherin, β-catenin, zonula occludins* (*ZO*), *claudins, desmoplakin* and *Crumbs3*, as well as mesenchyaml genes including *fibronectin, vimentin, N-cadherin* and *matrix metalloproteases* (*MMPs*) (Batlle *et al.*, 2000; Ikenouchi *et al.*, 2003; Yang *et al.*, 2004; Vandewalle *et al.*, 2005; Bindels *et al.*, 2006; Shirakihara *et al.*, 2007; Whiteman *et al.*, 2008).

4.1.4 TGF-β and Wnt signaling pathways are important regulators of EMT

The TGF-β pathway is an important regulator of cellular processes such as cell proliferation, apoptosis and differentiation in the gastrointestinal tract (Derynck *et al.*, 1997). It is regarded as a tumour suppressor pathway in this context as inactivation of the components of the TGF-β signaling cascade is prevalent in gastrointestinal cancers (Park *et al.*, 1994; Markowitz *et al.*, 1995; Howe *et al.*, 1998). The TGF-β signaling cascade has been well-delineated in which TGF-β signals through a heterodimeric complex of type I and type II trans-membrane receptors. Upon ligand binding to type II receptors, Smad2 and Smad3 are activated via phosphorylation by type I receptor kinases and form heterotrimeric complexes with Smad4. These complexes translocate into the nucleus and regulate the transcription of a variety of genes in collaboration with specific transcription factors and coactivators or corepressors (Massague *et al.*, 2006).

Members of the TGF-β family of cytokines are regarded as major inducers of EMT during embryogenesis. This is clearly demonstrated in the multiple developmental defects in the heart and palatal fusion in *TGF-β*-null embryos due to a

lack of EMT (Pelton *et al.*, 1990; Dickson *et al.*, 1995; Sanford *et al.*, 1997). Due to its diverse functions in various tissues, the role of TGF-β in carcinogenesis is distinctively pleiotropic. Although TGF-β acts as tumour suppressor through the induction of growth arrest and apoptosis at the early stage of cancer, surprisingly it also acts as a major driver of metastasis during cancer progression by inducing EMT (Heldin *et al.*, 2009; Massague, 2008). For instance, constitutive activation of TGF-β1 in transgenic mice led to the development of invasive spindle cell carcinomas from benign skin tumours (Cui *et al.*, 1996). Furthermore, cancer cells often produce autocrine TGF-β to activate EMT, which enhances survival and invasion of migratory cancer cells (Derynck *et al.*, 2001).

The canonical Wnt signaling pathway plays a central role in the development and regeneration of gastrointestinal tract, and its dysregulation is one of the best-characterised causes of gastrointestinal neoplasia (Clevers, 2006). The association between Wnt and EMT has been established during embryogenesis in which Wnt is a necessary component to drive EMT in neural crest formation and somitogenesis (Garcia-Castro and Bronner-Fraser, 1997; Galceran *et al.*, 2004). Wnt proteins regulate EMT through the control of β-catenin-mediated transcriptional activity. β-catenin plays dual roles in EMT: it enhances cell-cell adhesion when associated with the E-cadherin complex in adherens junctions (Ozawa *et al.*, 1989), it also functions as a transcription coactivator upon entry into the nucleus when Wnt pathway is activated (Behrens *et al.*, 1998). Consistent with the key roles that EMT and an activated Wnt pathway play in cancer progression, the translocation of β-catenin from cell membrane to nucleus is often observed at the invasive front of the primary carcinomas in metastatic human cancers (Brabletz *et al.*, 2001).

4.1.5 EMT promotes the formation of "cancer stem cells"

Apart from its better studied involvement in advanced cancer, recent evidence suggests that EMT may have a role in tumour initiation by promoting the genesis of "cancer stem cells". Two independent groups have demonstrated that mammary epithelial cells undergoing EMT gained stem cell-like characteristics (Mani *et al.*, 2008; Morel *et al.*, 2008). Immortalised human mammary epithelial cells that were induced to undergo EMT upon the overexpression of Snai1 or Twist or TGF-β1 treatment were capable of forming mammospheres *in vitro*, indicating that they display properties of stem cells (Mani *et al.*, 2008). In a separate study, the constitutive activation of EMT in Ras-transformed mammary epithelial cells led to a significant increase in the number of cancer stem cells, marked by $CD44^{high}CD24^{low}$ antigen profile (Morel *et al.*, 2008). These data indicate that the aberrant activation of an EMT induces a genetic reprogramming in epithelial cells which enables them to become phenotypically plastic. As a result, epithelial cells acquire stem cell characteristics, mesenchymal features, resistance to apoptosis and eventually become tumorigenic (Polyak and Weinberg, 2009).

4.1.6 Experimental approach

In the *Runx3*$^{-/-}$ GIF-14 cell line, the P2 subpopulation was found to be depleted for epithelial-specific surface antigens CD133, EpCAM and CD49f, suggesting that P2 cells display reduced epithelial phenotype. As the P2 subpopulation was shown to be tumorigenic, the relationship between a loss of epithelial characteristics and the tumorigenicity in the GIF-14 cell line will be investigated in the context of EMT. To achieve this, the following experimental approaches are taken: (1) measuring the gene expression of specific markers by quantitative RT-PCR, and their sub-cellular distribution by immuno-fluorescent staining; and (2) live monitoring of cell behaviour by time-lapse imaging. In the former approach, gene expression profiling of epithelial markers *E-cadherin* and *EpCAM*, EMT-inducing transcription factors *Snai1, Snai2* and *Twist* and mesenchymal markers *N-cadherin*, *Vimentin*, *Fibronectin* will be performed in GIF-14 subpopulations. Secondly, immuno-fluroscent staining coupled with confocal microscopy will be employed to study the distribution of epithelial- and mesenchymal-related proteins. This technique is widely practiced as high resolution three-dimensional images displaying spatial localisation of proteins using specific fluorescent dyes can be generated (Wright *et al.*, 1993). To track the behaviour of cells in terms of their cell morphology and migration real-time, live cell imaging techniques such as time-lapse imaging will be performed. Time-lapse imaging is particular useful for sequence-capturing of dynamic cellular events over a long period of time (Jang *et al.*, 2011). Finally, the effects of various EMT-inducing growth factors, in particular TGF-β and Wnt, on gene expression and cell biology of GIF-14 cells will be investigated using the above experimental approaches.

4.2 Results

4.2.1 The P2 subpopulation displays mesenchymal-like characteristics

P1 and P2 subpopulations displayed distinct cell morphology when cultured on plastic culture dish and glass cover slips. Figure 4.1 shows the morphologies of FACS-purified P1 and P2 cells grown on plastic culture dish at sub-confluent densities. P1 cells resembled typical epithelial cells with polygonal shapes. In contrast, P2 cells displayed features similar to mesenchymal cells, such as elongated and spindle-like morphologies (Figure 4.1). Although both subpopulations were seeded at the same cell density, the P1 subpopulation formed cell clusters more readily than the P2 subpopulation, suggesting that the P1 cells have relatively stronger cell-cell adhesion (Figure 4.1).

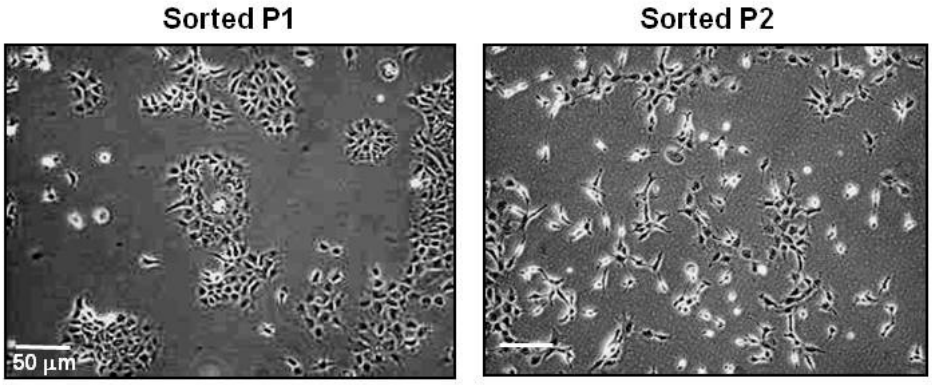

Figure 4.1. P1 and P2 cells in the GIF-14 cell line showed distinct differences in cell morphology. P1 and P2 cells were fractionated by FACS and they were expanded *in vitro*. Images of these cells at sub-confluent densities were captured by phase contrast microscopy. Scale bars, 50µm.

To confirm the above observations, time-lapse imaging was carried out to monitor the growth of P1 and P2 colonies. Freshly FACS-fractionated P1 and P2 cells were seeded at clonogenic densities on glass cover slips for the formation of single cell-derived colonies. The glass cover slips were transferred into a Sykes Moore chamber and mounted on a Nikon Ti Eclipse microscope through which images were captured at 3 min intervals. The progressive, time-lapse images of a representative colony from each subpopulation at indicated times of imaging are presented in Figure 4.2. P1 colonies took on a compact appearance and grew slowly in a cohesive manner, where neighboring cells were in constant contact with each other, thus displaying characteristics of epithelial cells (Figure 4.2). This observation was conserved in all P1 colonies monitored over the course of 18h. In striking contrast, cells within P2 colonies were disorganised in their arrangement and expanded rapidly with constant delamination and outward migration. These properties were particularly pronounced at the boundaries of P2 colonies (Figure 4.2). The dynamics and high motility of the P2 cells revealed by time-lapse imaging suggest that the P2 cells may possess weaker cell-cell adhesive force compared to P1 cells.

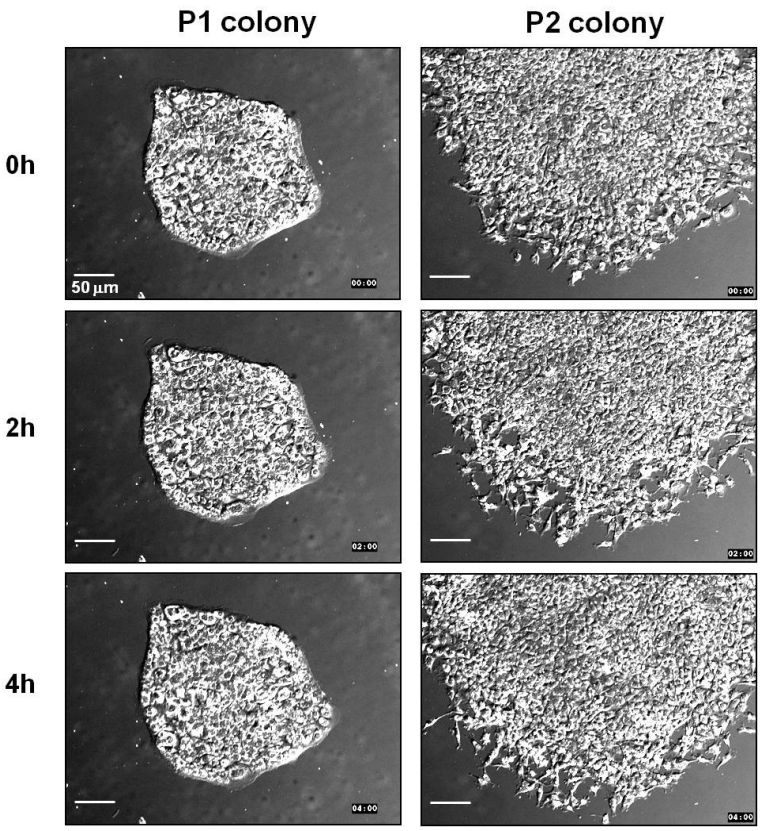

Figure 4.2. P1 and P2 colonies displayed markedly different morphology and migration. Time-lapse imaging of single-cell derived P1 and P2 colonies was performed in which images were captured by differential interference contrast (DIC) microscopy at 3min intervals over a period of 18h. Images of representative colonies at the indicated time points are presented. Scale bars, 50µm.

To further assess the mesenchymal nature of the P2 subpopulation, gene expression profiling experiments were performed in which the expression of well-established EMT- and mesenchymal-associated markers in P1 and P2 subpopulations were measured by quantitative RT-PCR. The gating strategy employed for the fractionation of P1 and P2 subpopulations by FACS is similar to that in Figure 3.9 in which P1 cells with the greatest dye efflux was captured by setting a small and selective gate. In total, three independent fractionations of GIF-14 cells were performed and the expression levels of each marker gene were calculated as ratios to those of the control samples (Figure 4.3). In all the experiments, mesenchymal markers such as *Fibronectin* (*Fn1*) were significantly elevated in the P2 subpopulation (Figure 4.3). Furthermore, the P2 subpopulation expressed markedly higher levels of key EMT-inducing transcription factors, *Snai1*, *Snai2* and *Twist* compared to the P1 subpopulation (Figure 4.3). Lastly, P2 cells had reduced expression of the epithelial cell marker, *EpCAM*, and this is in agreement with the lower EpCAM protein levels in these cells as determined by surface antigen staining and flow cytometry in Table 3.2. Taken together, our data indicate that the P2 subpopulation has reduced epithelial characteristics and concurrently displays morphological and molecular properties of mesenchymal cells.

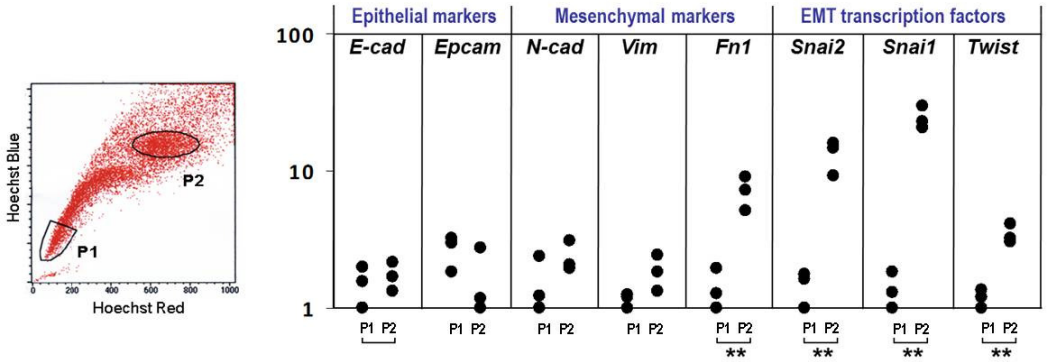

Figure 4.3. Expression levels of epithelial-, EMT- and mesenchymal-related markers in P1 and P2 cells. Left panel: Cells were fractionated based on Hoechst 33342 staining into P1 and P2 populations for qRT-PCR. A small gate was set to collect P1 cells with the greatest dye efflux potential. Right panel: Expression levels of epithelial-, EMT-, and mesenchymal-associated genes relative to those of control sorted cells (total population in the FACS plot). Data presented are a compilation of three independent experiments and each dot on the plot represents the read-out of a single experiment. Student's *t*-tests were performed on P1 and P2 values. Double asterisks denotes *p*-value <0.01.

4.2.2 TGF-β1 induces EMT- and mesenchymal-related genes in GIF-14 cells

To induce EMT experimentally in the GIF-14 cell line, parental GIF-14 cells were treated with human recombinant TGF-β1 ligand for 24h and 48h. Changes in EMT- and mesenchymal-related markers that were enriched in the P2 subpopulation were determined by qRT-PCR. These treatments resulted in robust induction of EMT/mesenchymal-associated genes (Figure 4.4). Induction was most prominently observed in *Snai1* at 24h post-treatment. In contrast, *N-cad, Fn1* and *Snai2* were strongly induced at 48h post-treatment (Figure 4.4). These observations suggest that the activation of *Snai1* by TGF-β1 is probably a primary event that leads to the secondary induction of its target genes, such as *N-cad* and *Fn1*. Collectively, the above results suggest that an EMT has been induced by TGF-β1 in GIF-14 cells. Unexpectedly, treatment of TGF-β1 also caused 5-fold induction of *Lgr5* transcript in GIF-14 cells at 48h post-treatment (Figure 4.4). As *Lgr5* is a specific gastrointestinal stem cell marker, this finding is consistent with the notion that EMT promotes the acquisition of stem cell-like properties in epithelial cells.

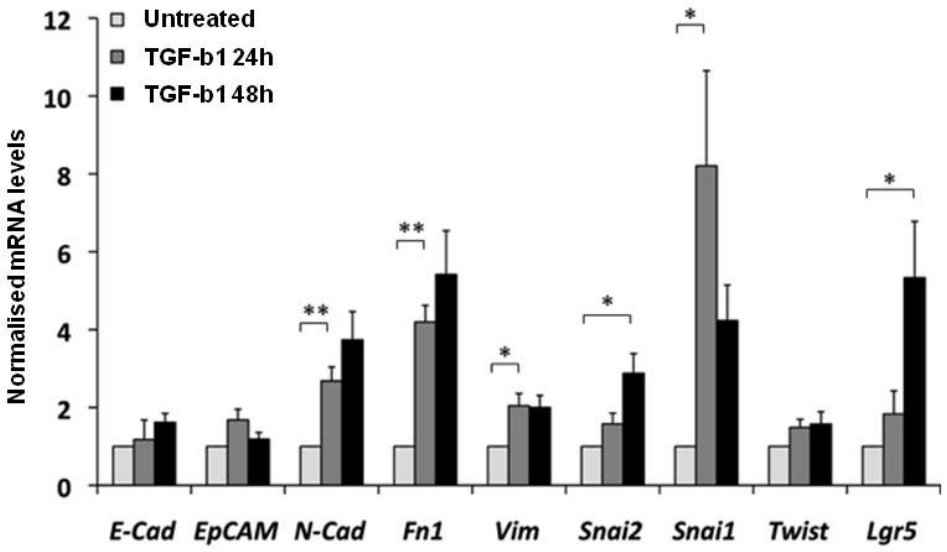

Figure 4.4. Changes in the expression of EMT- and mesenchymal-related genes in response to TGF-β1 treatment. Parental GIF-14 cells were treated with 2.5ng/ml of TGF-β1 for 24 or 48h and changes in the expression of epithelial-, EMT- and mesenchymal-related genes were determined by qRT-PCR. The values of each gene were normalised against those of *Gapdh* and expressed relative to the untreated controls. The data from three independent experiments were compiled (means ± SEM, n=3). Single and double asterisks represent *p*-value < 0.05 and *p*-value <0.01, respectively.

4.2.3 TGF-β1 and Wnt3a promotes the expansion of the P2 subpopulation

The strong resemblance between the P2 subpopulation and GIF-14 cells that have undergone TGF-β1-induced EMT suggests that P2 cells are the product of EMT. To demonstrate this, Hoechst 33342 staining was performed on GIF-14 cells treated with TGF-β1 at various time points across a 10-day period. To account for changes due to culture conditions, untreated cells were traced for the same period of time. Compared to the untreated cells, three days of TGF-β1 treatment resulted in an expansion of the P2 subpopulation from 4.8% to 10.1%. This was concomitant with shrinkage of the P1 subpopulation from 51.0% to 22.3% (Figure 4.5A). This trend was persistent and further enhanced over 10 days of TGF-β1 treatment period (Figure 4.5A). In this analysis, a small P1 gate was marked to highlight a receding of the "tip" of P1, which indicated a loss of dye efflux over time. It is worth noting that the same conclusion could be drawn when a larger gate was used.

As P1 and P2 cells could further be distinguished by their differential EpCAM and CD133 expression, changes in these markers were also measured by flow cytometry, and presented as a percentage of the total cell population. Consistent with the enlargement of P2 subpopulation, the fraction of the P2-associated $EpCAM^{low}CD133^{-}$ cells increased from 51% to 84% after 10 days of TGF-β1 treatment (Figure 4.5B). This was accompanied by a decrease in the percentage of the P1-associated $EpCAM^{high}CD133^{+}$ cells from 49% to 16% (Figure 4.5B). Together, these data provide strong evidence that TGF-β1 treatment promotes an expansion of the P2 subpopulation, and reduces P1 subpopulation in GIF-14 cells.

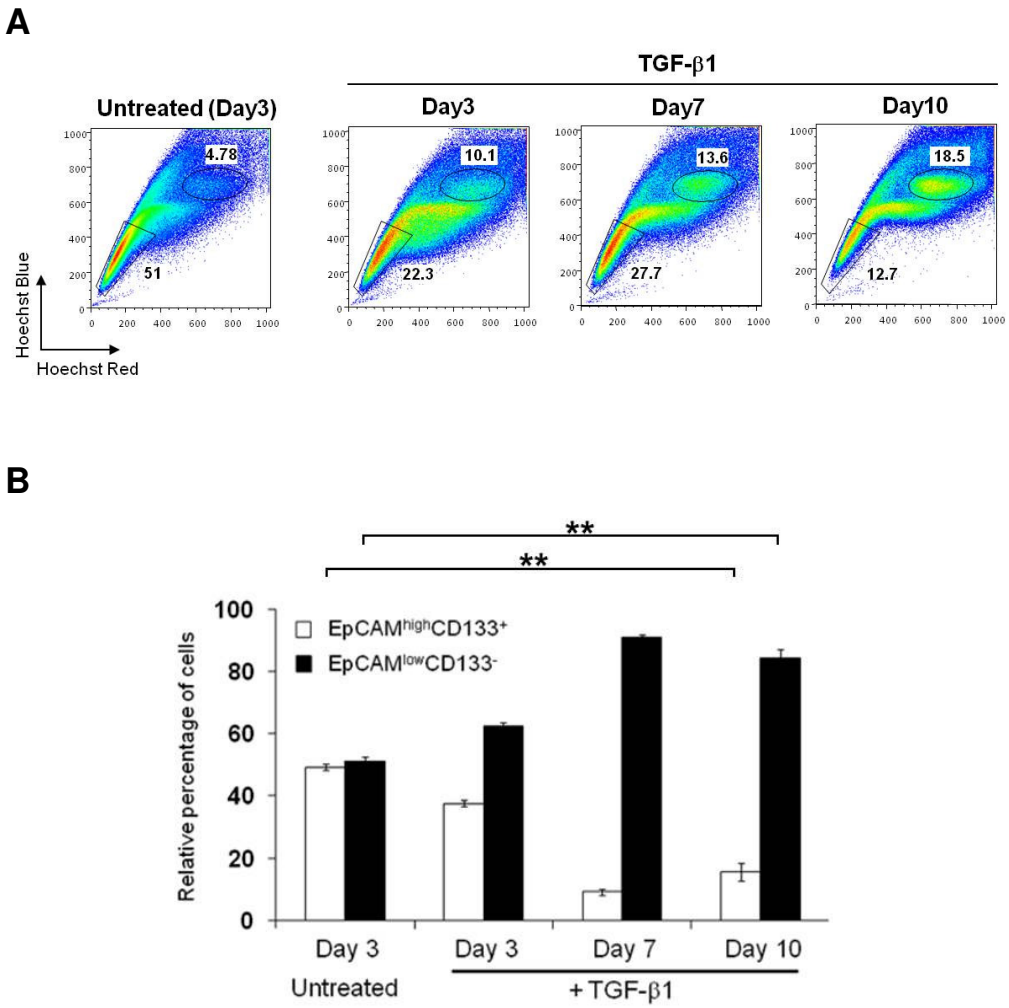

Figure 4.5. The effects of TGF-β1 treatment on Hoechst 33342 and cell surface marker staining profiles. GIF-14 cells were treated with 2.5ng/ml of TGF-β1 for a period of 10 days. Co-staining of Hoechst 33342 together with CD133 and EpCAM was performed at indicated time points and the cells were analysed on the flow cytometer. Changes in Hoechst 33342 staining profile were presented on the FACS plots (A) while the percentages of $EpCAM^{high}CD133^{+}$ and $EpCAM^{low}CD133^{-}$ cells relative to their combined values were shown in (B). Student's *t*-test was performed for day10 after TGF-β1 treatment and double asterisks denotes *p*-value <0.01.

The above observations prompted us to test the effects of Wnt3a, which is another well known inducer of EMT. To activate the canonical Wnt signaling, parental GIF-14 cells were treated with Wnt3a-conditioned medium (Wnt3a-Cm) or control-Cm over a period of 10 days. To determine the effects of Wnt, changes in $EpCAM^{high}CD133^{+}$ and $EpCAM^{low}CD133^{-}$ fractions were ascertained by flow cytometry over the course of the treatment. Relative to control-Cm, Wnt3a-Cm resulted in increased $EpCAM^{low}CD133^{-}$ cells from 43.1% to 56.3% after 3 days of treatment. Concomitantly, slight decrease in $EpCAM^{high}CD133^{+}$ cells was observed in Wnt3a-Cm treated cells (Figure 4.6). This effect was gradually enhanced with prolonged Wnt3a-Cm treatment (Figure 4.6). However, it was noted that control-Cm caused a milder but similar effect to that of Wnt3a-Cm, indicating that conditioned media may contain certain growth factors which would induce EMT (Figure 4.6).

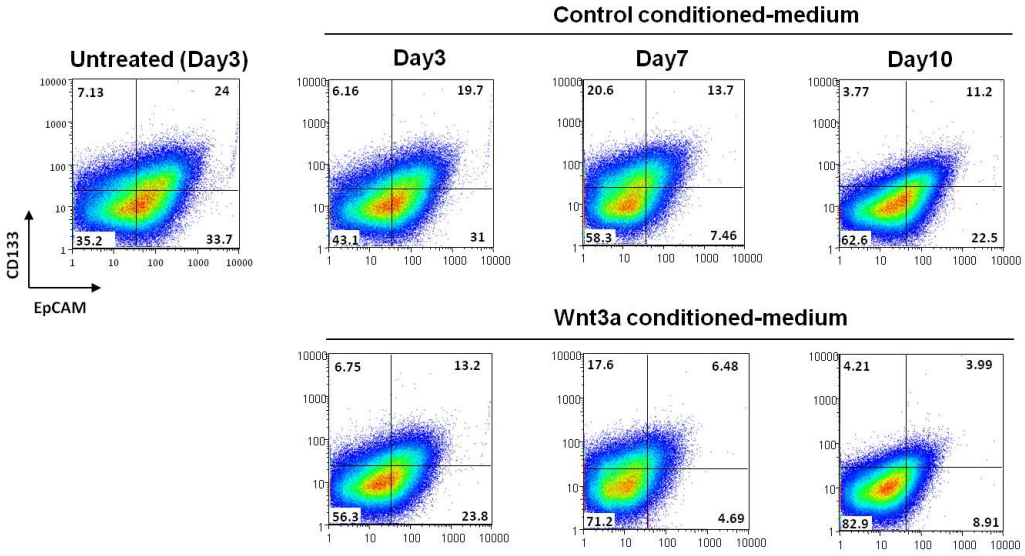

Figure 4.6. The effects of Wnt3a-Cm treatment on CD133/EpCAM marker profile. GIF-14 cells were subjected to CD133 and EpCAM staining at the indicated time points, following a period of 10 days of treatment with Control or Wnt3a-Cm (1:3 dilution with culture medium). Changes in CD133/EpCAM surface antigen profile were analysed by flow cytometry.

4.2.4 TGF-β1 causes a direct transition of P1 to P2 phenotype

The preliminary observation that TGF-β1 treatment leads to an expansion of the P2 subpopulation with simultaneous decrease in P1 subpopulation could be either due to: 1) TGF-β1 induces a direct transition of P1 to P2 phenotype or 2) a negative selection against P1 cells by TGF-β1. To exclude the latter possibility, time-lapse microscopy was employed to study changes in single-cell derived P1 colonies following TGF-β1 treatment. Two independent imaging experiments were conducted in which P1 colonies were cultured on plastic plates and glass cover slips for phase contrast (Figure 4.7A) and differential interference contrast (DIC) imaging (Figure 4.7B), respectively. The colonies were allowed to adapt to the environment in the culture chamber prior to TGF-β1 treatment for 67h. Images of representative colonies at indicated time points are shown in Figures 4.7A and 4.7B. Untreated colonies were imaged simultaneous in a separate well or chamber to account for the effects of culturing conditions on the behaviour of cells.

In these experiments, TGF-β1 treatment of P1 colonies did not trigger apoptosis; rather it resulted in a marked gain in mesenchymal-like phenotype (Figure 4.7A). As the treatment progressed, TGF-β1-treated cells took on a stretched and spindle-like morphology. Moreover, cells became increasingly detached and motile at the periphery of the colonies (Figure 4.7A). These changes were in striking contrast to the untreated control colonies which displayed epithelial properties. This phenomenon was clearly observed in two separate imaging experiment using different microscopy and culture substrata, namely plastic/phase-contrast and glass slip/DIC imaging (Figure 4.7B). Importantly, the resultant phenotype of P1 colonies following TGF-β1 treatment closely resembled that of P2-derived colonies (Figure 4.7 & 4.2). Therefore,

these data provide strong evidence that the expansion of P2 subpopulation in GIF-14 cells upon TGF-β1 treatment described in Section 4.2.3 is due to a direct transition of P1 cells to cells bearing P2 phenotypes.

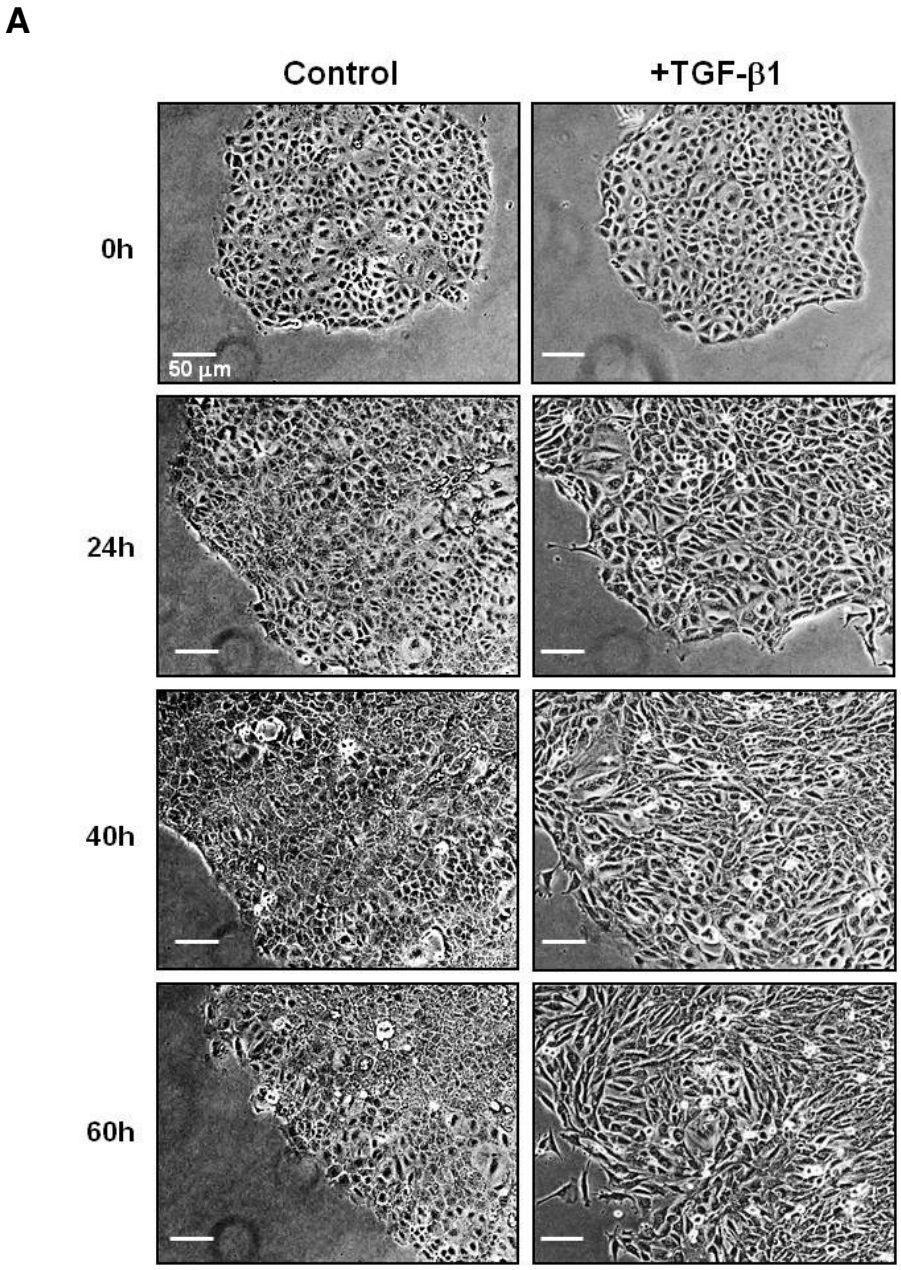

Figure 4.7A. Morphological changes in P1 colonies induced by TGF-β1. Time-lapse microscopy of single-cell derived P1 colonies treated with 2.5ng/ml of TGF-β1 was set up according the descriptions in Section 2.10. Phase contrast images of control and TGF-β1 treated P1 colonies cultured on low evaporation 6-well plastic plates were taken concurrently for 67h at 5min intervals. Images of the representative colonies at various treatment time points are shown. Scale bars, 50μm.

B

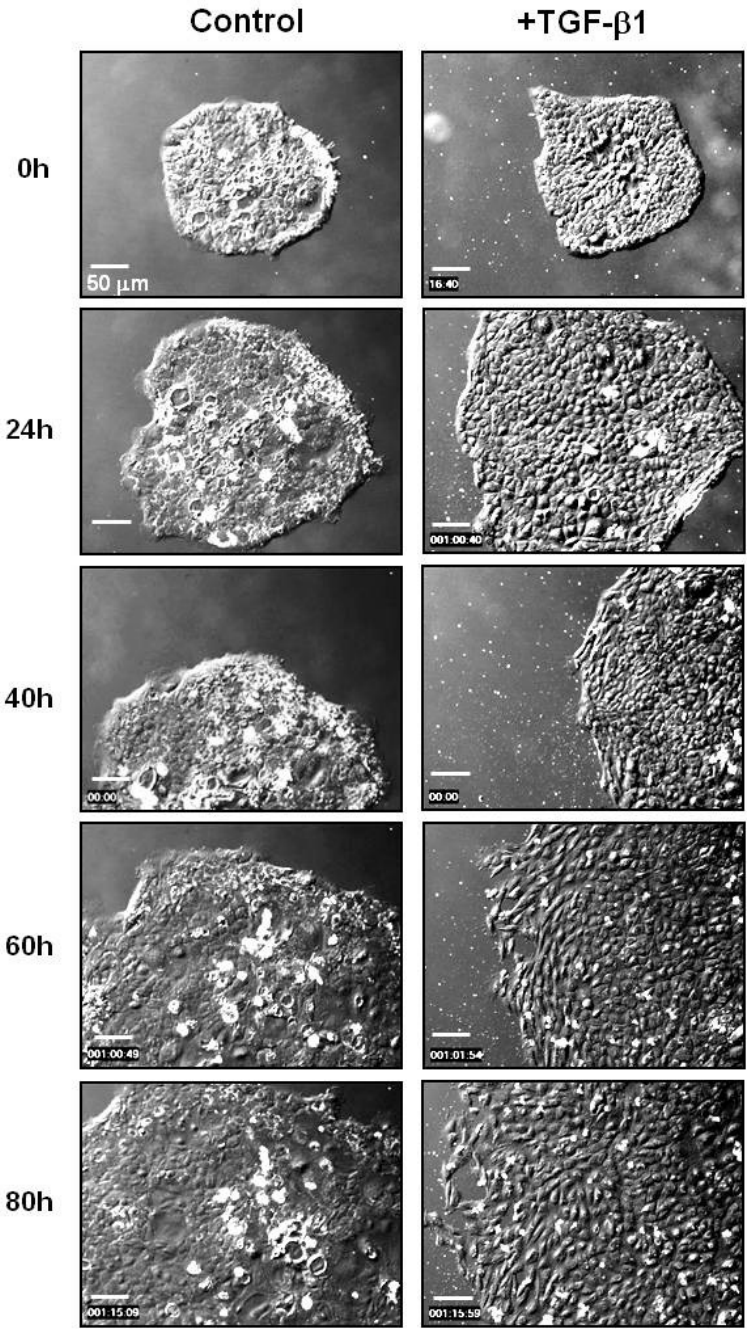

Figure 4.7B. Morphological changes in P1 colonies induced by TGF-β1. Time-lapse microscopy of single-cell derived P1 colonies treated with 1.25ng/ml of TGF-β1 was set up as described in Section 2.10. DIC images of control and TGF-β1 treated colonies grown on glass cover slips were captured in separate Sykes Moore chambers for 84h at 5min intervals. Images of the representative colonies at the indicated treatment time points are shown. Scale bars, 50μm.

4.2.5 TGF-β1 causes major sub-cellular changes in GIF-14 cells

The sub-cellular changes in cells undergoing EMT have been extensively studied. To provide conclusive evidence that TGF-β induces EMT in GIF-14 P1 colonies, immuno-fluorescent staining of cell-cell adhesion proteins and mesenchymal markers were performed. In this study, single-cell derived untreated or TGF-β1 treated P1 as well as P2 colonies were stained for desmoplakin, F-actin and β-catenin. High and low magnifications of confocal images of representative colonies were captured (Figure 4.8A and 4.8B). Desmoplakin is an essential component of the desmosomes that is a major feature of epithelial cells, as described in Section 4.1.3. In untreated P1 colonies, desmoplakin staining was prominent at intercellular boundaries where it appeared as punctate foci consistent with the presence of desmosomes. After 48h of TGF-β1 treatment, a pronounced redistribution of desmoplakin from the plasma membrane to the cytoplasm and nuclei was observed, indicating a disassembly of the desmosomes (Figures 4.8A and 4.8B).

F-actin filaments are important constituents of the cytoskeleton structures required for the maintenance of cell-cell junctions and cell shape. In untreated P1 colonies, F-actin was largely localised in close proximity to the cell membrane. TGF-β1 treatment of P1 cells resulted in a striking reorganisation of F-actin filaments in the form of stress fibres (Figures 4.8A and 4.8B). This is consistent with the observed increase in cell motility as shown in Figure 4.7. As stress fibres are part of the focal adhesion complex formed when cells make stable connections to the substratum, they enable cells to extend their leading edge to attach to the substratum for movement (Doherty and McMahon, 2008).

The immuno-fluorescent staining of β-catenin revealed its predominant localisation at intercellular junctions in untreated P1 colonies. TGF-β1 treatment caused a loss of membranous β-catenin staining in P1 cells, indicating a disruption of the adherent junctions (Figures 4.8A and 4.8B). In addition, increased nuclear β-catenin staining was observed in cells at the periphery of the colonies, suggesting an activated Wnt signaling (Figures 4.8A and 4.8B). Therefore, TGF-β1 treatment induced a change of cell-cell adhesion structures and increased cell motility in P1 colonies. More importantly, the resultant phenotype induced in P1 colonies by TGF-β1 resembled closely to those of P2-derived colonies (Figure 4.8A and 4.8B). This coincides with the adoption of P2-like cell morphology and motility by P1 colonies upon TGF-β1 treatment shown in Figure 4.7. Interestingly, a gradient of decreasing epithelial with concurrent increasing mesenchymal features from the centre towards the edge of single-cell derived P2 colonies was observed, reflecting an inherent state of plasticity in P2 cells (Figure 4.8B).

A

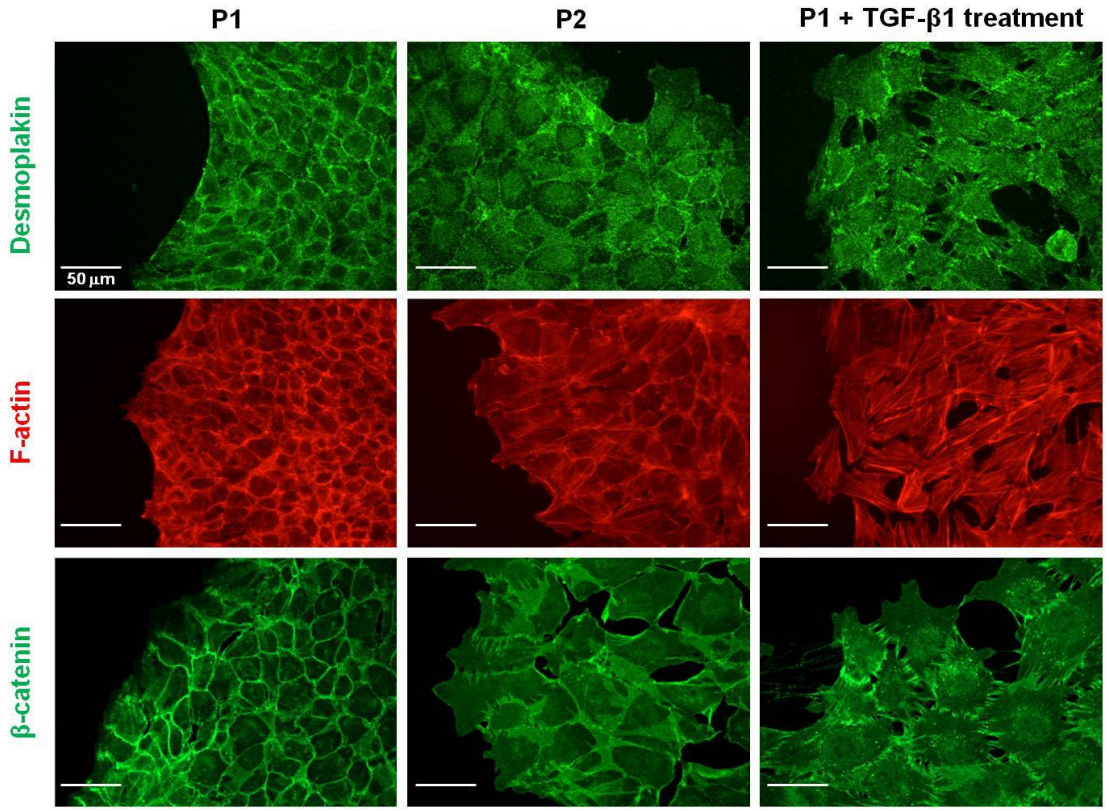

Figure 4.8A. Sub-cellular localisation of desmoplakin, F-actin and β-catenin in P1, P2 and TGF-β1 treated P1 colonies. Immuno-fluorescent staining of desmoplakin (top panel), F-actin (middle panel) and β-catenin (bottom panel) in P1, P2 and TGF-β1 (48h) treated P1 colonies was performed as described in Section 2.11. Confocal images of the periphery regions of representative colonies at high magnification views were taken. Scale bars, 50µm.

B

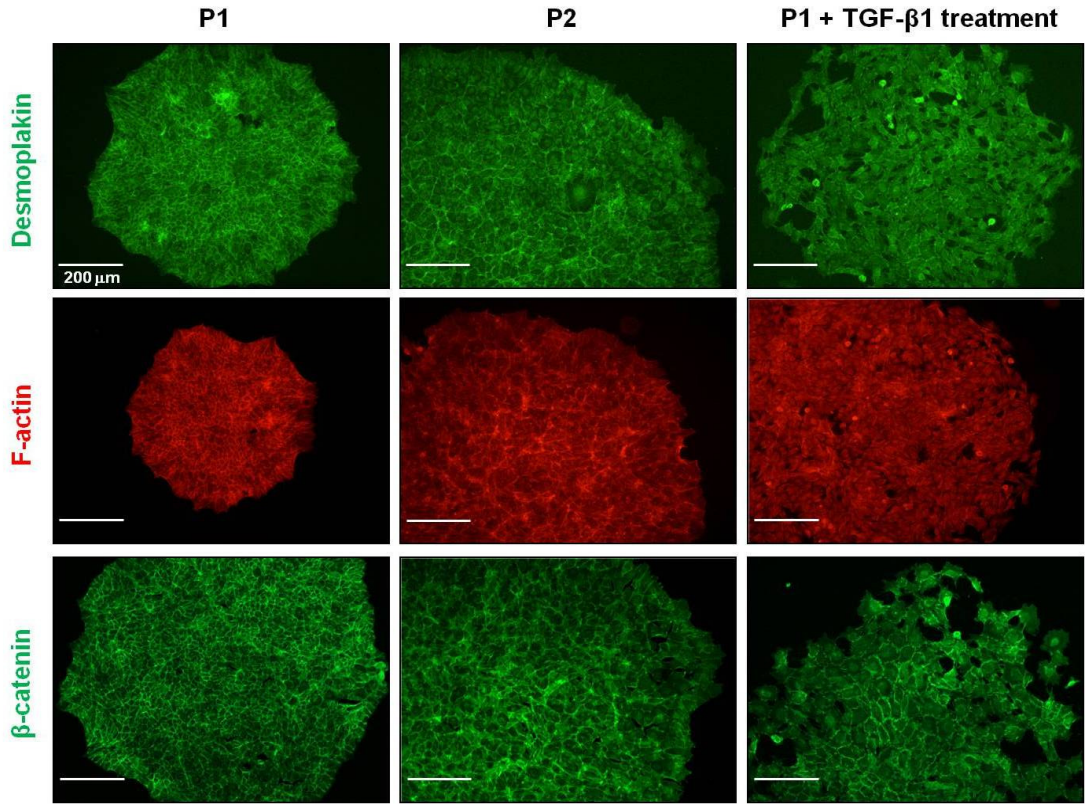

Figure 4.8B. Sub-cellular localisation of desmoplakin, F-actin and β-catenin in P1, P2 and TGF-β1 treated P1 colonies. Immuno-fluorescent staining of desmoplakin (top panel), F-actin (middle panel) and β-catenin (bottom panel) in P1, P2 and TGF-β1 (48h) treated P1 colonies was performed as described in Section 2.11. Confocal images of representative colonies were captured at low magnification views. Scale bars, 200µm.

4.2.6 Autocrine TGF-β drives spontaneous EMT in the GIF-14 line

The occurrence of a mesenchymal-like P2 subpopulation under normal culturing of GIF-14 cells suggests that these cells are undergoing spontaneous EMT. Therefore, the possibility that an autocrine and constitutively active TGF-β pathway which promotes and maintains the P2 subpopulation in steady state was investigated. In this study, a specific and potent TGF-β inhibitor, SB431542, abrogates TGF-β signaling by inhibiting the phosphorylation of Smad2 by type I TGF-β receptors (Inman *et al.*, 2002) was used. Parental GIF-14 cells were pre-treated with TGF-β inhibitor for 15h prior to the addition of TGF-β1 ligand for another 48h. TGF-β activity was assessed by immuno-fluorescent staining of total and phosphorylated Smad2/3, the nuclear effectors of TGF-β signaling. Untreated GIF-14 cells showed cytoplasmic and nuclear staining of total Smad2/3, indicating that the TGF-β pathway is partially and constitutively active in GIF-14 cells (Figure 4.9). Treatment with TGF-β1 triggered nuclear translocation of cytoplasmic Smad2/3, yielding exclusive nuclear total Smad2/3 staining (Figure 4.9). Pre-treatment with SB431542 blocked the nuclear accumulation of total Smad2/3 in both untreated and TGF-β1 treated cells, demonstrating the inhibition of autocrine and exogenous TGF-β signaling (Figure 4.9). However, despite the clear redistribution of total Smad2/3, persistent localisation of phosphorylated Smad2/3 in the nucleus was observed though the canonical TGF-β pathway was inhibited (Figure 4.9).

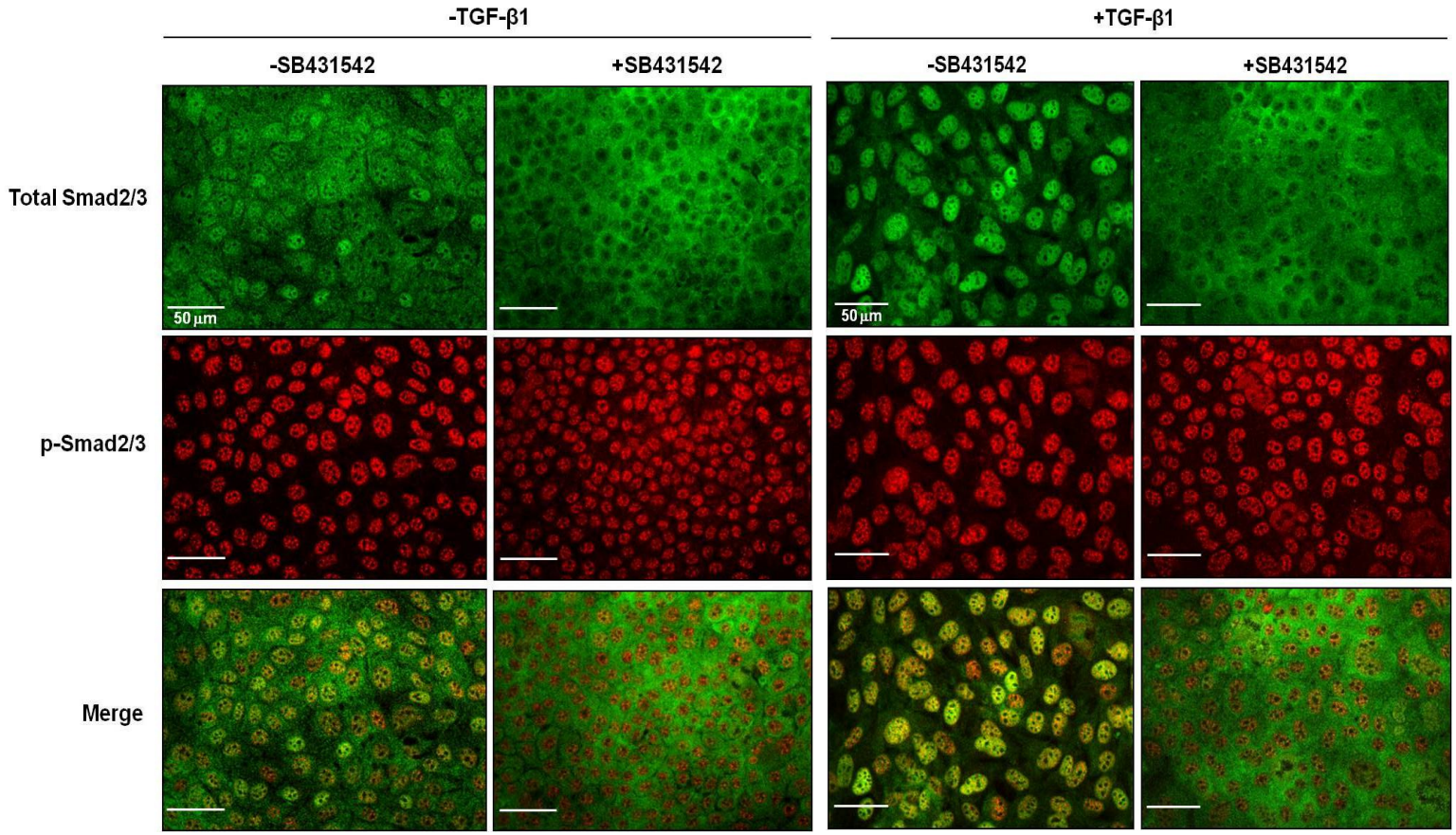

Figure 4.9. Sub-cellular localisation of Smad2/3 in GIF-14 cells upon TGF-β inhibitor (SB431542) treatment. Immuno-fluorescent staining of total Smad2/3 (top panel), phosphorylated Smad2/3 (middle panel) and merged (bottom panel) was performed on cells pre-treated with 10µM of SB431542 for 15h preceding 48h of TGF-β1 treatment at 2.5ng/ml. Representative confocal images are shown. Scale bars, 50µm.

Phase contrast images were captured to evaluate the changes in cell morphology in response to SB431542. GIF-14 cells were pre-treated with SB431542 for 15h before treatment with TGF-β1 for 24h. As described in Sections 4.2.4 and 4.2.5, TGF-β1 treatment resulted in distinct morphological changes in GIF-14 cells and endowing them with mesenchymal features (Figures 4.7 and 4.8). Concordant with the nuclear exclusion of total Smad2/Smad3, treatment with SB431542 effectively blocked the TGF-β1-induced morphological changes in GIF-14 (Figure 4.10). Moreover, uninduced GIF-14 cells treated with SB431542 appeared epithelial-like phenotype with greater compactness compared to resting GIF-14 cells (Figure 4.10). These data suggest that a constitutively active TGF-β pathway promotes mesenchymal-like morphology in some GIF-14 cells and its blockade by SB431542 would reverse these changes and promote epithelial cell phenotype.

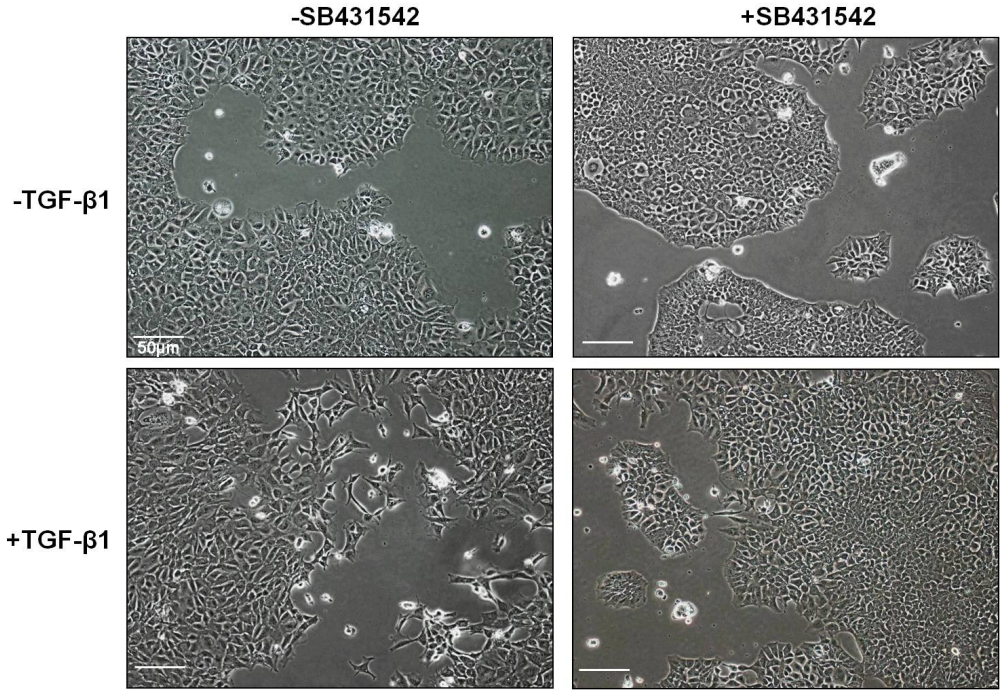

Figure 4.10. Changes in the cell morphology of GIF-14 cells upon TGF-β inhibitor (SB431542) treatment. GIF-14 cells were pre-treated with 10μM of SB431542 for 15h prior to the addition of 2.5ng/ml of TGF-β1 for another 24h. Phase contrast pictures of these cells are shown. Scale bars, 50μm.

To assess the effect of SB431542 on gene expression, qRT-PCR analyses were performed. Concordant with the observations described in Section 4.2.2, TGF-β1 treatment resulted in elevated expression of *Snai1, Snai2, Twist, Vim, Fn1* and *Hmga2* (Figure 4.11). Treatment with TGF-β inhibitor drastically reduced the basal and TGF-β1-induced expression of these genes to a level below those of untreated controls (Figure 4.11).

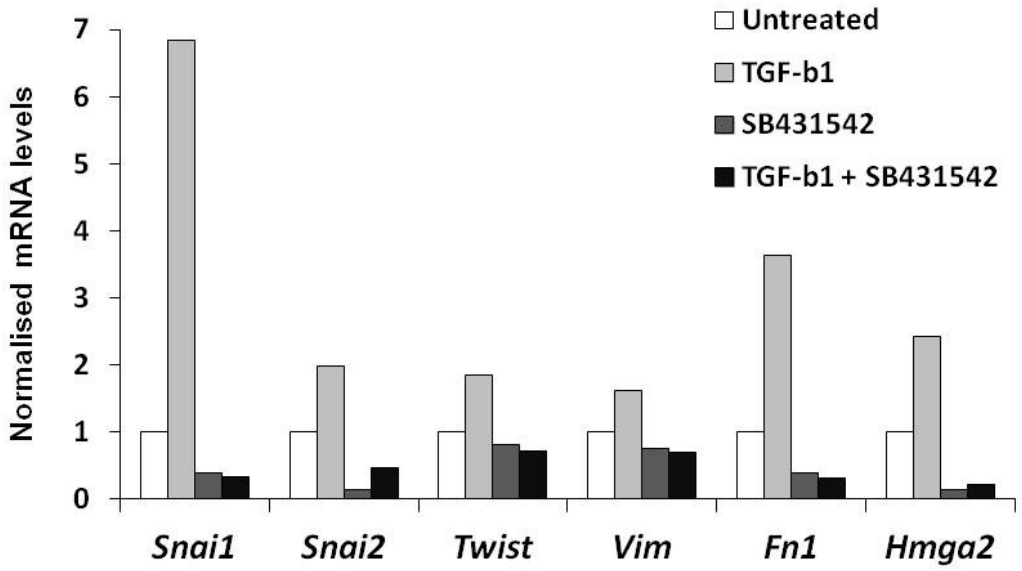

Figure 4.11. Changes in EMT- and mesenchymal-associated genes in GIF-14 cells upon TGF-β inhibitor (SB431542) treatment. GIF-14 cells were pre-treated with 10μM of TGF-β inhibitor for 15h prior to 24h of 2.5ng/ml TGF-β1 induction. EMT- and mesenchymal-related transcripts were ascertained by qRT-PCR. Expression levels were normalised against those of *Gapdh* and expressed relative to untreated control for each gene.

Finally, to demonstrate whether TGF-β inhibitor promotes the P1 subpopulation, Hoechst 33342 staining was performed on GIF-14 cells treated with TGF-β inhibitor for an extended period. Treatment with TGF-β inhibitor for 3 days resulted in an increase in P1 subpopulation from 22.7% to 53.8%. This was accompanied by a 40% reduction in the P2 subpopulation from 9.91% to 6.48% (Figure 4.12). These effects sustained for 7 days of TGF-β inhibitor treatment (Figure 4.12). Therefore, these data suggest that TGF-β inhibitor drives cells towards the P1 phenotype.

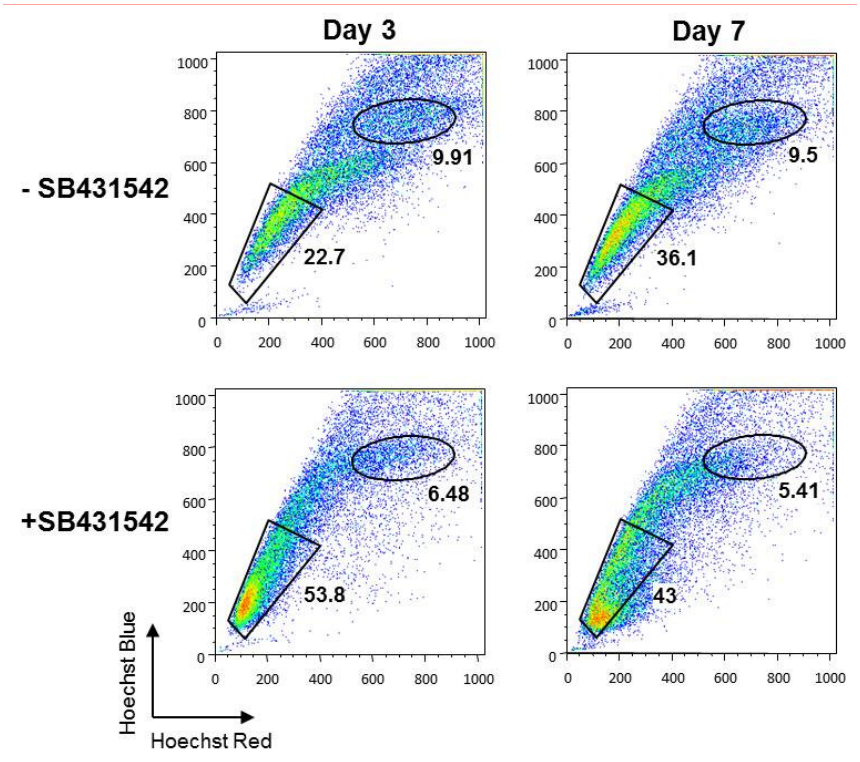

Figure 4.12. The effects of prolonged TGF-β inhibitor (SB431542) treatment on Hoechst 33342 staining profiles in GIF-14 cells. Parental GIF-14 cells were treated with 10μM of TGF-β inhibitor, SB431542 and Hoechst 33342 staining was performed on three and seven days post-treatment and analysed by flow cytometry.

4.2.7 EGF and HGF cooperate with TGF-β1 to induce EMT-related genes

In addition to TGF-β, EMT is also shown to be regulated by other growth factors pathways, such as epidermal growth factor (EGF), fibroblast growth factor (FGF), and hepatocyte growth factor (HGF) pathways. Therefore, their ability to activate EMT in GIF-14 cells was investigated. In addition, the potential cooperation between TGF-β and these growth factors was also studied. Parental GIF-14 cells were treated with EGFs, FGFs, HGF and TGF-β1 alone or together with TGF-β1 for 24h and gene expression profiling of EMT- and mesenchymal-related genes was performed. The results showed that robust activation of *Snai1*, *Fn1* and *Hmga2* was observed when cells were singly treated with TGF-β1, but not EGFs, FGFs and HGF (Figure 4.13). Co-treatment of EGFs or HGF together with TGF-β1 resulted in greater activation of *Snai1* and *Hmga2* transcripts (Figure 4.13). These data show that TGF-β is the primary factor that induces the EMT signature, though some degree of cooperation between TGF-β and EGF or HGF was observed.

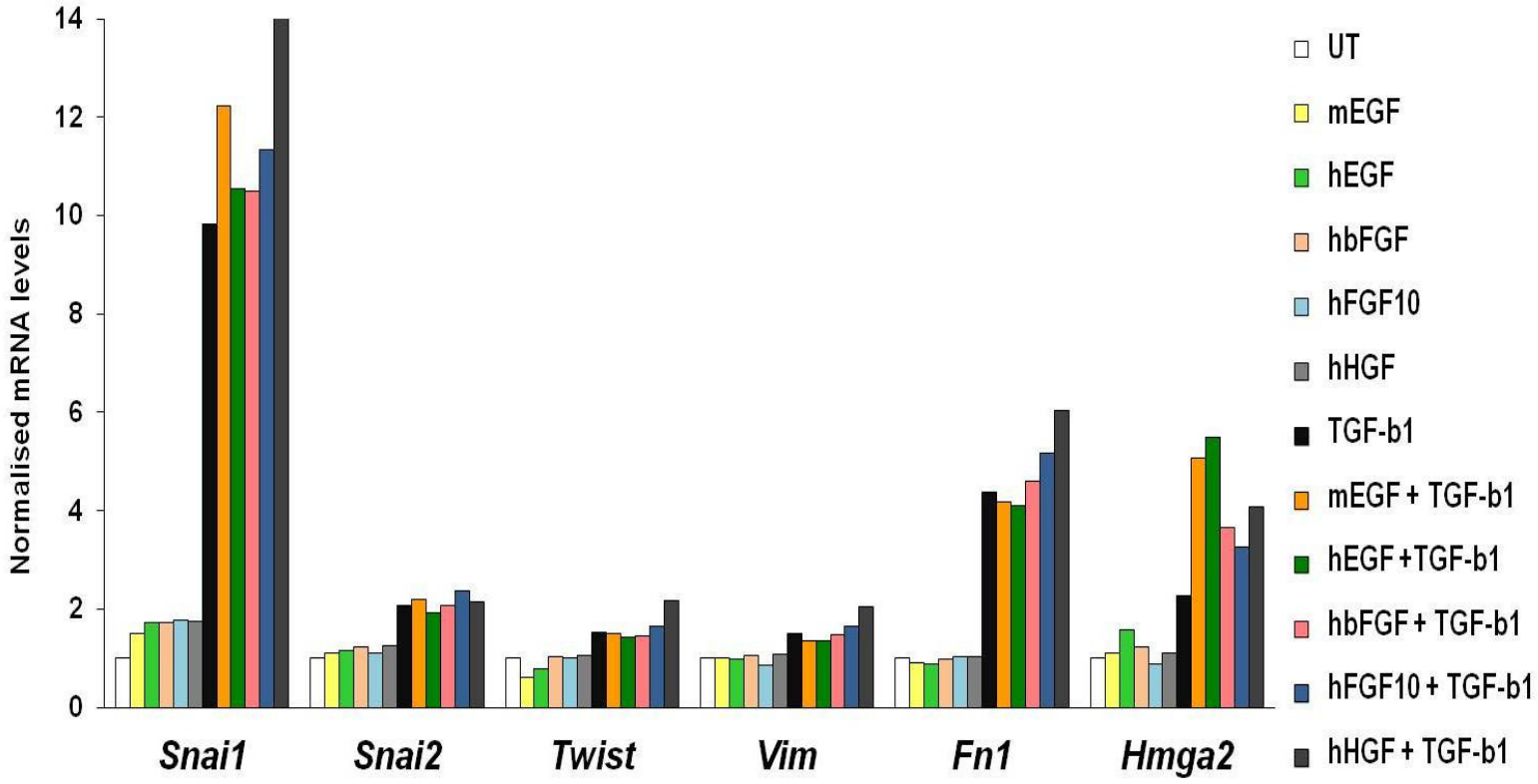

Figure 4.13. The effects of various growth factors on the expression of EMT- and mesenchymal-related genes. GIF-14 cells were singly treated with EGFs, FGFs, HGF and co-treated with TGF-β1 for 24h prior to the measurement of EMT- and mesenchymal-associated genes via qRT-PCR. (mEGF: murine EGF; hEGF: human EGF; hbFGF: human basic FGF; hFGF10: human FGF10).

4.3 Discussion

In the previous chapter, the P2 subpopulation in the GIF-14 cell line was found to have reduced epithelial characteristics. Thus, the possibility of GIF-14 cells undergoing EMT was investigated. Through time-lapse microscopy and gene expression profiling, the P2 subpopulation was shown to display mesenchymal-like features and was highly enriched for EMT- and mesenchymal-associated markers, indicating that the P2 cells are products of spontaneous EMT in GIF-14 cells. Furthermore, TGF-β1 treatment readily caused an expansion of the tumorigenic, *Lgr5*-positive P2 subpopulation as revealed by Hoechst 33342 staining, along with significant induction of EMT- and mesenchymal-related transcripts. These observations strongly implicate EMT as major contributor to the tumorigenicity of GIF-14 cells. However, it was noted that *E-cadherin* mRNA levels was comparable in P1 and P2 cells and its expression remained unaffected by TGF-β1 (Figures 4.3 and 4.4). The reason for these observations is currently unclear though known repressors of E-cadherin such as *Snai1* and *Snai2* were induced. At this point, it has yet been demonstrated that *Snai1* and *Snai2* are responsible for driving the EMT phenotype in GIF-14 cells, thus they are viewed as markers for TGF-β responsiveness. It would be necessary to verify the protein expression and sub-cellular localisation of E-cadherin in P1 and P2 subpopulations. As reported in Section 3.1.2, the GIF cell lines exist in an immortalised but untransformed, pre-malignant state. Hence, tumour initiation and growth requires additional mutations and/or growth stimuli from a permissive tissue microenvironment. In this context, the reprogramming properties of EMT may contribute to tumor formation by conferring greater adaptability and increased resistance to apoptosis to ensure better survival in graft niche when transplanted.

Moreover, cells that have undergone EMT may be more responsive to growth factors present in the microenvironment.

An unexpected and intriguing observation from this study is that prolonged TGF-β1 treatment induced *Lgr5*, hitherto known only as a Wnt target and an exclusive gastrointestinal stem cell marker (Figure 4.4) (Barker *et al*., 2007; Barker *et al*., 2010). This finding indicates that EMT promotes a stem cell-like state in GIF-14 cells by imparting greater cellular plasticity. This observation is analogous to the recently reported phenomenon that aberrant activation of EMT in mammary epithelial cells would generate "cancer stem cells" (Mani *et al*., 2008). A key implication of this phenomenon is that differentiated cells can revert to a stem cell-like state through the reprogramming properties of EMT, which challenges existing dogmas of carcinogenesis (Mani *et al*., 2008; Morel *et al*., 2008).

The phenotypic plasticity of GIF-14 cells was further demonstrated in two observations: 1) P1 readily took on a P2-like phenotype upon TGF-β1 treatment; and 2) a gradient of epithelial and mesenchymal characteristics within individual P2 colonies (Figures 4.7 and 4.8B). This phenomenon is akin to the intermediate "metastable" phenotype observed during EMT, in which co-expression of mixed epithelial and mesenchymal traits occur within the same cell population (Savagner *et al*., 2005). Interestingly, cells within the TGF-β1-treated P1 colonies displayed more drastic changes in membrane morphology than those in P2 colonies, suggesting that exogenous TGF-β1 and autocrine signals may induce different degree of "metastability" (Figure 4.8A). It would be worthwhile to investigate whether P2 cells could be further induced to completely lose epithelial characteristics by TGF-β1. The intermediate phenotype is considered unstable and contributes to the adaptability and

tumorigenicity of cells aberrantly altered by EMT. The co-existence and persistence of P1 and P2 in normal *in vitro* culture also suggests that a dynamic equilibrium may exist between P1 and P2. While epithelial-like P1 cells are primed to undergo EMT induced by TGF-β1 and Wnt3a (Figures 4.5, 4.6 and 4.7), P2 cells may revert to P1 phenotype through a reverse process, i.e. Mesenchymal-Epithelial Transition (MET).

An important observation from immuno-fluorescent staining experiments is the shift from membranous to nuclear staining of β-catenin when cells become more motile and detached at the boundary of P2 or TGF-β1 treated P1 colonies (Figure 4.8B). This indicates an activated Wnt signaling which is reminiscent of the invasive front of metastatic tumours, where activation of TGF-β and Wnt pathways drives EMT and metastasis (Brabletz *et al*., 2005; Klymkowsky and Savagner, 2009). As the immuno-fluorescent data are qualitative in nature, these could be corroborated with biochemical approach such as subcellular fractionation combined with Western blotting to verify the changes in membrane, cytosolic and nuclear localisation. Consistent with the involvement of Wnt pathway in EMT, Wnt3a treatment in GIF-14 cells induced $EpCAM^{low}CD133^{-}$ cells in a similar manner to TGF-β1 (Figure 4.6). It is plausible that TGF-β1 induces the Wnt pathway by depleting β-catenin at the adherens junctions which in turn cooperates with Wnt to reinforce EMT.

The spontaneous emergence of P2 cells in GIF-14 cells suggests the existence of constitutively active EMT-inducing pathways due to autocrine growth factors. The identity of these signals was investigated through two approaches: 1) the addition of exogenous growth factors; and 2) the use of a specific inhibitor for the canonical TGF-β pathway. The data from these experiments provide evidence that an autocrine TGF-β pathway is responsible for the promotion and maintenance of the P2

subpopulation within GIF-14 cells, in a Smad2/3-dependent manner. This was confirmed by the remarkable reversal to an epithelial phenotype in the presence of TGF-β inhibitor as measured by cell morphology, gene expression and Hoechst 33342 staining (Figures 4.9 to 4.12). These are concordant with the recent report that the maintenance of the mesenchymal state required sustained activation of TGF-β and Wnt pathways in an autocrine fashion in mammary epithelial cells. Importantly, disruption of autocrine signaling loops would suppress cell migration, self-renewal and tumorigencity (Scheel *et al*., 2011). In addition to the activation of Smads2/3, Smad–independent signaling such as the mitogen-activated protein kinase (MAPK) pathways, phosphatidylinositol 3-kinase-Akt and RhoA pathways are also involved in TGF-β-mediated EMT (Hartsough and Mulder, 1995; Atfi *et al*., 1997; Frey and Mulder, 1997; Hanafusa *et al*., 1999; Bakin *et al*., 2000; Bhowmick *et al*., 2001). For instance, TGF-β-mediated regulation of RhoA-GTPase activity through the Occludin/Par6/Smurf1 pathway at the tight functions of epithelial cells has been implicated in priming for EMT (Ozdamar *et al*., 2005). Activation of the Rho cascade induces the formation of stress fibres (Ridley and Hall, 1992) which was clearly observed in P2 and TGF-β1-treated P1 colonies. Therefore, the involvement of RhoA pathway in TGF-β-induced EMT could be investigated.

Taken together, our results show that the GIF-14 cell line undergoes EMT readily induced by autocrine or exogenous TGF-β1 or Wnt3a to give rise to the tumorigenic, stem cell-like and mesenchymal-like P2 subpopulation characterised in Chapter 3. An unexpected degree of phenotypic plasticity was observed in GIF-14 where P1 cells would dedifferentiate into the *Lgr5*-positive P2 cells through the reprogramming properties of EMT. The phenomenon of spontaneous EMT is likely to

be restricted to *Runx3*$^{-/-}$ GIF cell lines as *Runx3*$^{+/+}$ lines are not tumorigenic and possess intact cell-cell adhesions (Li *et al*., 2002; Fukamachi *et al*., 2004). In view of the previous reports that *Runx3*$^{-/-}$ GIF cell lines were refractory to the growth suppressive and apoptotic effects of TGF-β1 compared to *Runx3*$^{+/+}$ cells (Li *et al*., 2002), it is surprising that *Runx3*$^{-/-}$ GIF-14 cells are susceptible to EMT-promoting effects of TGF-β1. Therefore, Runx3 may play an important role in modulating the TGF-β pathway. For this reason, the relationship between the loss of Runx3 and susceptibility to EMT will be further investigated in the following chapter.

CHAPTER 5

Runx3 safeguards gastric epithelial cells against aberrant activation of EMT and phenotypic plasticity

5.1 Introduction

5.1.1 *Runx3*$^{-/-}$ GIF cell lines display altered differentiation and epithelial phenotype

Despite the observation of a hyper-proliferative stomach in the *Runx3*-null mouse model, the study of Runx3 function in gastric epithelial cells was severely hampered by the early death (postnatal day1) of C57BL/6 *Runx3*$^{-/-}$ mice. To alleviate this problem, a series of mouse gastric epithelial cell lines, termed the GIF cell lines were established by the immortalisation of *Runx3*$^{+/+}$.*p53*$^{-/-}$ or *Runx3*$^{-/-}$.*p53*$^{-/-}$ gastric epithelial cells isolated from E16.5 fetuses. In the initial characterisation of these embryonic cell lines, it was revealed that when cultured between collagen sheets, *Runx3*$^{+/+}$ GIF lines readily formed simple columnar epithelia with glandular structures. Like normal gastric epithelial cells, these cells exhibited polarity with mucus droplets localised on the luminal surface (Fukamachi *et al*., 2004). In contrast, *Runx3*$^{-/-}$ GIF lines under the same culturing conditions displayed an altered *in vitro* phenotype that was characterised by poor organisation and disrupted differentiation. Of particular note, these cells failed to develop apical-basal polarity and glandular structures (Fukamachi *et al*., 2004). The former was subsequently found to be caused by the reduced expression of tight junction proteins important for cell-cell contact, such as Claudin-1 which was found to be a positive target of Runx3 (Chang *et al*., 2010). These data indicate that Runx3 is required for the proper differentiation into glandular epithelial sheet with established cell-cell adhesion and polarity in collagen gel cultures.

When subcutaneously transplanted into immuno-compromised nude mice, it was found that only *Runx3*$^{-/-}$ GIF lines and not their *Runx3*$^{+/+}$ counterparts were tumorigenic (Li *et al*., 2002). The resultant *Runx3*$^{-/-}$ GIF-generated tumours were

studied to provide further insights into their differentiation potentials. Remarkably, histological analysis of tumours in nude mice and *in vitro* culture in three dimensional matrigel showed that *Runx3*$^{-/-}$ GIF lines were capable of trans-differentiating into intestinal-type cells (Fukamachi *et al*., 2004; Fukamachi *et al*., 2008). Together, all the above data indicate that *Runx3*$^{-/-}$ cells are prone to losing their identity as gastric epithelial cells when perturbed by extracellular morphogenetic cues. These observations are further supported by recent finding from adult BALB/c *Runx3*$^{-/-}$ mice, which showed altered differentiation and intestinalisation of the gastric epithelium, characterised by the loss of chief cells and aberrant expression of the intestinal specific transcription factor Cdx2 (Ito *et al*., 2011).

5.1.2 Altered TGF-β and Wnt signaling in *Runx3*$^{-/-}$ GIF lines

A prominent feature of *Runx3*$^{-/-}$ GIF lines is their resistance to TGF-β1-mediated growth arrest and apoptosis (Li *et al*., 2002). This is consistent with the critical function of RUNX3 as a mediator of the TGF-β/Smad tumour suppressor pathway in gastric epithelial cells. Through direct interactions with the Smad transcription factors, RUNX3 transcriptionally activate the expression of *p21*$^{WAF/Cip1}$ and *BIM,* a negative regulator of cell cycle and a pro-apoptotic gene respectively (Chi *et al*., 2005; Yano *et al*., 2006; Ito 2008). Indeed, the ability to escape TGF-β-mediated apoptosis is considered to be an important basis for the tumorigenicity of the *Runx3*$^{-/-}$ GIF lines. However, the TGF-β signaling pathway is remarkably pleiotropic in that while it serves as a major cancer barrier in early carcinogenesis due to its tumour suppressive activities, its ability to aberrantly activate EMT renders it a major driver of cancer progression and metastasis in late stage cancers (Wakefield and

Roberts, 2002). It is therefore possible that the resistance of *Runx3*$^{-/-}$ GIF lines to TGF-β-mediated apoptosis is a result of the skewing of TGF-β signaling towards EMT-activating properties due to the absence of Runx3. Apart from its involvement in TGF-β signaling, RUNX3 acts as a molecular antagonist to the canonical Wnt pathway through direct interaction with the TCF4/β-catenin complex in human colorectal cancer cell lines (Ito *et al*., 2008). Consistent with this, *Runx3*$^{-/-}$ intestinal epithelial cells in primary cultures displayed higher sensitivity to Wnt stimulation than their *Runx3*$^{+/+}$ equivalents (Ito *et al*., 2008). However, the response to Wnt signaling has yet been addressed in gastric epithelial cells. In our study, Wnt responsiveness was demonstrated in the *Runx3*$^{-/-}$ GIF-14 cell line through the activation of *Lgr5* by Wnt3a. Hence, Runx3 is also involved in modulating the Wnt pathway in the stomach and the dysregulation of which is heavily implicated in gastrointestinal neoplasia as well as aberrant activation of EMT (Brabletz *et al*., 2001; Kim *et al*., 2002, Kolligs *et al*., 2002; Vincan and Barker, 2008).

In the previous chapter, it was demonstrated that the *Runx3*$^{-/-}$ GIF-14 cell line underwent spontaneous EMT to give rise to a tumorigenic and stem cell-like P2 subpopulation. This was attributed to a constitutively active TGF-β pathway caused by an autocrine TGF-β loop in GIF-14 cells during normal *in vitro* culture. Furthermore, the canonical Wnt pathway was also shown to promote the formation of EpCAM^{low}CD133^{-}/P2 subpopulation. Given that Runx3 is involved in both TGF-β and Wnt pathways, the roles of Runx3 in EMT and tumorigenicity of gastric epithelial cells will now be investigated through the use of *Runx3*-null and *Runx3*-expressing GIF cell lines.

5.1.3 Experimental approach

The contribution of Runx3 in the regulation of EMT would be studied by two approaches: 1) Comparing the TGF-β and Wnt responsiveness of *Runx3*$^{+/+}$ and *Runx3*$^{-/-}$ GIF cell lines; and 2) Studying the effects of exogenous RUNX3 on the TGF-β and Wnt responsiveness of *Runx3*$^{-/-}$ GIF-14 cells. For the former, TGF-β and Wnt responsiveness of multiple *Runx3*$^{+/+}$ and *Runx3*$^{-/-}$ GIF cell lines would be quantified and compared. To accomplished the latter, lentiviruses will be employed which enables the sustained and stable expression of RUNX3 due to their ability to integrate into the host genome following transduction (Naldini *et al*., 1996; Kafri *et al*., 1997; Miyoshi *et al*., 1997). Furthermore, lentiviruses are capable of delivering the transgenes into dividing as well as non-dividing cells (Burkrinsky *et al*., 1993), hence enabling the study of all subpopulations within the GIF-14 cell line. The response of multiple GIF lines to various treatments and exogenous RUNX3 will be quantified by the methodologies established in the studying of GIF-14 cells, as described in previous chapters.

5.2 Results

5.2.1 *Runx3*$^{-/-}$ GIF lines are sensitised to TGF-β1-induced EMT

To investigate whether the reduced epithelial and EMT-prone phenotype observed was a unique characteristic of GIF-14 cells or a general phenomenon among the *Runx3*$^{-/-}$ GIF cells lines, the expression of EpCAM and CD133 were measured in four individual *Runx3*$^{-/-}$ and *Runx3*$^{+/+}$ GIF cell lines. Flow cytometry analyses revealed that the EpCAM^{low}CD133^{-} fraction associated with the tumorigenic, mesenchyml-like P2 cells in GIF-14 was significantly represented only in *Runx3*$^{-/-}$ GIF-5 and GIF-14 cells. Moreover, the average expression of EpCAM was also significantly lower in *Runx3*$^{-/-}$ cell lines, reflecting an overall loss of epithelial phenotype (Figure 5.1A). The loss of epithelial characteristics in *Runx3*$^{-/-}$ cell lines is in agreement with published reports in which these cell lines showed defective epithelial morphology when grown in collagen cultures (Fukamachi *et al*., 2004). The relative expression of Runx3 in these GIF cell lines was assessed by Western blotting using two separate Runx3-specific monoclonal antibodies, R3-5G4 and -8C9. This also confirmed the absence of contaminating Runx3-expressing cells in *Runx3*$^{-/-}$ GIF lines (Figures 5.1B and C).

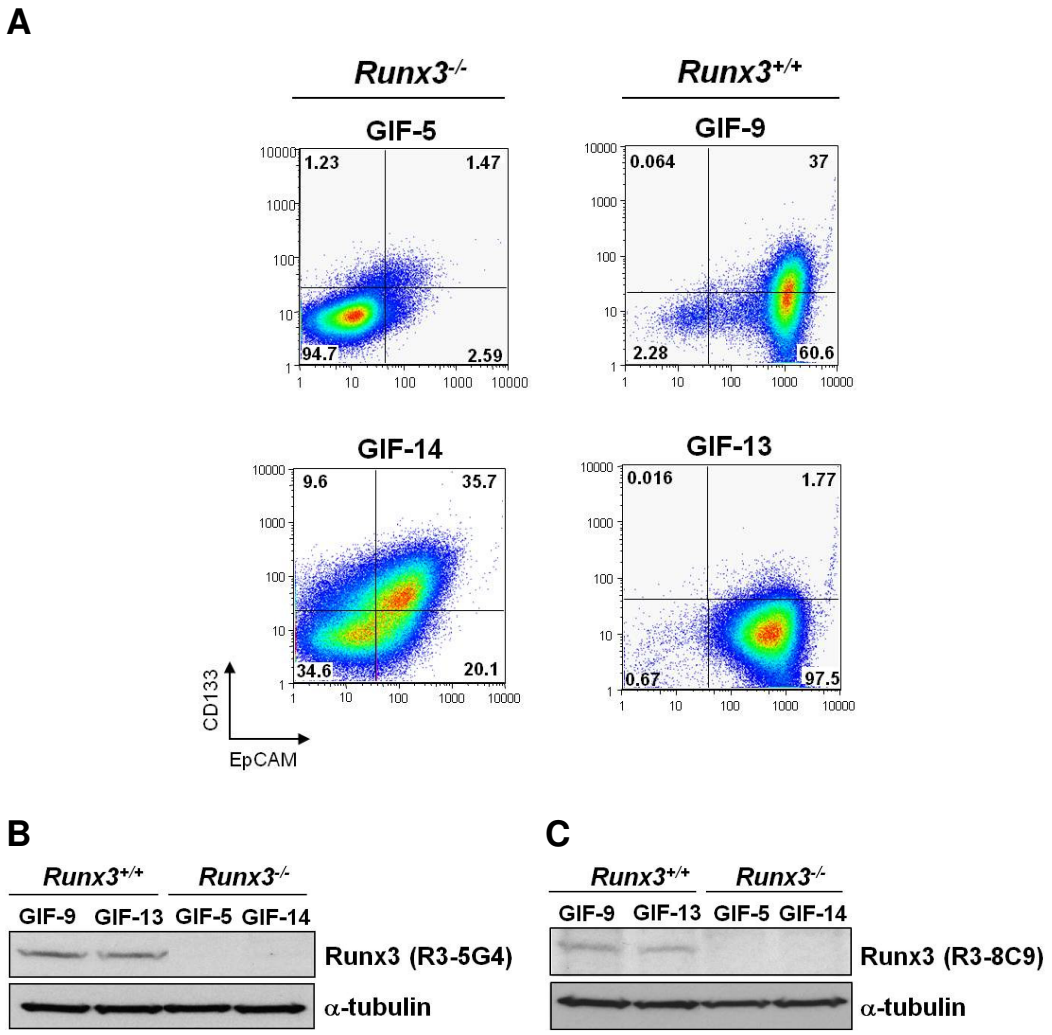

Figure 5.1. EpCAM/CD133 antigen profiles and the expression of Runx3 in *Runx3*$^{-/-}$ and *Runx*3$^{+/+}$ GIF cell lines. (A) *Runx*3$^{+/+}$ (GIF-9 and GIF-13) and *Runx3*$^{-/-}$ (GIF-5 and GIF-14) cell lines were subjected to co-staining of antibodies against surface markers EpCAM and CD133 and analysed on the flow cytometer. To determine the relative expression levels of Runx3, total cell lysates were used in Western blot analysis (Section 2.14) using anti-Runx3 monoclonal antibodies (B) R3-5G4 and (C) R3-8C9. As loading control, immunoblotting of α-tubulin was performed.

The reduced epithelial characteristics in *Runx*3$^{-/-}$ lines suggest that they may be prone to undergo EMT. To test this, *Runx*3$^{-/-}$ and *Runx3*$^{+/+}$ lines were treated with TGF-β1 and changes in gene expression was measured by qRT-PCR. This revealed remarkable differences in TGF-β1 responsiveness between the two groups. In *Runx*3-null GIF-5 and GIF-14 lines, induction of EMT- and mesenchymal-related marker genes were observed within 24h, with the levels of *Snai1* prominently elevated (Figure 5.2). In contrast, only marginal induction of these marker genes were observed in *Runx*3$^{+/+}$ GIF-9 and GIF-13 lines (Figure 5.2). These results provide sufficient evidence that an important function of Runx3 in gastric epithelial cells is to protect them against the aberrant activation of EMT.

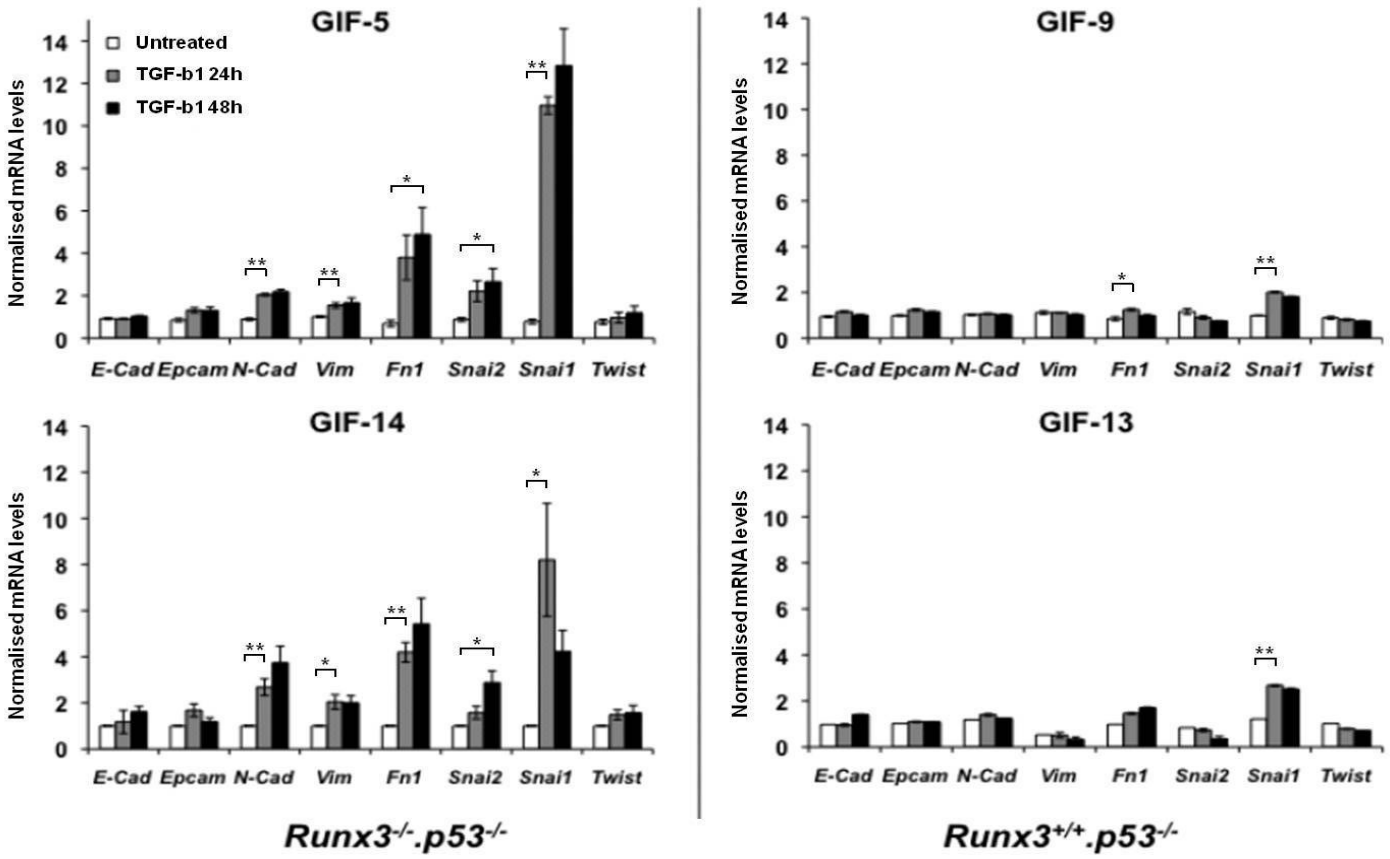

Figure 5.2. Comparison of TGF-β1-responsiveness of *Runx3*$^{-/-}$ and *Runx3*$^{+/+}$ GIF cell lines. *Runx3*$^{-/-}$ (GIF-5 and GIF-14) and *Runx3*$^{+/+}$ (GIF-9 and GIF-13) lines were treated with 2.5ng/ml of TGF-β1 for 24h and 48h for gene expression profiling of EMT- and mesenchymal-related markers by qRT-PCR. The expression levels were normalised against those of *Gapdh* and expressed relative to untreated controls for each gene (means ± SEM, n=3). Single and double asterisks represent *p*-value <0.05 and *p*-value <0.01, respectively.

5.2.2 Exogenous RUNX3 reduces the P2 subpopulation

To verify the negative correlation between Runx3 and mesenchymal-like phenotype in *Runx3*$^{-/-}$ GIF lines, wild-type human RUNX3 and RUNX3^{R178Q} were stably re-introduced into *Runx3*-null GIF-14 cells by lentiviruses. RUNX3^{R178Q} is a DNA-binding defective mutant of RUNX3 which bears an amino acid substitution of arginine to glutamine in the Runt domain and used as a negative control (Inoue *et al*. 2007). As *RUNX3/RUNX3*^{R178Q} was cloned upstream of the *IRES-EGFP* sequences in the iG2 lentiviral vector (Section 2.12.1), RUNX3/RUNX3^{R178Q} and enhanced green fluorescent protein (EGFP) could be co-expressed in infected cells. Thus, this strategy enables the tracing of transduced cells by flow cytometry and fractionation by FACS based on stable expression of EGFP. The transduction effeciency achieved by iG2 lentiviruses was approximately 50%. However, the percentage of EGFP^{+} cells in iG2-RUNX3 infected samples would steadily decline over the course of an experiment, indicating that RUNX3 exerts a negative selection pressure that is consistent with its tumor suppressor activity. GIF-14 cells transduced with lentiviruses encoding iG2-Control, iG2-RUNX3 or iG2-RUNX3^{R178Q} were subjected to Hoechst 33342 staining and analyses by flow cytometry 4 and 6 days post-infection. The ectopic expression of RUNX3 markedly altered the Hoechst 33342 staining profile. RUNX3 caused a reduction of P2 subpopulation 4 days post-infection and this trend was persistent and further enhanced at six days post-infection (Figure 5.3). In contrast, stable introduction of RUNX3^{R178Q} resulted in Hoechst 33342 staining pattern indistinguishable from that of cells infected with the iG2-Control lentivirus. This indicates that the effect of RUNX3 is dependent on its DNA-binding activity (Figure 5.3). To demonstrate that there is a close coupling of EGFP expression and that of ectopic proteins, EGFP^{+} and EGFP^{-} cells were fractionated and analysed by Western

blot using RUNX3-specific R3-5G4 antibody. This revealed that exogenous proteins were detectable in the $EGFP^+$ but not in $EGFP^-$ fractions, indicating that the purity of the FACS-enriched cells was high (Figure 5.3). The expression levels of exogenous RUNX3/$RUNX^{R178Q}$ were estimated to be ~130-fold that of endogenous Runx3 in GIF-13 cells relative to α-tubulin (data not shown).

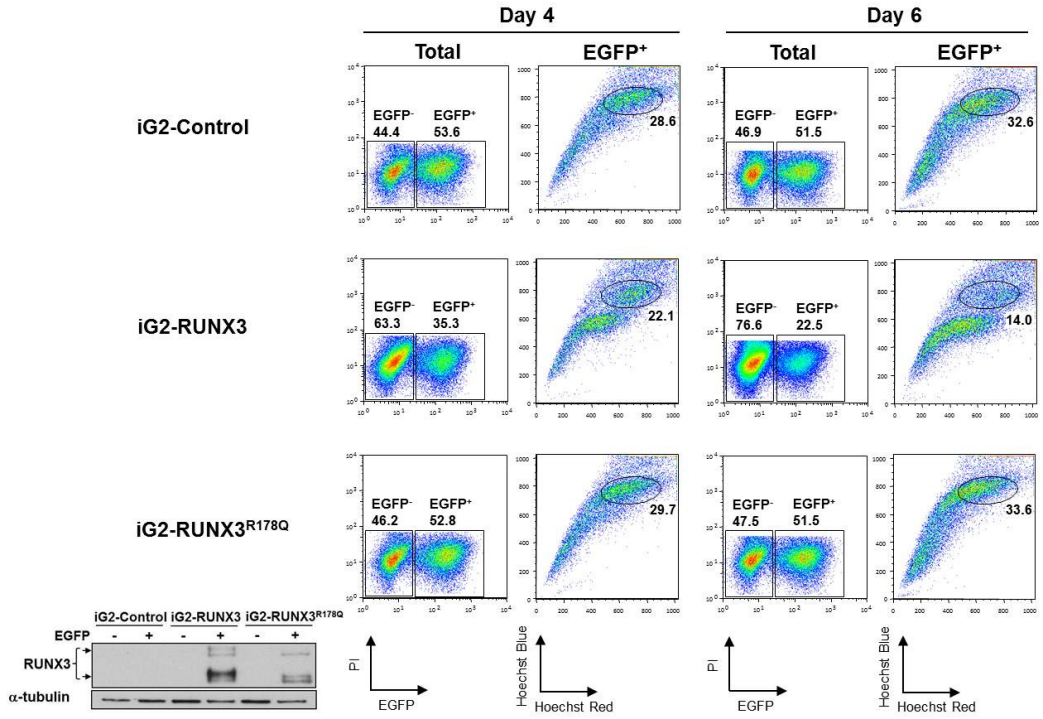

Figure 5.3. Optimisation of lentivirus transduction for the over-expression of RUNX3 in GIF-14 cells. GIF-14 cells were transduced with lentiviruses encoding encoding wild-type RUNX3 or its DNA-binding defective mutant, $RUNX3^{R178Q}$. Transduction efficiency was determined by the percentage of $EGFP^+$ cells and the Hoechst 33342 staining patterns in $EGFP^+$ cells were analysed by flow cytometry 4 and 6 days post-transduction. PI denotes propidium iodide. The expression of exogenous proteins in FACS-enriched GIF-14 cells 6 days post-transduction was confirmed by Western blot analysis. Exogenous RUNX3 amd $RUNX3^{R178Q}$ was detected using R3-5G4 antibody. Immunoblotting of α-tubulin was included as loading control.

The results from the previous experiment showed that at least six days of infection was required for RUNX3 to exert pronounced effects, this infection regime was employed in the subsequent sections. GIF-14 cells were transduced with lentiviruses encoding iG2-Control, iG2-RUNX3 or iG2-RUNX3^{R178Q}. At two days post-infection, cells were treated with TGF-β1 for 4 days prior to Hoechst 33342 staining for flow cytometric analysis. Three separate experiments were performed and the FACS plots from a representative experiment were shown in Figure 5.4A. Our results revealed that ectopic expression of RUNX3 resulted in an ablation of the P2 subpopulation and this effect was augmented when cells were treated with TGF-β1 (Figure 5.4A). The data from three experiments were compiled in which P2 cells was presented as a percentage of combined P1 and P2 cell populations (Figure 5.4B). Importantly, the Hoechst 333242 staining pattern from RUNX3^{R178Q} infected cells was indistinguishable from that of the iG2-Control, confirming that the effect of RUNX3 is dependent on its DNA-binding activity (Figures 5.4A and 5.4B). Interestingly, over expression of RUNX3 also caused P1 cells to display lower dye efflux capacity (Figure 5.4A), possibly due to a downregulation of the ATP binding cassette protein transporters by RUNX3.

As P1 and P2 cells could be demarcated based on their differential EpCAM and CD133 expression, changes in these markers were also determined by flow cytometry and expressed as a percentage of combined EpCAM^{high}CD133^{+} and EpCAM^{low}CD133^{-} populations. Consistent with the Hoechst 33342 staining data, exogenous RUNX3 but not RUNX3^{R178Q} reduced the P2-associated EpCAM^{low}CD133^{-} fraction. In addition, an increase in the P1-associated EpCAM^{high}CD133^{+} fraction in RUNX3 infected cells was observed (Figure 5.4C).

Therefore, our data suggest that exogenous RUNX3 exerts an antagonistic effect on the mesenchymal-like P2 cells.

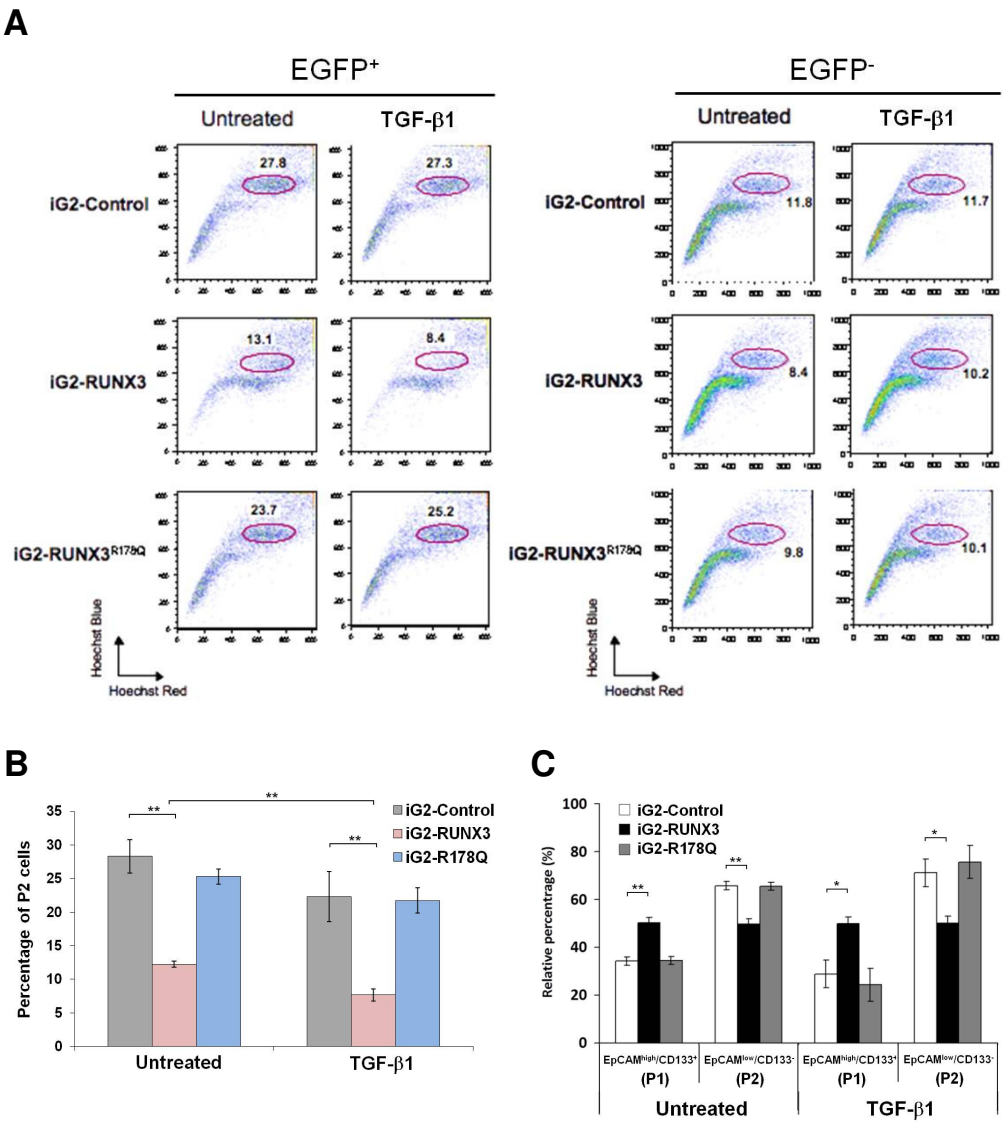

Figure 5.4. The effects of exogenous RUNX3 on Hoechst 33342 staining and EpCAM/CD133 profiles in GIF-14 cells. (A) GIF-14 cells were transduced with EGFP-tagged iG2-Control, -RUNX3 or -RUNX3^{R178Q} lentiviruses for 48h preceding the treatment with 2.5ng/ml of TGF-β1 for 4 days. EGFP^{+} infected cells were subjected to Hoechst 33342 staining and analysed by flow cytometry. Profiles of EGFP^{-} cells served as negative controls. The experiments were performed in triplicates and the FACS charts from one representative experiment were shown here. (B) Changes in the P2 subpopulation following TGF-β1 treatment in EGFP^{+} cells in three separate experiments were compiled. The relative levels of P2 cells are presented as a percentage of P1 and P2 combined values (means ± SEM, n=3). (C) Corresponding changes in EpCAM and CD133 surface antigen expression in EGFP^{+} cells from three independent experiments were compiled. The relative levels of EpCAM^{high}CD133^{+} and EpCAM^{low}CD133^{-} populations are presented as a percentage of their combined values (means ± SEM, n=3). Single and double asterisks represent *p*-value <0.05 and *p*-value <0.01, respectively.

5.2.3 RUNX3 suppresses TGF-β1-induced EMT-related genes and *Lgr5*

To assess the effect of RUNX3 on TGF-β1-induced genes, gene expression profiling was performed. Three independent infections were set up as described in Section 5.2.2, with the exception that GIF-14 cells were infected for 6 days prior to 24h of TGF-β1 treatment. Infected cells were enriched by FACS based on EGFP fluorescence and harvested for qRT-PCR analyses. The results showed that RUNX3 partially and completely abrogated TGF-β1-induced *Snai1* and *Hmga2* respectively, but not $RUNX3^{R178Q}$ (Figure 5.5). As TGF-β1 treatment was shown to activate *Lgr5* in Section 4.2.2, the effect of RUNX3 on TGF-β-induced *Lgr5* was therefore tested. The results showed that exogenous RUNX3 strongly inhibited TGF-β1-induced *Lgr5* and *Sox9*. Interestingly, the basal expression of these genes was also suppressed by RUNX3 in contrast to those of *Snai1* and *Hmga2* (Figure 5.5). Together, these data indicate that RUNX3 plays a negative role in the regulation of TGF-β1-induced EMT genes and *Lgr5* in a DNA-binding dependent manner. To confirm the expression of exogenous proteins, Western blotting was performed, which revealed that exogenous RUNX3 and $RUNX3^{R178Q}$ were expressed at comparable levels in lentivirus-transduced GIF-14 cells (Figure 5.5).

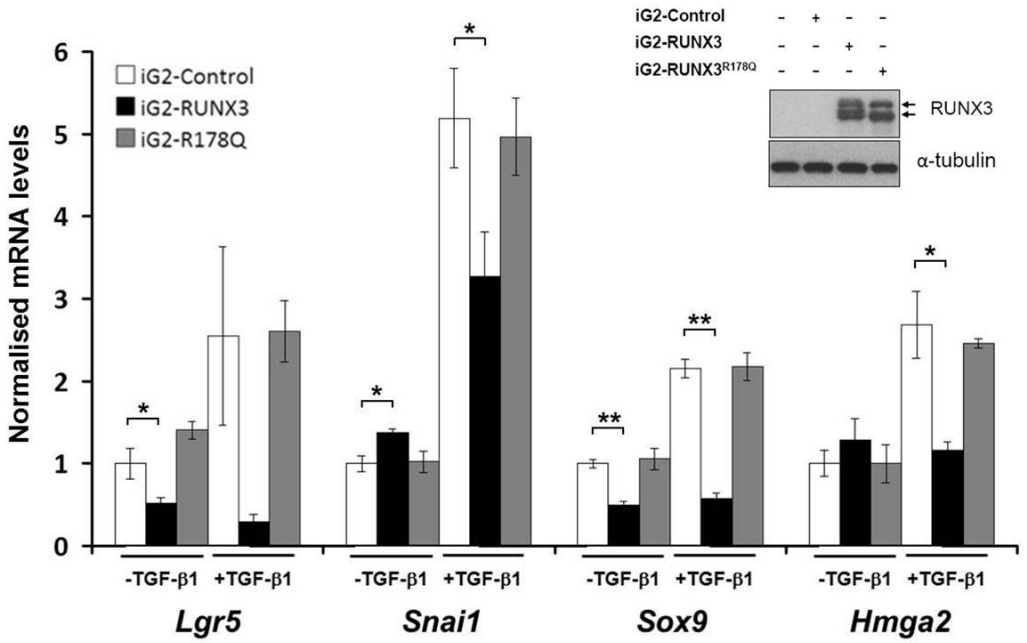

Figure 5.5. Changes in EMT- and stemness-related genes in the presence of exogenous RUNX3. (A) GIF-14 cells were treated with TGF-β1 for 24h following 6 days of infection by lentiviruses encoding Control, RUNX3 or RUNX3^{R178Q}. EGFP^{+} infected cells were enriched by FACS and changes in EMT- and stemness-associated markers were measured by qRT-PCR. Three separate infection experiments were carried out and the expression levels were normalised against those of *Gapdh* and presented as a ratio to the untreated iG2-Control sample for individual genes (means ± SEM, n=3). Single and double asterisks represent *p*-value <0.05 and *p*-value <0.01, respectively. Western blotting was performed to confirm the expression levels of exogenous RUNX3 and RUNX3^{R178Q} 48h post-infection using R3-5G4 antibody. Immunoblotting of α-tubulin was included as loading control.

5.2.4 *Runx3*$^{-/-}$ GIF cells display increased Wnt responsiveness

The Wnt target gene and stem cell marker *Lgr5* was shown to be highly induced by Wnt3a-Cm in *Runx3*$^{-/-}$ GIF-14 cells in Section 3.2.7. As RUNX3 is known to be a potent molecular antagonist of the Wnt pathway through its direct interaction with the TCF4/β-catenin complex, the Wnt responsiveness of *Runx3*$^{-/-}$ and *Runx3*$^{+/+}$ cells were compared (Ito *et al*., 2008). GIF-14 (*Runx3*$^{-/-}$) and GIF-13 (*Runx3*$^{+/+}$) cells were treated with Wnt3a- or Control-Cm for 15h and the expression of *Lgr5* transcript was ascertained by qRT-PCR. The results revealed that GIF-14 cells were highly sensitised to Wnt3a-Cm as reflected in the strong induction of *Lgr5* while GIF-13 cells were not responsive to Wnt3a (Figure 5.6). Moreover, GIF-14 cells showed a 6-fold greater basal expression of *Lgr5* than GIF-13 cells, indicative of a constitutively active Wnt signaling (Figure 5.6). These data indicate that similar to earlier observations in colorectal epithelial cells, Runx3 has an inhibitory effect on the canonical Wnt pathway in GIF cells.

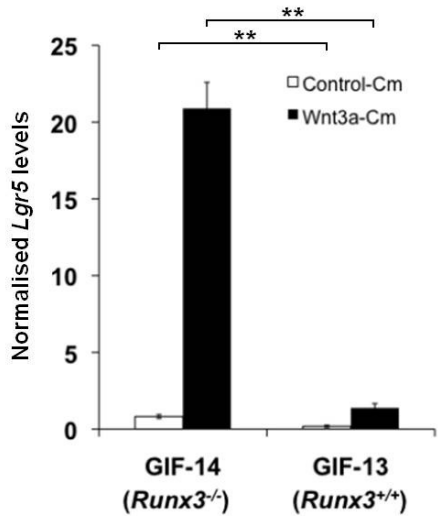

Figure 5.6. Comparison of Wnt responsiveness of *Runx3*$^{-/-}$ and *Runx*3$^{+/+}$ GIF cell lines. *Runx3*$^{-/-}$ GIF-14 and *Runx*3$^{+/+}$ GIF-13 lines were treated with Control or Wnt3a-Cm diluted 1:3 by culture medium for 15h prior to measurement of *Lgr5* transcripts by qRT-PCR. The expression levels were normalised against those of *Gapdh* and expressed relative to GIF-14 treated with control-Cm. Double asterisks denotes *p*-value < 0.01.

To assess whether higher basal *Lgr5* expression correlates to increased sphere formation, the sphere-forming potential of *Runx3*$^{-/-}$ GIF-14 and *Runx3*$^{+/+}$ GIF-13 cells were compared. These two cell lines were cultured in serum-free sphere medium and the number of spheres was scored. The results revealed that GIF-14 cells possessed 4-fold higher sphere-forming activity than GIF-13 cells (Figure 5.7). While spheres formed by GIF-14 cells could be maintained for a long period of time, GIF-13 cells gave rise to sphere-like structures that quickly disintegrated into clusters of mixed cell morphologies indicative of differentiation (Figure 5.7). Collectively, these data indicate that Runx3 is a negative regulator of a stem cell-like state through the suppression of *Lgr5* and sphere formation.

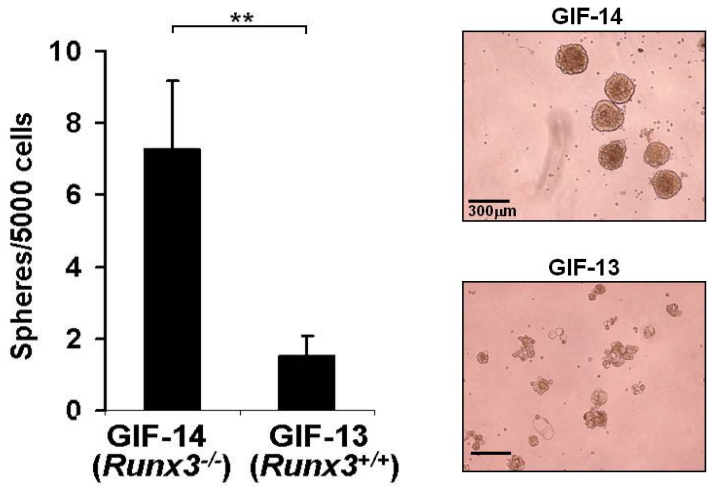

Figure 5.7. Relative sphere-initiation potential of GIF-14 and GIF-13 cells. Sphere-forming assay was set up using GIF-14 and GIF-13 cells in the presence of 0.1% of methylcellulose as described in materials and methods. Data are presented as number of spheres (≥250μm in size) generated from 5000 cells after 25 days in culture (means ± SEM, n=4). Double asterisks denotes *p*-value < 0.01. Representative phase contrast images of spheres are shown. Scale bars, 300μm.

5.2.5 Exogenous RUNX3 abrogates Wnt3a-induction of *Lgr5* and sphere formation

To verify the negative role of Runx3 on the canonical Wnt pathway in GIF gastric epithelial cells, exogenous wild-type RUNX3 or RUNX3^{R178Q} (a DNA-binding defective mutant) were ectopically introduced into *Runx3*-null GIF-14 cells by the pBOBI series of lentiviruses. As the transduction efficiency for these viruses was approximately 80%, the cells were harvested *in situ* following 15h of Control- or Wnt3a-Cm treatment, without enrichment by FACS. Our results revealed that RUNX3 partially abrogated the robust induction of *Lgr5* by Wnt3a while the ectopic expression of RUNX3^{R178Q} had no effect (Figure 5.8). These data indicate that RUNX3 antagonises the canonical Wnt pathway in a DNA-binding dependent manner in gastric epithelial cells. The relative expression of exogenous proteins in GIF-14 cells was assessed by Western blot analysis. This confirmed that the expression levels of ectopic RUNX3 and RUNX3^{R178Q} were similar (Figure 5.8).

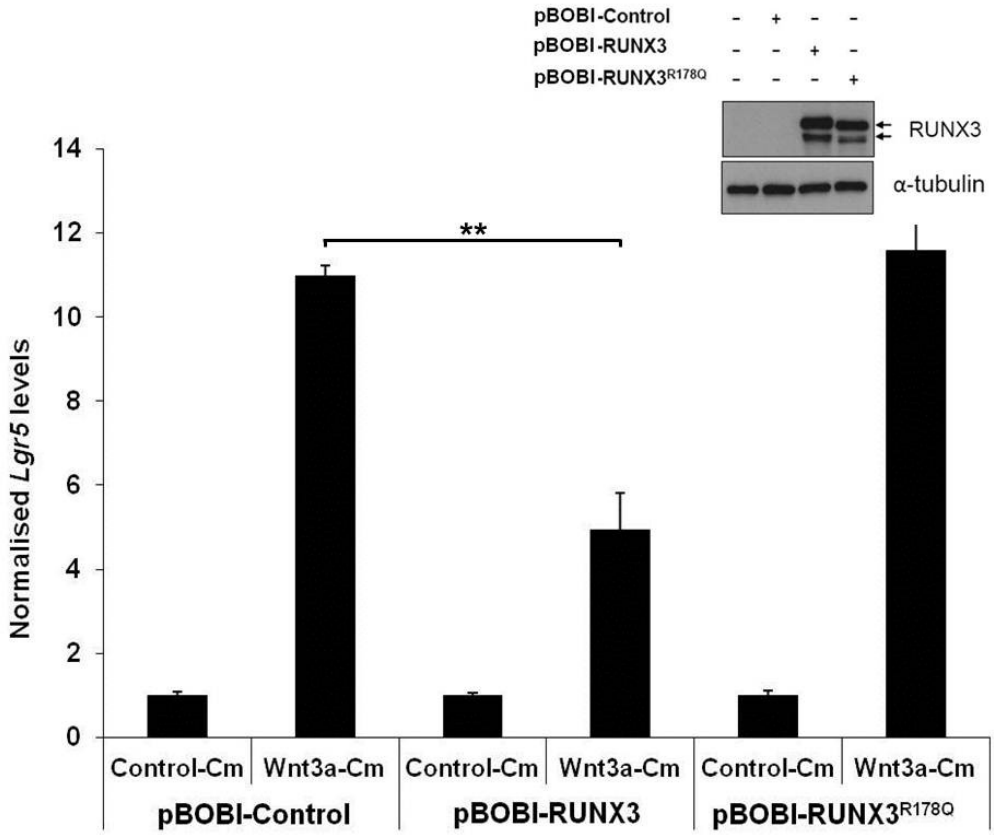

Figure 5.8. The effects of exogenous RUNX3 on Wnt3a-induced *Lgr5*. (A) GIF-14 cells were infected with pBOBI-Control, -RUNX3 or -RUNX3^{R178Q} lentiviruses for 48h preceding treatment with control or Wnt3a-Cm (1:3 dilution with culture medium) for another 15h. Cells were harvested for quantification of *Lgr5* mRNA levels by qRT-PCR. Values are normalised against those of *Gapdh* and expressed as ratios to that of control-Cm treated cells for each sample. Double asterisks denotes *p*-value < 0.01. (B) GIF-14 cells were transduced with the pBOBI-based series of lentiviruses for 48h. The expression levels of exogenous proteins were confirmed by Western blot analysis 48h post-infection using R3-5G4 antibody. Immunblotting of α-tubulin served as loading control.

The strong inhibition of Wnt3a-induction of *Lgr5* by exogenous RUNX3 prompted the testing of its effect on sphere formation. GIF-14 cells were infected with lentiviruses encoding wild-type RUNX3 or iG2-Control for 6 days and subjected to enrichment by FACS. Sphere-forming capacities of FACS-purified cells were evaluated. The results revealed that ectopic expression of RUNX3 dramatically reduced sphere formation by 4-fold compared to iG2-Control (Figure 5.9A). In a similar experiment, GIF-14 cells infected with wild-type RUNX3 or iG2-Control viruses were pre-treated with Control- or Wnt3a-Cm prior to purification by FACS. Sphere-forming assay was performed on enriched cells cultured in Control- or Wnt3a-Cm diluted 1:10 by sphere medium. Under this condition, ectopically expressed RUNX3 consistently suppressed sphere-formation (Figure 5.9B). Moreover, RUNX3 also completely blocked the induction of sphere-formation by Wnt3a (Figure 5.9B). Together, these data clearly demonstrate that RUNX3 acts as a negative regulator of stem cell-like phenotype by strong blockade of Wnt3a-induction of *Lgr5*.

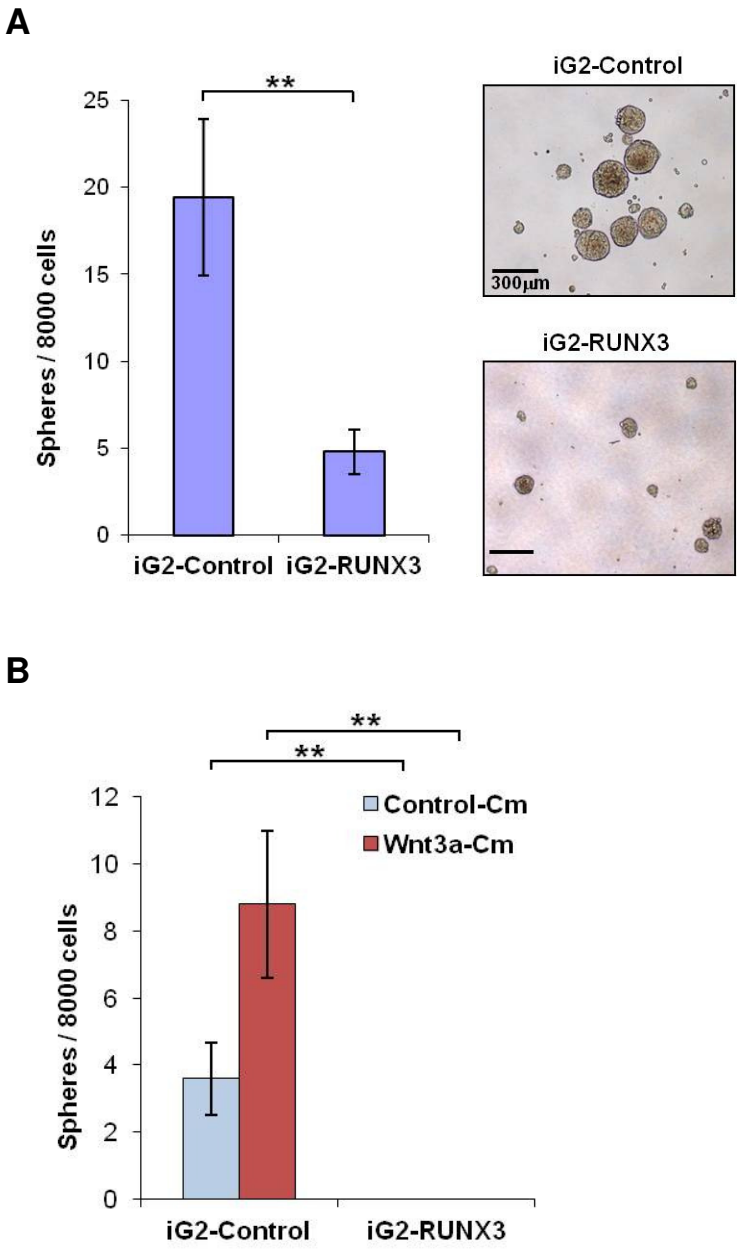

Figure 5.9. The effects of exogenous RUNX3 on sphere-initiation. (A) GIF-14 cells were transduced with lentiviruses encoding Control, RUNX3 or RUNX3^{R178Q}. Six days post-infection, EGFP^{+} cells were fractionated by FACS and cultured in sphere medium containing 0.5% of methylcellulose. Spheres (≥150µm in size) generated from 8000 cells were counted after 34 days of culture (means ± SEM, n=5). Double asterisks denotes *p*-value < 0.01. Phase contrast images of spheres are shown. Scale bars, 300µm. (B) Transduced GIF-14 cells were pre-treated with control or Wnt3a-Cm for 2 days prior to enrichment of EGFP^{+} cells by FACS 6 days post-infection and sphere-forming assay was performed. Conditioned media was supplied in 1:10 dilution with sphere medium containing 1% of methylcellulose. Number of spheres formed from 8000 cells was scored 25 days after culture (means ± SEM, n=5). Double asterisks denotes *p*-value < 0.01.

5.2.6 Runx3 abrogates the synergistic activation of *Lgr5* by TGF-β and Wnt3a

To investigate the tripartite relationship between EMT, stemness and Runx3, a co-induction with TGF-β1 and Wnt3a was performed on GIF-14 (*Runx3*$^{-/-}$) and GIF-13 (*Runx3*$^{+/+}$) cells. Cells were pre-treated with TGF-β1 for varying periods before they were co-treated with control- or Wnt3a-Cm for a further 15h. Quantitative RT-PCR measurement of *Lgr5* and *Snai1* of treated cells revealed distinct induction patterns in GIF-14 cells. Notably, *Snai1* was strongly activated by TGF-β1 within 15h of treatment, but was unresponsive to Wnt3a (Figure 5.10). In comparison, *Lgr5* transcript was initially suppressed by TGF-β1 at 15h, but was moderately induced upon prolonged treatment for 48h. Surprisingly, Wnt3a-induction of *Lgr5* was dramatically augmented with TGF-β1 pre-treatment for 48h from 9-fold to 30-fold. This synergistic effect was not observed at shorter TGF-β1 pre-treatment time points (Figure 5.10). These data implies that the strong synergy between TGF-β1 and Wnt3a in activating *Lgr5* transcription involves an independent but cooperative mechanism. Remarkably, the Wnt3a- and TGF-β1-responsiveness observed for these two genes was completely muted in *Runx3*$^{+/+}$ GIF-13 cells, underscoring the strong opposing effects of Runx3 on the cooperative activation of *Lgr5* by TGF-β1 and Wnt3a (Figure 5.10).

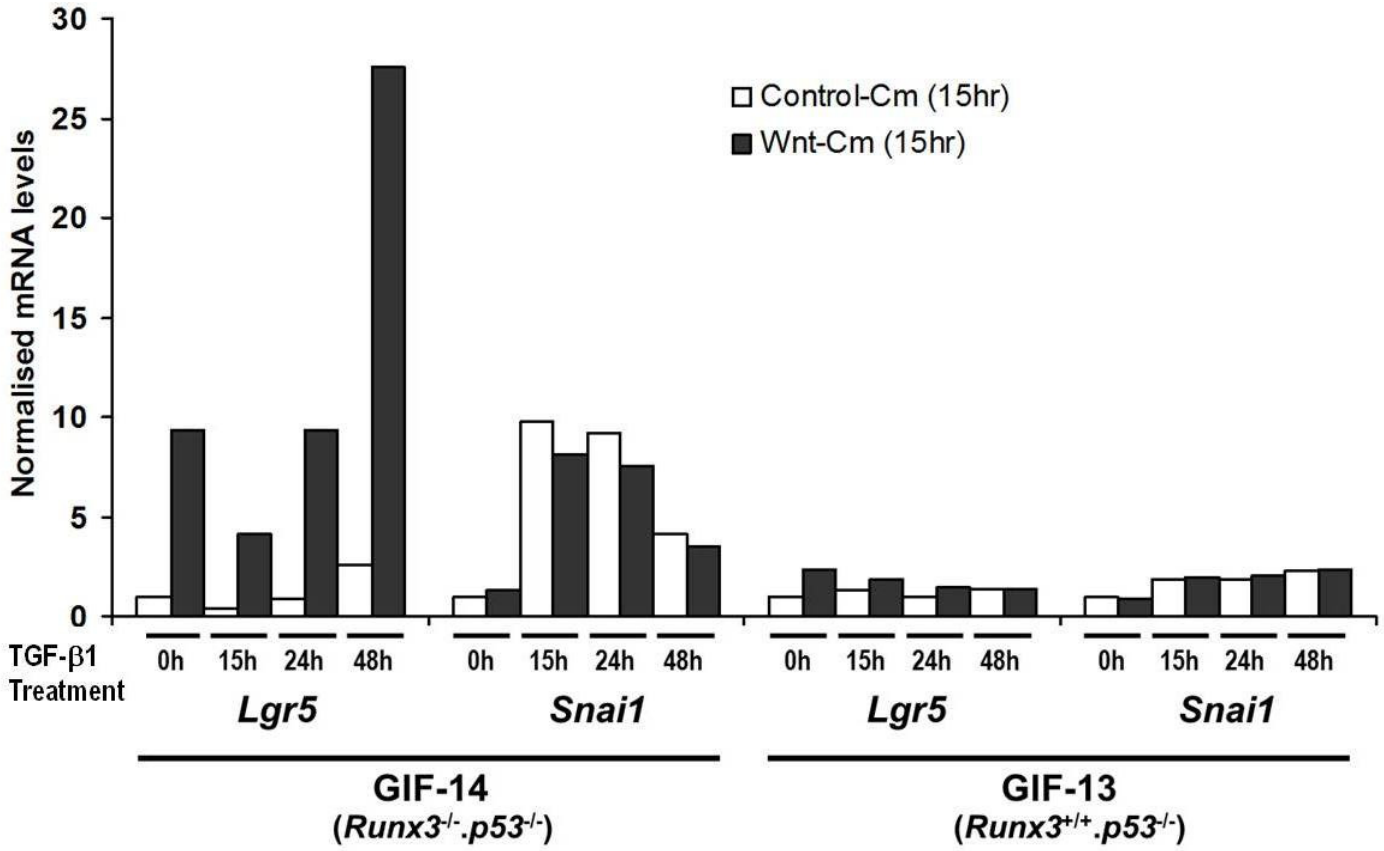

Figure 5.10. The effects of co-treatment of Wnt3a-Cm and TGF-β1 in *Runx3*$^{-/-}$ and *Runx3*$^{+/+}$ GIF cell lines. GIF-14 (*Runx3*$^{-/-}$) and GIF-13 (*Runx3*$^{+/+}$) cell lines were pre-treated with 2.5ng/ml of TGF-β1 for the indicated periods prior to co-treatment with control- or Wnt3a-Cm (1:3 dilution with culture medium) for another 15h. Changes in *Lgr5* and *Snai1* mRNA levels were quantified by qRT-PCR. Expression levels were normalised against those of *Gapdh* and presented as ratios to that of Control-Cm treated cells in the absence of TGF-β1.

5.3 Discussion

The identification of a tumorigenic and stem cell-like subpopulation in the *Runx3*$^{-/-}$ GIF-14 cell line and the discovery of its induction by TGF-β1 and Wnt3a signals raised important questions. These pathways are critical for the development, homeostasis and carcinogenesis in the gastrointestinal tract and RUNX3 is known to act in cooperation or in antagonism with them in this specific context (Chi *et al*., 2005; Yano *et al*., 2006; Ito *et al*., 2008). This chapter addresses the relationship between the absence of Runx3 and the susceptibility to spontaneous EMT in gastric epithelial cells; and to further understand the contribution of the dysregulated TGF-β and Wnt pathways to the observed cellular plasticity.

The cell surface markers analysis revealed that *Runx3*$^{-/-}$ GIF lines displayed a reduced epithelial phenotype that is in contrast to *Runx3*$^{+/+}$ lines (Figure 5.1A). Indeed, further analysis showed that the *Runx3*$^{-/-}$ GIF cells lines were highly sensitised for TGF-β1-induced expression of EMT- and mesenchymal-associated markers (Figure 5.2). This is a paradoxical and intriguing observation as it was previously reported that *Runx3*$^{-/-}$ GIF lines were refractory to TGF-β1-induced apoptosis, consistent with the tumour suppressor activity of RUNX3 (Li *et al*., 2002). The data from the current study suggests that in the absence of Runx3, the TGF-β signal would be diverted from its tumour suppressive and growth modulating functions, towards its EMT-inducing, morphogenetic functions. This point could be tested by analysing activation of the components or target genes of TGF-β-induced growth inhibition and EMT pathways through biochemical methods. These results further suggest that the pleiotropic effects of TGF-β pathway in gastrointestinal carcinogenesis could be due

to the silencing or mutation of an integral component, such as a partner transcription factor like RUNX3.

A negative role of Runx3 in EMT is supported in the reduction of P2 cells by exogenous RUNX3 in GIF-14 cells as revealed by Hoechst 33342 staining (Figure 5.4A and B). Moreover, the re-introduction of RUNX3 also caused a partial blockade of TGF-β1-induced key EMT-promoting factors, *Snail* and *Hmga2* in a DNA-binding dependent manner (Figure 5.5A) Apart from being a negative regulator of EMT, RUNX3 strongly antagonises TGF-β1-induced stem cell-like state as demonstrated in the complete abrogation of stemness-related markers, *Lgr5* and *Sox9* induced by TGF-β1. However, unlike *Snai1* and *Hmga2*, the basal levels of *Lgr5* and *Sox9* were also suppressed by ectopic RUNX3 (Figure 5.5A). As *Lgr5* and *Sox9* are also known Wnt targets, this observation could be due in part to the antagonistic function of RUNX3 against the canonical Wnt pathway, as reported in intestinal epithelial cells (Ito *et al*., 2008). Indeed, the altered response to extracellular cues observed in *Runx3*$^{-/-}$ GIF cell lines is not restricted to TGF-β signaling, but also the Wnt pathway. GIF-14 cells were sensitised to Wnt3a-induction of *Lgr5* and formed spheres more readily compared to *Runx3*$^{+/+}$ GIF-13 cells (Figures 5.6 and 5.7). This negative correlation between *Runx3*-deletion and sphere initiation was further supported by the abolishment of Wnt3a-induction of *Lgr5* and sphere formation by exogenous RUNX3 (Figures 5.8A and 5.9). Together, these data demonstrate that Runx3 acts as a barrier to the acquisition of stem cell-like or plastic state induced either by TGF-β1 or Wnt3a. The negative effects of ectopic RUNX3 on EMT and sphere formation were apparent only 6 days after lentivirus-mediated delivery. These observations are surprising as RUNX3 is known to regulate gene expression through direct transcriptional control. It

is possible that RUNX3 could act through an indirect mechanism in which its target gene is a transcription regulator. Alternatively, RUNX proteins has been reported to control gene expression by remodeling the chromatin structure through interactions with proteins such as histone deacetylases and p300 (Kitabayashi, *et al*. 1998; Lutterbach *et al*. 2000; Amann *et al*. 2001; Westendorf *et al*. 2002; Schroeder *et al*. 2004). Therefore, RUNX3 could function through epigenetic mechanisms and these global changes may occur in a progressive manner.

Lastly, the combined effects of dysregulated TGF-β and Wnt signaling were seen in their strongly cooperative induction of *Lgr5* in GIF-14 cells. A notable aspect of this observation is that the two treatments induced *Lgr5* expression with different kinetics. While Wnt3a transiently activated *Lgr5*, the effect of TGF-β1 was latent (Figure 5.10). The delayed actions of TGF-β1 may indicate that its effects were indirect and possibility acting through intermediate effectors. Alternatively, TGF-β1 may function via epigenetic mechanisms involving the remodeling of chromatin structures, which makes the *Lgr5* locus more accessible to transcription factors. Indeed, this increased accessibility may be the basis of the strong cooperation between TGF-β1 and Wnt3a in inducing *Lgr5* at the later time point (Figure 5.10). The implication herein is that the reprogramming properties of EMT induced by an aberrant TGF-β signal would increase cellular plasticity, as reflected in the reactivation of *Lgr5*. This in turn sensitises cells to the mitogenic effects of the Wnt pathway. In GIF-14 cells, these compounding defects are causal to the genesis of the tumorigenic and stem cell-like P2 subpopulation. This novel molecular mechanism may underlie the tumorigenicity of all *Runx3*$^{-/-}$ GIF cell lines. Finally, our findings may also provide an explanation for the increased phenotypic plasticity and

precancerous conditions observed in adult BALB/c *Runx3*$^{-/-}$ gastric mucosa, characterised by hyperproliferation, development of preneoplastic metaplasia (SPEM) and transdifferentiation into intestinal-like cells.

CHAPTER 6:

Overall discussion

6.1 Summary of findings

Based on the data presented in this study, a model is illustrated in Figure 6.1, where a tumorigenic and mesenchymal-like subpopulation, P2 was identified in the *Runx3*$^{-/-}$.*p53*$^{-/-}$ GIF-14 cell line. Interestingly, the P2 subpopulation expresses high levels of *Lgr5* which is a target gene of the canonical Wnt pathway, and a gastrointestinal stem cell marker. The P2 subpopulation arises through the induction of spontaneous EMT by a constitutively active TGF-β pathway. Moreover, *Runx3*$^{-/-}$ GIF-14 cells were prone to the induction of *Lgr5* and stemness by Wnt3a. The combined effects of overly active TGF-β and Wnt pathways led to the synergistic induction of *Lgr5* expression through cooperative but independent mechanisms. These defects were largely restricted to *Runx3*$^{-/-}$ GIF cell lines, and not observed in *Runx3*$^{+/+}$ lines. Furthermore, the re-introduction of exogenous RUNX3 in GIF-14 cells led to an ablation of P2 cells, suppression of TGF-β1-induced EMT- and stemness-related genes, and abrogation of Wnt3a-induction of *Lgr5*, confirming the negative effect of RUNX3 on EMT and stemness. Collectively, our results demonstrate the critical role of Runx3 in maintaining the gastric epithelial cell phenotype, the absence of which predisposes cells to EMT-induced phenotypic plasticity and the appearance of a tumorigenic and stem cell-like subpopulation.

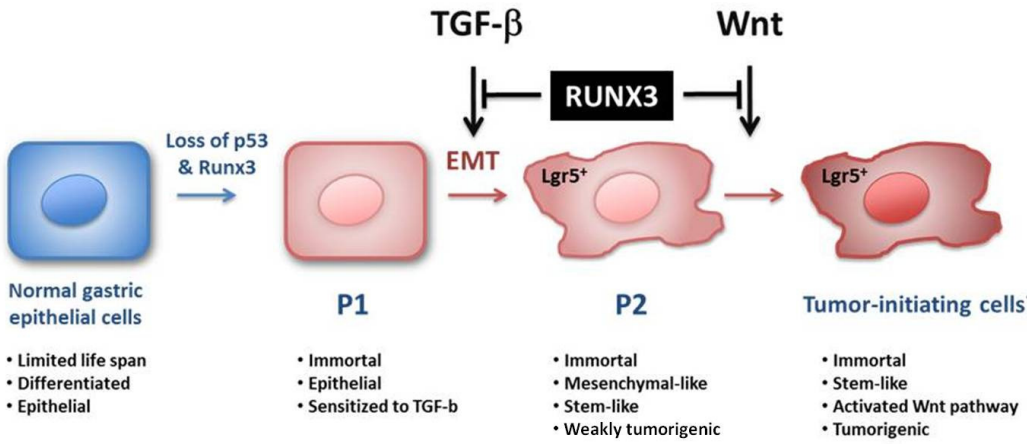

Figure 6.1. A model summarising the role of Runx3 in protecting gastric epithelial cells against EMT-induced cellular plasticity and tumorigenicity.

6.2 Significance of findings

The model of carcinogenesis that involves cumulative genetic mutations typically in tumour suppressors and oncogenes is a well established paradigm. These genetic alterations drive the immortalisation and eventual transformation of normal cells into their malignant derivatives (Nowell, 1976). The multi-step progression of tumours is thought to follow a sequence of clonal successions which ultimately produces a malignant clone most suitable for uncontrolled proliferation in the micro-environment (Nowell, 1976). Recent data from the study of leukemias have revealed that the maintenance and continual evolution of a malignant clone is supported by a small minority of cells, termed "cancer stem cells". Based on their existence, a refined model that holds a hierarchical organisation exists within a tumour mass, and the tumour is propagated by a small subpopulation of cancer cells (Lapidot *et al.*, 1994; Clarke *et al.*, 2006).

Related to the advent of the cancer stem cell theory, recent discovery of aberrant EMT reactivation could generate a stem cell-like state in differentiated mammary epithelial cells further challenge the stem cell origin of cancer (Mani *et al.*, 2008; Morel *et al.*, 2008). The ability of differentiated tumour cells to dedifferentiate into stem cell-like, tumour-initiating cells *in vivo* might resolve some of the conceptual difficulties over the cell-of-origin of cancer. In particular, the observed multipotency of EMT-induced "cancer stem cells" argues that cancer need not to be derived from mutated stem cells, but could derive from differentiated cells (Scheel and Weinberg, 2011). Therefore, EMT has emerged as an important path to a state of phenotypic plasticity, enabling cancer cells to dynamically enter into and exit from stem cell-like state. This notion is strongly supported by our observation that

spontaneous EMT promotes the emergence of a stem cell-like subpopulation within a *Runx3*$^{-/-}$ gastric epithelial cell line, that is concurrently tumorigenic. Furthermore, it implicates a safeguarding role for Runx3 against EMT-induced cellular plasticity and tumour-initiation in gastric epithelial cells, thus fulfilling its tumour suppressor function.

Analogous to the reprogramming properties of EMT to induce phenotypic plasticity, the recently described somatic cell reprogramming has succeeded in converting differentiated cells to pluoripotent stem cells. Of relevance to our study, p53 is shown to play an important regulatory role in both EMT and somatic cell reprogramming. Inactivation of the p53-related pathways was required to greatly enhance the generation of induced pluoripotent stem (iPS) cells, through the escape of p53-mediated senescence and apoptosis (Hong *et al.*, 2009; Kawamaura *et al.*, 2009; Li *et al.*, 2009; Marion *et al.*, 2009; Utikal *et al.*, 2009) Similarly, inactivation of p53 function that enabled cells to evade senescence and apoptosis facilitated the induction of EMT by Twist and Zeb1 proteins as well as growth factors such TGF-β and EGF (Ansieau *et al.*, 2008; Liu *et al.*, 2008; Araki *et al.*, 2010; Ohashi *et al.*, 2010). Thus, it is plausible that the immortalisation of GIF cell lines against a *p53*$^{-/-}$ background may reduce the threshold for the induction of EMT. Given that the *Runx3*$^{+/+}$.*p53*$^{-/-}$ remained resistant to EMT, the protective role of Runx3 against EMT-induced cellular plasticity is highlighted even in the absence of p53.

The representation of stem cell-like cells within tumour cell populations *in vivo* is likely to be influenced by both the intrinsic phenotypic plasticity of these cells and contextual signals (Chaffer *et al.*, 2011). The spontaneous conversion of a stem cell-like subpopulation in GIF-14 cells may be augmented *in vivo* by contextual cues

in the tumour niche, particularly those that drive the EMT. TGF-β and the Wnt pathways are the best known activators of EMT, and the dysregulation of these signaling pathways would collaborate to amplify the induction of EMT and cellular plasticity. This cooperation is clearly demonstrated in the synergistic induction of *Lgr5* by TGF-β1 and Wnt3a in *Runx3*$^{-/-}$ GIF-14 cells, but not in *Runx3*$^{+/+}$ GIF-13 cells. Therefore, an important part the tumour suppressor function of RUNX3 is to ensure that TGF-β and Wnt signaling pathways are properly regulated. In the case of TGF-β pathway, it is conceivable that Runx3 acts as a molecular switch to transduce the tumour suppressive functions of TGF-β and inhibit its EMT-promoting effects by orchestrating a set of genetic programs in gastric epithelial cells. In the absence of Runx3, the transcriptional circuitry would be disrupted and this is reflected in the ability of *Runx3*$^{-/-}$ GIF lines to bypass the tumour suppressive effects of TGF-β1, while becoming sensitised to its EMT-inducing functions.

6.3 Future work

The precise mechanism through which Runx3 interferes with the EMT process remains unknown. Two complementary approaches could be carried out to elucidate this: 1) genome-wide comparative study of P1 and P2 cells to identify putative regulators of EMT; and 2) investigate the potential candidates of RUNX3 target genes. An important finding uncovered from this study is the existence of two distinct cellular states P1 and P2 within the GIF-14 cells, thus genome-wide microarray of P1 and P2 cells would shed light on the potential key regulators of EMT. As TGF-β signaling pathway is a well-established central player in EMT in our model, several candidates mediating the effects of TGF-β have been found. One of the promising candidates is Hmga2, a non-histone chromatin protein which acts as a architectural factor that alters the chromatin structure, and promotes the assembly of protein complexes to regulate transcription (Fusco and Fedele, 2007). This was demonstrated in the cooperation of HMGA2 and Smads to transactivate the transcription of *Snai1* in mammary epithelial cells (Thuault *et al.*, 2008). To gain an insight into the global epigenetic changes mediated by Hmga2, genome-wide chromatin immuno-precipitation (ChIP) of Hmga2 will be performed upon ectopic Hmga2 expression in GIF cells. To demonstrate that *Hmga2* is a direct target of RUNX3, promoter studies could be performed in which *Hmga2* proximal promoter and intronic enhancers containing putative Runx binding sequences will be cloned to study the effects of exogenous RUNX3 on these cis-regulatory elements.

The discovery of a negative role of Runx3 in protecting gastric epithelial cells against EMT-mediated cellular plasticity is made in immortalised GIF cell lines. These lines are pre-conditioned to undergo EMT in the absence of p53 and Runx3. To

validate these data *in vivo*, conditional targeting of *Runx3* using stomach-specific Cre recombinase will be performed to assess whether the loss of Runx3 would cause greater phenotypic plasticity in the gastric mucosa. To complement this, *ex vivo* culture systems using normal gastric epithelial cells and stem cells will be employed. Previously, Barker *et al.* succeeded in generating long-lived gastric organoid structures from single *Lgr5*-positive pyloric stomach stem cells. The gastric organoid cultures would serve as an important platform for *in vitro* deletion of *Runx3* in normal gastric epithelial cells, and specifically in *Lgr5*-positive stem cells.

The aberrant reactivation of EMT in advanced cancer is believed to be a major contributor to tumour metastasis, which allows tumour cells to disseminate from primary tumours to distal sites (Thiery, 2002). As Runx3 is a negative regulator of EMT, its inactivation may render tumour cells prone to the pro-metastatic effects of EMT at later stages of gastric cancer. Indeed, preliminary studies have revealed that the loss of RUNX3 is significantly associated with poor clinical outcome in gastric cancer patients, and its reactivation leads to abrogation of metastasis in animal models (Wei *et al.*, 2005). Therefore, the protective role of Runx3 against gastric cancer metastasis could be further investigated. In conclusion, our findings implicate a safeguarding function of Runx3 against EMT-induced cellular plasticity and tumour-initiation, and perhaps metastasis would partly explain the frequent inactivation of RUNX3 in human gastric cancers Thus, this reinforces that the reactivation of RUNX3 through the administration of DNA methylation inhibitors such as decitabine and azacitidine may present a novel therapeutic strategy for gastric cancer.

PUBLICATIONS

Voon DC*, **Wang H***, Koo JK, Nguyen TA, Hor YT, Chu YS, Ito K, Fukamachi H, Chan SL, Thiery JP, Ito Y (2012). Runx3 protects gastric epithelial cells against epithelial-mesenchymal transition-induced cellular plasticity and tumorigenicity. *Stem Cells*. **30**, 2088-2099. *Equal contribution.

Ito K, Lim AC, Salto-Tellez M, Motoda L, Osato M, Chuang LS, Lee CW, Voon DC, Koo JK, **Wang H**, Fukamachi H, Ito Y (2008). RUNX3 attenuates beta-catenin/T cell factors in intestinal tumorigenesis. *Cancer Cell*. **14**, 226-237.

BIBLIOGRAPHY

Ahmed N, Maines-Bandiera S, Quinn MA, Unger WG, Dedhar S, Auersperg N (2006). Molecular pathways regulating EGF-induced epithelio-mesenchymal transition in human ovarian surface epithelium. *Am J Physiol Cell Physiol.* **290**, C1532–C1542.

Aigner K, Dampier B, Descovich L, Mikula M, Sultan A, Schreiber M, Mikulits W, Brabletz T, Strand D, Obrist P, Sommergruber W, Schweifer N, Wernitznig A, Beug H, Foisner R, Eger A (2007). The transcription factor ZEB1 (deltaEF1) promotes tumour cell dedifferentiation by repressing master regulators of epithelial polarity. *Oncogene*. **26**, 6979–6988.

Akech J, Wixted JJ, Bedard K, van der Deen M, Hussain S, Guise TA, van Wijnen AJ, Stein JL, Languino LR, Altieri DC, Pratap J, Keller E, Stein GS, Lian JB (2010). Runx2 association with progression of prostate cancer in patients: mechanisms mediating bone osteolysis and osteoblastic metastatic lesions. *Oncogene*. **29**, 811–821.

Al-Hajj M, Wicha MS, Benito-Hernandez A, Morrison SJ, Clarke MF (2003). Prospective identification of tumorigenic breast cancer cells. *Proc Nat Acad Sci USA*. **100**, 3983–3988.

Alliston T, Choy L, Ducy P, Karsenty G, Derynck R (2001). TGF-beta-induced repression of CBFA1 by Smad3 decreases cbfa1 and osteocalcin expression and inhibits osteoblast differentiation. *EMBO J.* **20**, 2254-2272.

Ansieau S, Bastid J, Doreau A, Morel AP, Bouchet BP, Thomas C, Fauvet F, Puisieux I, Doglioni C, Piccinin S, Maestro R, Voeltzel T, Selmi A, Valsesia-Wittmann S, Caron de Fromentel C, Puisieux A (2008). Induction of EMT by twist proteins as a collateral effect of tumor-promoting inactivation of premature senescence. *Cancer Cell*. **14**, 79-89.

Araki S, Eitel JA, Batuello CN, Bijangi-Vishehsaraei K, Xie XJ, Danielpour D, Pollok KE, Boothman DA, Mayo LD (2010). TGF-beta1-induced expression of human Mdm2 correlates with late-stage metastatic breast cancer. *J Clin Invest.* **120**, 290-302.

Aronson BD, Fisher AL, Blechman K, Caudy M, Gergen JP (1997). Groucho-dependent and -independent repression activities of Runt domain proteins. *Mol Cell Biol.* **17**, 5581-5587.

Atfi A, Djelloul S, Chastre E, Davis R, Gespach C (1997). Evidence for a role of Rho-like GTPases and stress-activated protein kinase/c-Jun N-terminal kinase (SAPK/JNK) in transforming growth factor beta-mediated signaling. *J Biol Chem*. **272**, 1429-1432.

Bae SC, Takahashi E, Zhang YW, Ogawa E, Shigesada K, Namba Y, Satake M, Ito Y (1995). Cloning, mapping and expression of PEBP2 alpha C, a third gene encoding the mammalian Runt domain. *Gene*. **159**, 245-248.

Bakin AV, Tomlinson AK, Bhowmick NA, Moses HL, Arteaga CL (2000). Phosphatidylinositol 3-kinase function is required for transforming growth factor beta-mediated epithelial to mesenchymal transition and cell migration. *J Biol Chem*. **275**, 36803-36810.

Barker N, van Es JH, Kuipers J, Kujala P, van den Born M, Cozijnsen M, Haegebarth A, Korving J, Begthel H, Peters PJ, Clevers H (2007). Identification of stem cells in small intestine and colon by marker gene Lgr5. *Nature*. **449**, 1003-1007.

Barker N, Ridgway RA, van Es JH, van de Wetering M, Begthel H, van den Born M, Danenberg E, Clarke AR, Sansom OJ, Clevers H (2009). Crypt stem cells as the cells-of-origin of intestinal cancer. *Nature*. **457**, 608-611.

Barker N, Huch M, Kujala P, van de Wetering M, Snippert HJ, van Es JH, Sato T, Stange DE, Begthel H, van den Born M, Danenberg E, van den Brink S, Korving J, Abo A, Peters PJ, Wright N, Poulsom R, Clevers H (2010). Lgr5(+ve) stem cells drive self-renewal in the stomach and build long-lived gastric units in vitro. *Cell Stem Cell*. **6**, 25-36.

Batlle E, Henderson JT, Beghtel H, van den Born MM, Sancho E, Huls G, Meeldijk J, Robertson J, van de Wetering M, Pawson T, Clevers H (2002). Beta-catenin and TCF mediate cell positioning in the intestinal epithelium by controlling the expression of EphB/EphrinB. *Cell*. **111**, 251–263.

Baum B, Settleman J, Quinlan MP (2008). Transitions between epithelial and mesenchymal states in development and disease. *Semin Cell Dev Biol.* **19**, 294–308.

Beachy PA, Karhadkar SS, Berman DM (2004). Tissue repair and stem cell renewal in carcinogenesis. *Nature*. **432**, 324-331.

Behrens J, Jerchow BA, Wurtele M, Grimm J, Asbrand C, Wirtz R, Kuhl M, Wedlich D, Birchmeier W (1998). Functional interaction of an axin homolog, conductin, with beta-catenin, APC, and GSK3beta. *Science*. **280**, 596-599.

Bhowmick NA, Ghiassi M, Bakin A, Aakre M, Lundquist CA, Engel ME, Arteaga CL, Moses HL (2001). Transforming growth factor-beta1 mediates epithelial to mesenchymal transdifferentiation through a RhoA-dependent mechanism. *Mol Biol Cell*. **12**, 27-36.

Bienz M, Clevers H (2000). Linking colorectal cancer to Wnt signaling. *Cell.* **103**, 311-320.

Bindels S, Mestdagt M, Vandewalle C, Jacobs N, Volders L, Noël A, van Roy F, Berx G, Foidart JM, Gilles C (2006). Regulation of vimentin by SIP1 in human epithelial breast tumor cells. *Oncogene*. **25**, 4975-4985.

Bjornson CR, Rietze RL, Reynolds BA, Magli MC, Vescovi AL (1999). Turning brain into blood: a hematopoietic fate adopted by adult neural stem cells in vivo. *Science*. **283**, 534-537.

Bodnar AG, Ouellette M, Frolkis M, Holt SE, Chiu CP, Morin GB, Harley CB, Shay JW, Lichtsteiner S, Wright WE (1998). Extension of life-span by introduction of telomerase into normal human cells. *Science*. **279**, 349-352.

Boyer B, Valles AM, Edme N (2000). Induction and regulation of epithelial-mesenchymal transitions. *Biochem Pharmacol*. **60**, 1091-1099.

Brabletz T, Jung A, Reu S, Porzner M, Hlubek F, Kunz-Schughart LA, Knuechel R, Kirchner T (2001). Variable beta-catenin expression in colorectal cancers indicates tumor progression driven by the tumor environment. *Proc Natl Acad Sci USA*. **98**, 10356–10361.

Britos-Bray M, Friedman AD (1997). Core binding factor cannot synergistically activate the myeloperoxidase proximal enhancer in immature myeloid cells without c-Myb. *Mol Cell Biol*. **17**, 5127–5135.

Bukrinsky MI, Haggerty S, Dempsey MP, Sharova N, Adzhubel A, Spitz L, Lewis P, Goldfarb D, Emerman M, Stevenson M (1993). A nuclear localization signal within HIV-1 matrix protein that governs infection of non-dividing cells. *Nature.* **365**, 666-669.

Bunting KD, Zhou S, Lu T, Sorrentino BP (2000). Enforced P-glycoprotein pump function in murine bone marrow cells results in expansion of side population stem cells in vitro and repopulating cells in vivo. *Blood*. **96**, 902-909.

Burkert J, Otto WR, Wright NA (2008). Side populations of gastrointestinal cancers are not enriched in stem cells. *J Pathol.* **214**, 564-573.

Carver EA, Jiang R, Lan Y, Oram KF, Gridley T (2001). The mouse snail gene encodes a key regulator of the epithelial-mesenchymal transition. *Mol Cell Biol.* **21**, 8184-8188.

Chaffer CL, Brennan JP, Slavin JL, Blick T, Thompson EW, Williams ED (2006). Mesenchymal-to-epithelial transition facilitates bladder cancer metastasis: Role of fibroblast growth factor receptor-2. *Cancer Res*. **66**, 11271–11278.

Chaffer CL, Brueckmann I, Scheel C, Kaestli AJ, Wiggins PA, Rodrigues LO, Brooks M, Reinhardt F, Su Y, Polyak K, Arendt LM, Kuperwasser C, Bierie B, Weinberg RA (2011). Normal and neoplastic nonstem cells can spontaneously convert to a stem cell-like state. *Proc Natl Acad Sci USA*. **108**, 7950-7955.

Challen GA, Little MH (2006). A side order of stem cells: the SP phenotype. *Stem Cells*. **24**, 3-12.

Chang TL, Ito K, Ko TK, Liu Q, Salto-Tellez M, Yeoh KG, Fukamachi H, Ito Y (2010). Claudin-1 has tumor suppressive activity and is a direct target of RUNX3 in gastric epithelial cells. *Gastroenterology*. **138**, 255-265.

Chi XZ, Yang JO, Lee KY, Ito K, Sakakura C, Li QL, Kim HR, Cha EJ, Lee YH, Kaneda A, Ushijima T, Kim WJ, Ito Y, Bae SC (2005). RUNX3 suppresses gastric epithelial cell growth by inducing p21(WAF/Cip1) expression in cooperation with transforming growth factor beta-activated SMAD. *Mol Cell Biol*. **25**, 8097–8107.

Chiba T, Kita K, Zheng YW, Yokosuka O, Saisho H, Iwama A, Nakauchi H, Taniguchi H (2006). Side population purified from hepatocellular carcinoma cells harbors cancer stem cell-like properties. *Hepatology*. **44**, 240-251.

Cifone MA, Fidler IJ (1980). Correlation of patterns of anchorage-independent growth with in vivo behavior of cells from a murine fibrosarcoma. *Proc Natl Acad Sci USA*. **77**, 1039-1043.

Clarke MF, Dick JE, Dirks PB, Eaves CJ, Jamieson CH, Jones DL, Visvader J, Weissman IL, Wahl GM (2006). Cancer stem cells--perspectives on current status and future directions: AACR Workshop on cancer stem cells. *Cancer Res*. **66**, 9339-9344.

Clevers H (2006). Wnt/beta-catenin signaling in development and disease. *Cell.* **127**, 469-480.

Cui W, Fowlis DJ, Bryson S, Duffie E, Ireland H, Balmain A, Akhurst RJ (1996). TGFbeta1 inhibits the formation of benign skin tumors, but enhances progression to invasive spindle carcinomas in transgenic mice. *Cell*. **86**, 531-542.

Das K, Leong DT, Gupta A, Shen L, Putti T, Stein GS, van Wijnen AJ, Salto-Tellez M (2009). Positive association between nuclear Runx2 and oestrogen-progesterone receptor gene expression characterises a biological subtype of breast cancer. *Eur J Cancer*. **45**, 2239–2248.

Derynck R, Feng XH (1997). TGF-beta receptor signaling. *Biochim Biophys Acta*. **1333,** F105-150.

Derynck R, Akhurst RJ, Balmain A (2001). TGF-beta signaling in tumor suppression and cancer progression. *Nat Genet.* **29**, 117–129.

Dickson MC, Martin JS, Cousins FM, Kulkarni AB, Karlsson S, Akhurst RJ (1995). Defective haematopoiesis and vasculogenesis in transforming growth factor-beta 1 knock out mice. *Development*. **121**, 1845-1854.

Doherty GJ, McMahon HT (2008). Mediation, modulation, and consequences of membrane-cytoskeleton interactions. *Annu Rev Biophys*. **37**, 65-95.

Dong HY, Wilkes S, Yang H (2011). CD71 is selectively and ubiquitously expressed at high levels in erythroid precursors of all maturation stages: a comparative immunochemical study with glycophorin A and hemoglobin A. *Am J Surg Pathol*. **35**, 723-732.

Dontu G, Abdallah WM, Foley JM, Jackson KW, Clarke MF, Kawamura MJ, Wicha MS (2003). In vitro propagation and transcriptional profiling of human mammary stem/progenitor cells. *Genes Dev*. **17**, 1253-1270.

Drayton S, Peters G (2002). Immortalisation and transformation revisited. *Curr Opin Genet Dev*. **12**, 98-104.

Ducy P, Starbuck M, Priemel M, Shen J, Pinero G, Geoffroy V, Amling M, Karsenty G (1999). A Cbfa1-dependent genetic pathway controls bone formation beyond embryonic development. *Genes Dev*. **13**, 1025-1036.

Duffy JB, Gergen JP (1991). The Drosophila segmentation gene *runt* acts as a position-specific numerator element necessary for the uniform expression of the sex-determining gene *Sex-lethal*. *Genes Dev*. **5**, 2176–2187.

Duffy JB, Kania MA, Gergen JP (1991). Expression and function of the Drosophila gene *runt* in early stages of neural development. *Development.* **113**, 1223–1230.

Feng XH, Derynck R (2005). Specificity and versatility in TGF-beta signaling through Smads. *Annu Rev Cell Dev Biol*. **21**, 659-93.

Flanagan SP (1966). 'Nude', a new hairless gene with pleiotropic effects in the mouse. *Genet Res*. **8**, 295-309.

Frey RS, Mulder KM (1997). Involvement of extracellular signal-regulated kinase 2 and stress-activated protein kinase/Jun N-terminal kinase activation by transforming growth factor beta in the negative growth control of breast cancer cells. *Cancer Res*. 57, 628-633.

Fristrom D (1988). The cellular basis of epithelial morphogenesis. *Tissue Cell*. **20**, 645-690.

Fukamachi H, Ito K, Ito Y (2004). *Runx3*$^{-/-}$ gastric epithelial cells differentiate into intestinal type cells. *Biochem Biophys Res Commun.* **321**, 58-64.

Fukamachi H, Mimata A, Tanaka I, Ito K, Ito Y, Yuasa Y (2008). In vitro differentiation of *Runx3*$^{-/-}$ *p53*$^{-/-}$ gastric epithelial cells into intestinal type cells. *Cancer Sci*. **99**, 671-676.

Fusco A, Fedele M (2007). Roles of HMGA proteins in cancer. *Nat Rev Cancer*. **7**, 899-910.

Galceran J, Sustmann C, Hsu SC, Folberth S, Grosschedl R (2004). LEF1-mediated regulation of Delta-like1 links Wnt and Notch signaling in somitogenesis. *Genes Dev*. **18**, 2718-2723.

Garcia-Castro M, Bronner-Fraser M (1999). Induction and differentiation of the neural crest. *Curr Opin Cell Biol*. **11**, 695-698.

Golub TR, Barker GF, Bohlander SK, Hiebert SW, Ward DC, Bray-Ward P, Morgan E, Raimondi SC, Rowley JD, Gilliland DG (1995). Fusion of the TEL gene on 12p13 to the AML1 gene on 21q22 in acute lymphoblastic leukemia. *Proc Natl Acad Sci USA*. **92**, 4917-4921.

Goodell MA, Brose K, Paradis G, Conner AS, Mulligan RC (1996). Isolation and functional properties of murine hematopoietic stem cells that are replicating in vivo. *J Exp Med*. **183**, 1797-1806.

Goodell MA, Rosenzweig M, Kim H, Marks DF, DeMaria M, Paradis G, Grupp SA, Sieff CA, Mulligan RC, Johnson RP (1997). Dye efflux studies suggest that hematopoietic stem cells expressing low or undetectable levels of CD34 antigen exist in multiple species. *Nat Med*. **3**, 1337-1345.

Growney JD, Shigematsu H, Li Z, Lee BH, Adelsperger J, Rowan R, Curley DP, Kutok JL, Akashi K, Williams IR, Speck NA, Gilliland DG (2005). Loss of Runx1 perturbs adult hematopoiesis and is associated with a myeloproliferative phenotype. *Blood.* **106**, 494-504.

Hanafusa H, Ninomiya-Tsuji J, Masuyama N, Nishita M, Fujisawa J, Shibuya H, Matsumoto K, Nishida E (1999). Involvement of the p38 mitogen-activated protein kinase pathway in transforming growth factor-beta-induced gene expression. *J Biol Chem*. **274**, 27161-27167.

Hanai J, Chen LF, Kanno T, Ohtani-Fujita N, Kim WY, Guo WH, Imamura T, Ishidou Y, Fukuchi M, Shi MJ, Stavnezer J, Kawabata M, Miyazono K, Ito Y (1999). Interaction and functional cooperation of PEBP2/CBF with Smads. Synergistic induction of the immunoglobulin germline C alpha promoter. *J Biol Chem.* **274**, 31577-31582.

Haraguchi N, Utsunomiya T, Inoue H, Tanaka F, Mimori K, Barnard GF, Mori M (2006). Characterization of a side population of cancer cells from human gastrointestinal system. *Stem Cells*. **24**, 506-513.

Hartsough MT, Mulder KM (1995). Transforming growth factor beta activation of p44mapk in proliferating cultures of epithelial cells. *J Biol Chem*. **270**, 7117-7124.

Hay ED (1968). Organization and fine structure of epithelium and mesenchyme in the developing chick embryo. In *Epithelial-Mesenchymal Interactions; 18th Hahnemann Symposium*, (eds. R. Fleischmajer, & R. E. Billingham), Williams & Wilkins, Baltimore.

Hay ED (1995). An overview of epithelio-mesenchymal transformation. *Acta Anat*. **154**, 8-20.

He TC, Sparks AB, Rago C, Hermeking H, Zawel L, de Costa LT, Morin PJ, Vogelstein B, Kinzler KW (1998). Identification of c-MYC as a target of the APC pathway. *Science.* **281**, 1509–1512.

Heldin CH, Landstrom M, Moustakas A (2009). Mechanism of TGF-beta signaling to growth arrest, apoptosis, and epithelial-mesenchymal transition. *Curr Opin Cell Biol*. **21**, 166-176.

Hernandez-Munain C, Krangel MS (1994). Regulation of the T-cell receptor delta enhancer by functional cooperation between c-Myb and core-binding factors. *Mol Cell Biol*. **14**, 473–483.

Ho MM, Ng AV, Lam S, Hung JY (2007). Side population in human lung cancer cell lines and tumors is enriched with stem cell-like cancer cells. *Cancer Res*. **67**, 4827-4833.

Hong H, Takahashi K, Ichisaka T, Aoi T, Kanagawa O, Nakagawa M, Okita K, Yamanaka S (2009). Suppression of induced pluripotent stem cell generation by the p53-p21 pathway. *Nature.* **460**, 1132-1135.

Howe JR, Roth S, Ringold JC, Summers RW, Jarvinen HJ, Sistonen P, Tomlinson IP, Houlston RS, Bevan S, Mitros FA, Stone EM, Aaltonen LA (1998). Mutations in the SMAD4/DPC4 gene in juvenile polyposis. *Science*. **280**, 1086−1088.

Ibrahim SF, Diercks AH, Petersen TW, van den Engh G (2007). Kinetic analyses as a critical parameter in defining the side population (SP) phenotype. *Exp Cell Res*. **313**, 1921-1926.

Ichikawa M, Asai T, Saito T, Seo S, Yamazaki I, Yamagata T, Mitani K, Chiba S, Ogawa S, Kurokawa M, Hirai H (2004). AML-1 is required for megakaryocytic maturation and lymphocytic differentiation, but not for maintenance of hematopoietic stem cells in adult hematopoiesis. *Nat Med*. **10**, 299-304.

Ikenouchi J, Matsuda M, Furuse M, Tsukita S (2003). Regulation of tight junctions during the epithelium-mesenchyme transition: direct repression of the gene expression of claudins/occluding by Snail. *J Cell Sci.* **116**, 1959-1967.

Imai Y, Kurokawa M, Tanaka K, Friedman AD, Ogawa S, Mitani K, Yazaki Y, Hirai H (1998). TLE, the human homolog of groucho, interacts with AML1 and acts as a repressor of AML1-induced transactivation. *Biochem Biophys Res Commun*. **252**, 582-589.

Ingham P, Gergen P (1988). Interactions between the pairrule genes *runt, hairy, even-skipped* and *fushi tarazu* and the establishment of periodic pattern in Drosophila embryo. *Development.* **104**, 51–60.

Inman GJ, Nicolas FJ, Callahan JF, Harling JD, Gaster LM, Reith AD, Laping NJ, Hill CS (2002). SB-431542 is a potent and specific inhibitor of transforming growth factor-beta superfamily type I activin receptor-like kinase (ALK) receptors ALK4, ALK5, and ALK7. *Mol Pharmacol*. **62**, 65-74.

Inoue K, Ozaki S, Shiga T, Ito K, Masuda T, Okado N, Iseda T, Kawaguchi S, Ogawa M, Bae SC, Yamashita N, Itohara S, Kudo N, Ito Y (2002). *Runx3* controls the axonal projection of proprioceptive dorsal root ganglion neurons. *Nat Neurosci.* **5**, 946–954.

Inoue K, Ito K, Osato M, Lee B, Bae SC, Ito Y (2007). The transcription factor Runx3 represses the neurotrophin receptor TrkB during lineage commitment of dorsal root ganglion neurons. *J Biol Chem.* **282**, 24175-24184.

Irie HY, Pearline RV, Grueneberg D, Hsia M, Ravichandran P, Kothari N, Natesan S, Brugge JS (2005). Distinct roles of Akt1 and Akt2 in regulating cell migration and epithelial-mesenchymal transition. *J Cell Biol*. **171**, 1023–1034.

Ito K, Liu Q, Salto-Tellez M, Yano T, Tada K, Ida H, Huang C, Shah N, Inoue M, Rajnakova A, Hiong KC, Peh BK, Han HC, Ito T, Teh M, Yeoh KG, Ito Y (2005). RUNX3, a novel tumor suppressor, is frequently inactivated in gastric cancer by protein mislocalization. *Cancer Res.* **65**, 7743-7750.

Ito K, Lim AC, Salto-Tellez M, Motoda L, Osato M, Chuang LS, Lee CW, Voon DC, Koo JK, Wang H, Fukamachi H, Ito Y (2008). RUNX3 attenuates beta-catenin/T cell factors in intestinal tumorigenesis. *Cancer Cell.* **14**, 226-237.

Ito K, Chuang LS, Ito T, Chang TL, Fukamachi H, Salto-Tellez M, Ito Y (2011). Loss of Runx3 is a key event in inducing precancerous state of the stomach. *Gastroenterology.* **140**, 1536-1546.

Ito K, Inoue KI, Bae SC, Ito Y (2009). Runx3 expression in gastrointestinal tract epithelium: resolving the controversy. *Oncogene*. **28**, 1379-1384.

Ito M, Hiramatsu H, Kobayashi K, Suzue K, Kawahata M, Hioki K, Ueyama Y, Koyanagi Y, Sugamura K, Tsuji K, Heike T, Nakahata T (2002). NOD/SCID/gamma(c)(null) mouse: an excellent recipient mouse model for engraftment of human cells. *Blood*. **100,** 3175-3182.

Ito Y (1999). Molecular basis of tissue-specific gene expression mediated by the Runt domain transcription factor PEBP2/CBF. *Genes Cells.* **4**, 685-696.

Ito Y (2004). Oncogenic potential of the RUNX gene family, 'Overview'. *Oncogene.* **23**, 4198-4208.

Ito Y (2008). RUNX genes in development and cancer: regulation of viral gene expression and the discovery of RUNX family genes. *Adv Cancer Res*. **99**, 33–76.

Jacob B, Osato M, Yamashita N, Wang CQ, Taniuchi I, Littman DR, Asou N, Ito Y (2010). Stem cell exhaustion due to Runx1 deficiency is prevented by Evi5 activation in leukemogenesis. *Blood.* **115**, 1610-1620.

Jang YY, Ye Z, Cheng L (2011). Molecular imaging and stem cell research. *Mol Imaging*. **10**, 111-122.

Javed A, Barnes GL, Pratap J, Antkowiak T, Gerstenfeld LC, van Wijnen AJ, Stein JL, Lian JB, Stein GS (2005). Impaired intranuclear trafficking of Runx2 (AML3/CBFA1) transcription factors in breast cancer cells inhibits osteolysis in vivo. *Proc Natl Acad Sci USA*. **102**, 1454–1459.

Javed A, Guo B, Hiebert S, Choi JY, Green J, Zhao SC, Osborne MA, Stifani S, Stein JL, Lian JB, van Wijnen AJ, Stein GS (2000). Groucho/TLE/R-esp proteins associate with the nuclear matrix and repress RUNX (CBF(alpha)/AML/PEBP2(alpha)) dependent activation of tissue-specific gene transcription. *J Cell Sci*. **113**, 2221-2231.

Kafri T, Blomer U, Peterson DA, Gage FH, Verma IM (1997). Sustained expression of genes delivered directly into liver and muscle by lentiviral vectors. *Nat Genet*. **17**, 314–317.

Kamachi Y, Ogawa E, Asano M, Ishida S, Murakami Y, Satake M, Ito Y, Shigesada K (1990). Purification of a mouse nuclear factor that binds to both the A and B cores of the polyomavirus enhancer. *J Virol*. **64**, 4808-4819.

Kania MA, Bonner AS, Duffy JB, Gergen JP (1990). The *Drosophila* segmentation gene runt encodes a novel nuclear regulatory protein that is also expressed in the developing nervous system. *Genes Dev*. **4**, 1701–1713.

Kawamura T, Suzuki J, Wang YV, Menendez S, Morera LB, Raya A, Wahl GM, Izpisua Belmonte JC (2009). Linking the p53 tumour suppressor pathway to somatic cell reprogramming. *Nature*. **460**, 1140-1144.

Kim K, Lu Z, Hay ED (2002). Direct evidence for a role of beta-catenin/LEF-1 signaling pathway in induction of EMT. *Cell Biol Int.* **26**, 463-476.

Kim WY, Sieweke M, Ogawa E, Wee HJ, Englmeier U, Graf T, Ito Y (1999). Mutual activation of Ets-1 and AML1 DNA binding by direct interaction of their autoinhibitory domains. *EMBO J*. **18**, 1609–1620.

Kinzler KW, Vogelstein B (1996). Lessons from hereditary colorectal cancer. *Cell.* **87**, 159-170.

Kitabayashi I, Yokoyama A, Shimizu K, Ohki M (1998). Interaction and functional cooperation of the leukemia-associated factors AML1 and p300 in myeloid cell differentiation. *EMBO J*. **17**, 2994-3004.

Klymkowsky MW, Savagner P (2009). Epithelial-mesenchymal transition: a cancer researcher's conceptual friend and foe. *Am J Pathol*. **174**, 1588-1593.

Kolega J (1985). The cellular basis of epithelial morphogenesis. *Dev Biol*. **2**:103-143.

Kolligs FT, Bommer G, Goke B (2002). Wnt/β-catenin/Tcf signaling, A critical pathway in gastrointestinal tumorigenesis. *Digestion.* **66,** 131-144.

Komori T, Yagi H, Nomura S, Yamaguchi A, Sasaki K, Deguchi K, Shimizu Y, Bronson RT, Gao YH, Inada M, Sato M, Okamoto R, Kitamura Y, Yoshiki S, Kishimoto T (1997). Targeted disruption of *Cbfa1* results in a complete lack of bone formation owing to maturational arrest of osteoblasts. *Cell.* **89**, 755–764.

Kondo T, Setoguchi T, Taga T (2004). Persistence of a small subpopulation of cancer stem cell-like cells in the C6 glioma cell line. *Proc Natl Acad Sci USA.* **101**, 781–786.

Kong D, Li Y, Wang Z, Sarkar FH (2011). Cancer Stem Cells and Epithelial-to-Mesenchymal Transition (EMT)-Phenotypic Cells: Are They Cousins or Twins? *Cancers (Basel).* **3**, 716-729.

Korinek V, Barker N, Moerer P, van Donselaar E, Huls G, Peters PJ, Clevers H (1998). Depletion of epithelial stem-cell compartments in the small intestine of mice lacking Tcf-4. *Nat Genet.* **19**, 379-383.

Krieger M, Scott MP, Matsudaira PT, Lodish HF, Darnell JE, Zipursky L, Kaiser C, Berk A (2004). *Molecular cell biology*. (5th edition).

Latza U, Niedobitek G, Schwarting R, Nekarda H, Stein H (1990). Ber-EP4: new monoclonal antibody which distinguishes epithelia from mesothelial. *J Clin Pathol.* **43**, 213-219.

Lee KS, Kim HJ, Li QL, Chi XZ, Ueta C, Komori T, Wozney JM, Kim EG, Choi JY, Ryoo HM, Bae SC (2000). Runx2 is a common target of transforming growth factor beta1 and bone morphogenetic protein 2, and cooperation between Runx2 and Smad5 induces osteoblast-specific gene expression in the pluripotent mesenchymal precursor cell line C2C12. *Mol Cell Biol.* **20**, 8783-8792.

Levanon D, Bettoun D, Harris-Cerruti C, Woolf E, Negreanu V, Eilam R, Bernstein Y, Goldenberg D, Xiao C, Fliegauf M, Kremer E, Otto F, Brenner O, Lev-Tov A and Groner Y (2002). The Runx3 transcription factor regulates development and survival of TrkC dorsal root ganglia neurons. *EMBO J.* **21**, 3454-3463.

Levanon D, Negreanu V, Bernstein Y, Bar-Am I, Avivi L, Groner Y (1994). AML1, AML2, and AML3, the human members of the runt domain gene-family: cDNA structure, expression, and chromosomal localization. *Genomics.* **23**, 425-432.

Li C, Heidt DG, Dalerba P, Burant CF, Zhang L, Adsay V, Wicha M, Clarke MF, Simeone DM (2007). Identification of pancreatic cancer stem cells. *Cancer Res.* **67**, 1030-1037.

Li H, Collado M, Villasante A, Strati K, Ortega S, Cañamero M, Blasco MA, Serrano M (2009). The Ink4/Arf locus is a barrier for iPS cell reprogramming. *Nature*. **460**, 1136-1139.

Li QL, Ito K, Sakakura C, Fukamachi H, Inoue K, Chi XZ, Lee KY, Nomura S, Lee CW, Han SB, Kim HM, Kim WJ, Yamamoto H, Yamashita N, Yano T, Ikeda T, Itohara S, Inazawa J, Abe T, Hagiwara A, Yamagishi H, Ooe A, Kaneda A, Sugimura T, Ushijima T, Bae SC, Ito Y (2002). Causal relationship between the loss of *RUNX3* expression and gastric cancer. *Cell.* **109**, 113-124.

Liao MJ, Zhang CC, Zhou B, Zimonjic DB, Mani SA, Kaba M, Gifford A, Reinhardt F, Popescu NC, Guo W, Eaton EN, Lodish HF, Weinberg RA (2007). Enrichment of a

population of mammary gland cells that form mammospheres and have in vivo repopulating activity. *Cancer Res*. **67**, 8131-8138.

Lim M, Zhong C, Yang S, Bell AM, Cohen MB, Roy-Burman P (2010). Runx2 regulates
survivin expression in prostate cancer cells. *Lab Invest*. **90**, 222–233.

Linardopoulos S, Street AJ, Quelle DE, Parry D, Peters G, Sherr CJ, Balmain A (1995). Deletion and altered regulation of p16INK4a and p15INK4b in undifferentiated mouse skin tumors. *Cancer Res*. **55**, 5168-5172.

Liu Y, El-Naggar S, Darling DS, Higashi Y, Dean DC (2008). Zeb1 links epithelial-mesenchymal transition and cellular senescence. *Development.* **135**, 579–588.

Llorens A, Rodrigo I, López–βarcons L, Gonzalez-Garrigues M, Lozano E, Vinyals A, Quintanilla M, Cano A, Fabra A (1998). Down-regulation of E-cadherin in mouse skin carcinoma cells enhances a migratory and invasive phenotype linked to matrix metalloproteinase-9 gelatinase expression. *Lab Invest.* **78**, 1131-1142.

Lo PK, Kanojia D, Liu X, Singh UP, Berger FG, Wang Q, Chen H (2011). CD49f and CD61 identify Her2/neu-induced mammary tumor-initiating cells that are potentially derived from luminal progenitors and maintained by the integrin-TGFbeta signaling. *Oncogene*. **31**, 2614-2626.

Look AT (1997). Oncogenic transcription factors in the human acute leukemias. *Science.* **278**, 1059–1064.

Lorenz K, Rupf T, Salvetter J, Bader A (2009). Enrichment of human beta 1 bri/alpha 6 bri/CD71 dim keratinocytes after culture in defined media. *Cells Tissues Organs*. **189**, 382-390.

Lu SL, Zhang WC, Akiyama Y, Nomizu T, Yuasa Y (1996). Genomic structure of the transforming growth factor β type II receptor gene and its mutations in hereditary nonpolyposis colorectal cancers. *Cancer Res.* **56**, 4595–4598.

Mani SA, Guo W, Liao MJ, Eaton EN, Ayyanan A, Zhou AY, Brooks M, Reinhard F, Zhang CC, Shipitsin M, Campbell LL, Polyak K, Brisken C, Yang J, Weinberg RA (2008). The epithelial-mesenchymal transition generates cells with properties of stem cells. *Cell*. **133**, 704–715.

Markowitz S, Wang J, Myeroff L, Parsons R, Sun L, Lutterbaugh J, Fan RS, Zborowska E, Kinzler KW, Vogelstein B, Markowitz, S (1995). Inactivation of the type II TGF-β receptor in colon cancer cells with microsatellite instability. *Science*. **268**, 1336–1338.

Marieb EM (1995). *Human Anatomy and Physiology*. (3rd edition).

Marion RM, Strati K, Li H, Murga M, Blanco R, Ortega S, Fernandez-Capetillo O, Serrano M, Blasco MA (2009). A p53-mediated DNA damage response limits reprogramming to ensure iPS cell genomic integrity. *Nature.* **460**, 1149-1153.

Massague J (2008). TGFbeta in Cancer. *Cell*. **134**, 215-230.

Massague J, Gomis RR (2006). The logic of TGFbeta signaling. *FEBS Lett*. **580**, 2811-2820.

Massague J, Seoane J, Wotton D (2005). Smad transcription factors. *Genes Dev*. **19**, 2783-2810.

Mishra L, Shetty K, Tang Y, Stuart A, Byers SW (2005). The role of TGF-beta and Wnt signaling in gastrointestinal stem cells and cancer. *Oncogene*. **24**, 5775–5789.

Mitani K, Ogawa S, Tanaka T, Miyoshi H, Kurokawa M, Mano H, Yazaki Y, Ohki M, Hirai H (1994). Generation of the AML1-EVI-1 fusion gene in the t(3;21)(q26;q22) causes blastic crisis in chronic myelocytic leukemia. *EMBO J.* **13**, 504-510.

Miyazono K, Maeda S, Imamura T (2004). Coordinate regulation of cell growth and differentiation by TGF-beta superfamily and Runx proteins. *Oncogene*. **23**, 4232-4237.

Molofsky AV, Pardal R, Morrison SJ (2004). Diverse mechanisms regulate stem cell self-renewal. *Curr Opin Cell Biol*. **16**, 700-707.

Miyoshi H, Takahashi M, Gage FH, Verma IM (1997). Stable and efficient gene transfer into the retina using an HIV-based lentiviral vector. *Proc Natl Acad Sci USA*. **94**, 10319-10323.

Moore KA, Lemischka IR (2006). Stem cells and their niches. *Science*. **311**, 1880-1885.

Morel AP, Lievre M, Thomas C, Hinkal G, Ansieau S, Puisieux A (2008). Generation of breast cancer stem cells through epithelial-mesenchymal transition. *PLoS ONE.* **3**, e2888.

Moreno-Bueno G, Portillo F, Cano A (2008). Transcriptional regulation of cell polarity in EMT and cancer. *Oncogene*. **27**, 6958-6969.

Morita Y, Ema H, Yamazaki S, Nakauchi H (2006). Non-side-population hematopoietic stem cells in mouse bone marrow. *Blood.* **108,** 2850-2856.

Moser AR, Pitot HC, Dove WF (1990). A dominant mutation that predisposes to multiple intestinal neoplasia in the mouse. *Science*. **247**, 322–324.

Motoda L, Osato M, Yamashita N, Jacob B, Chen LQ, Yanagida M, Ida H, Wee HJ, Sun AX, Taniuchi I, Littman D, Ito Y (2007). Runx1 protects hematopoietic stem/progenitor cells from oncogenic insult. *Stem Cells.* **25**, 2976-2986.

Moustakas A, Heldin CH (2007). Signaling networks guiding epithelial-mesenchymal transitions during embryogenesis and cancer progression. *Cancer Sci*. **98**, 1512–1520.

Naldini L, Blomer U, Gage FH, Trono D, Verma IM (1996). Efficient transfer, integration, and sustained long-term expression of the transgene in adult rat brains injected with a lentiviral vector. *Proc Natl Acad Sci USA*. **93**, 11382-11388.

Nieto MA (2011).The ins and outs of the epithelial to mesenchymal transition in health and disease. *Annu Rev Cell Dev Biol*. **27**, 347-376.

North T, Gu TL, Stacy T, Wang Q, Howard L, Binder M, Marín-Padilla M, Speck NA (1999). Cbfa2 is required for the formation of intraaortic hematopoietic clusters. *Development.* **126**, 2563– 2575.

Nowell PC (1976). The clonal evolution of tumor cell populations. *Science*. **194**, 23-28.

Nucifora G, Begy CR, Erickson P, Drabkin HA, Rowley JD (1993). The 3;21 translocation in myelodysplasia results in a fusion transcript between the AML1 gene and the gene for EAP, a highly conserved protein associated with the Epstein-Barr virus small RNA EBER 1. *Proc Natl Acad Sci USA.* **90**, 7784-7788.

Ogawa E, Inuzuka M, Maruyama M, Satake M, Naito-Fujimoto M, Ito Y, Shigesada K (1993). Molecular cloning and characterization of PEBP2 beta, the heterodimeric partner of a novel Drosophila runt-related DNA binding protein PEBP2 alpha. *Virology*. **194**, 314-331.

Ogawa E, Maruyama M, Kagoshima H, Inuzuka M, Lu J, Satake M, Shigesada K, Ito Y. PEBP2/PEA2 represents a family of transcription factors homologous to the products of the Drosophila runt gene and the human AML1 gene (1993). *Proc Natl Acad Sci USA.* **90**, 6859-6863.

Ohashi S, Natsuizaka M, Wong GS, Michaylira CZ, Grugan KD, Stairs DB, Kalabis J, Vega ME, Kalman RA, Nakagawa M, Klein-Szanto AJ, Herlyn M, Diehl JA, Rustgi AK, Nakagawa H (2010). Epidermal growth factor receptor and mutant p53 expand an esophageal cellular subpopulation capable of epithelial-to-mesenchymal transition through ZEB transcription factors. *Cancer Res*. **70**, 4174-4184.

Ohkuma M, Haraguchi N, Ishii H, Mimori K, Tanaka F, Kim HM, Shimomura M, Hirose H, Yanaga K, Mori M (2011). Absence of CD71 Transferrin Receptor Characterizes Human Gastric Adenosquamous Carcinoma Stem Cells. *Ann Surg Oncol.* **19**, 1357-1364.

Okuda T, van Deursen J, Hiebert SW, Grosveld G, Downing JR (1996). AML1, the target of multiple chromosomal translocations in human leukemia, is essential for normal fetal liver hematopoiesis. *Cell.* **84**, 321–330.

Otto F, Thornell AP, Crompton T, Denzel A, Gilmour KC, Rosewell IR, Stamp GW, Beddington RS, Mundlos S, Olsen BR, Selby PB, Owen MJ (1997). *Cbfa1*, a

candidate gene for cleidocranial dysplasia syndrome, is essential for osteoblast differentiation and bone development. *Cell.* **89**, 765–771.

Ozawa M, Baribault H, Kemler R (1989). The cytoplasmic domain of the cell adhesion molecule uvomorulin associates with three independent proteins structurally related in different species. *EMBO J*. **8**, 1711-1717.

Ozdamar B, Bose R, Barrios-Rodiles M, Wang HR, Zhang Y, Wrana JL (2005). Regulation of the polarity protein Par6 by TGFbeta receptors controls epithelial cell plasticity. *Science*. **307**, 1603-1609.

Pardal R, Clarke MF, Morrison SJ (2003). Applying the principles of stem-cell biology to cancer. *Nat Rev Cancer*. **3**, 895-902.

Pardali E, Xie XQ, Tsapogas P, Itoh S, Arvanitidis K, Heldin CH, ten Dijke P, Grundström T, Sideras P (2000). Smad and AML proteins synergistically confer transforming growth factor beta1 responsiveness to human germ-line IgA genes. *J Biol Chem.* **275**, 3552-3560.

Park K, Kim SJ, Bang YJ, Park JG, Kim NK, Roberts AB, Sporn MB (1994). Genetic changes in the transforming growth factor β (TGF-β) type II receptor gene in human gastric cancer cells: correlation with sensitivity to growth inhibition by TGF-β. *Proc. Natl Acad Sci USA*. **91**, 8772–8776.

Parrinello S, Samper E, Krtolica A, Goldstein J, Melov S, Campisi J (2003). Oxygen sensitivity severely limits the replicative lifespan of murine fibroblasts. *Nat Cell Biol*. **5**, 741-747.

Pelton RW, Hogan BL, Miller DA, Moses HL (1990). Differential expression of genes encoding TGFs beta 1, beta 2, and beta 3 during murine palate formation. *Dev Biol*. **141**, 456-460.

Petersen BE, Bowen WC, Patrene KD, Mars WM, Sullivan AK, Murase N, Boggs SS, Greenberger JS, Goff JP (1999). Bone marrow as a potential source of hepatic oval cells. *Science*. **284**, 1168-1170.

Petrovick MS, Hiebert SW, Friedman AD, Hetherington CJ, Tenen DG, Zhang DE (1998). Multiple functional domains of AML1: PU.1 and C/EBPalpha synergize with different regions of AML1. *Mol Cell Biol*. **18**, 3915–3925.

Pfannkuche K, Summer H, Li O, Hescheler J, Dröge P (2009). The high mobility group protein HMGA2: a co-regulator of chromatin structure and pluripotency in stem cells? *Stem Cell Rev*. **5**, 224-230.

Polyak K, Weinberg RA (2009). Transitions between epithelial and mesenchymal states: acquisition of malignant and stem cell traits. *Nat Rev Cancer*, **9**, 265-273.

Pratap J, Wixted JJ, Gaur T, Zaidi SK, Dobson J, Gokul KD, Hussain S, van Wijnen AJ, Stein JL, Stein GS, Lian JB (2008). Runx2 transcriptional activation of Indian

hedgehog and a downstream bone metastatic pathway in breast cancer cells. *Cancer Res*. **68**, 7795–7802.

Rassoulzadegan M, Cowie A, Carr A, Glaichenhaus N, Kamen R, Cuzin F (1982). The roles of individual polyoma virus early proteins in oncogenic transformation. *Nature*. **300**, 713-718.

Reya T, Morrison SJ, Clarke MF, Weissman IL (2001). Stem cells, cancer, and cancer stem cells. *Nature*. **414**, 105–111.

Ridley AJ, Hall A. The small GTP-binding protein rho regulates the assembly of focal adhesions and actin stress fibers in response to growth factors (1992). *Cell*. **70**, 389-399.

Sadler TW (2006). *Langman's Medical Embryology*. (10^{th} edition).

Salven P, Mustjoki S, Alitalo R., Alitalo K, Rafii S (2003). VEGFR-3 and CD133 identify a population of CD341 lymphatic/vascular endothelial precursor cells. *Blood*. **101**, 168–172.

Sanford LP, Ormsby I, Gittenberger-de Groot AC, Sariola H, Friedman R, Boivin GP, Cardell EL, Doetschman T (1997). TGFbeta2 knockout mice have multiple developmental defects that are non-overlapping with other TGFbeta knockout phenotypes. *Development*. **124**, 2659-2670.

Sato T, van Es JH, Snippert HJ, Stange DE, Vries RG, van den Born M, Barker N, Shroyer NF, van de Wetering M, Clevers H (2011). Paneth cells constitute the niche for Lgr5 stem cells in intestinal crypts. *Nature*. **469**, 415-418.

Sato T, Vries RG, Snippert HJ, van de Wetering M, Barker N, Stange DE, van Es JH, Abo A, Kujala P, Peters PJ, Clevers H (2009). Single Lgr5 stem cells build crypt-villus structures in vitro without a mesenchymal niche. *Nature*. **459**, 262-265.

Savagner P, Kusewitt DF, Carver EA, Magnino F, Choi C, Gridley T, Hudson LG (2005). Developmental transcription factor slug is required for effective re-epithelialization by adult keratinocytes. *J Cell Physiol.* **202**, 858–866.

Scheel C, Eaton EN, Li SH, Chaffer CL, Reinhardt F, Kah KJ, Bell G, Guo W, Rubin J, Richardson AL, Weinberg RA (2011). Paracrine and autocrine signals induce and maintain mesenchymal and stem cell states in the breast. *Cell*. **145**, 926-940.

Scheel C, Weinberg RA (2011). Phenotypic plasticity and epithelial-mesenchymal transitions in cancer and normal stem cells? *Int J Cancer.* **129**, 2310-2314.

Schock F, Perrimon N (2002). Molecular mechanisms of epithelial morphogenesis. *Annu Rev Cell Dev Biol*. **18**, 463-493.

Schreier AA, Gruber J (1990). Viral T-antigen interactions with cellular proto-oncogene and anti-oncogene products. *J Natl Cancer Inst*. **82,** 354-360.

Sebe-Pedros A, de Mendoza A, Lang BF, Degnan BM, Ruiz-Trillo I (2011). Unexpected repertoire of metazoan transcription factors in the unicellular holozoan Capsaspora owczarzaki. *Mol Biol Evol*. **28**, 1241-1254.

Shirakihara T, Saitoh M, Miyazono K (2007). Differential regulation of epithelial and mesenchymal markers by deltaEF1 proteins in epithelial mesenchymal transition induced by TGF-beta. *Mol Biol Cell.* **18**, 3533-3544.

Shmelkov SV, Butler JM, Hooper AT, Hormigo A, Kushner J, Milde T, St Clair R, Baljevic M, White I, Jin DK, Chadburn A, Murphy AJ, Valenzuela DM, Gale NW, Thurston G, Yancopoulos GD, D'Angelica M, Kemeny N, Lyden D, Rafii S (2008). CD133 expression is not restricted to stem cells, and both CD133+ and CD133- metastatic colon cancer cells initiate tumors. *J Clin Invest.* **118**, 2111-2120.

Singh SK, Hawkins C, Clarke ID, Squire JA, Bayani J, Hide T, Henkelman RM, Cusimano MD, Dirks PB (2004). Identification of human brain tumour initiating cells. *Nature*. **432**, 396–401.

Speck NA, Renjifo B, Hopkins N (1990). Point mutations in the Moloney murine leukemia virus enhancer identify a lymphoid-specific viral core motif and 1,3-phorbol myristate acetate-inducible element. *J Virol*. **64,** 543-550.

Stewart M, Terry A, Hu M, O'Hara M, Blyth K, Baxter E, Cameron E, Onions DE, Neil JC (1997). Proviral insertions induce the expression of bone-specific isoforms of PEBP2alphaA (CBFA1): evidence for a new myc collaborating oncogene. *Proc Natl Acad Sci USA*. **94**, 8646-8651.

Stingl J, Eirew P, Ricketson I, Shackleton M, Vaillant F, Choi D, Li HI, Eaves CJ (2006). Purification and unique properties of mammary epithelial stem cells. *Nature*. **439**, 993-997.

Sullivan JC, Sher D, Eisenstein M, Shigesada K, Reitzel AM, Marlow H, Levanon D, Groner Y, Finnerty JR, Gat U (2008). The evolutionary origin of the Runx/CBFbeta transcription factors-studies of the most basal metazoans. *BMC Evol Biol*. **8**, 228.

Sun W, Graves BJ, Speck NA (1995). Transactivation of the Moloney murine leukemia virus and T-cell receptor b-chain enhancers by cbf and ets requires intact binding sites for both proteins. *J Virol*. **69**, 4941–4949.

Takaishi S, Okumura T, Tu S, Wang SS, Shibata W, Vigneshwaran R, Gordon SA, Shimada Y, Wang TC (2009). Identification of gastric cancer stem cells using the cell surface marker CD44. *Stem Cells*. **27**, 1006-1020.

Taniuchi I, Osato M, Egawa T, Sunshine MJ, Bae SC, Komori T, Ito Y and Littman DR (2002). Differential requirements for Runx proteins in *CD4* repression and epigenetic silencing during T lymphocyte development. *Cell.* **111**, 621-633.

Tessa A, Salvi S, Casali C, Garavelli L, Digilio MC, Dotti MT, Di Giandomenico S, Valoppi M, Grieco GS, Comanducci G, Bianchini G, Fortini D, Federico A, Giannotti A, Santorelli FM (2003). Six novel mutations of the RUNX2 gene in Italian patients with cleidocranial dysplasia. *Hum Mutat.* **22**, 104.

Tetsu O, McCormick F (1999). Beta-catenin regulates expression of cyclin D1 in colon carcinoma cells. *Nature*. **398**, 422–426.

Thiery JP (2002). Epithelial-mesenchymal transitions in tumour progression. *Nat Rev Cancer*. **2**, 442–454.

Thiery JP, Acloque H, Huang RY, Nieto MA (2009). Epithelial-mesenchymal transitions in development and disease. *Cell*. **139**, 871-890.

Thiery JP, Chopin D (1999). Epithelial cell plasticity in development and tumor progression. *Cancer Metastasis Rev*. **18**, 31-42.

Thiery JP, Sleeman JP (2006).Complex networks orchestrate epithelial-mesenchymal transitions. *Nat Rev Mol Cell Biol*. **7**, 131-42.

Thuault S, Tan EJ, Peinado H, Cano A, Heldin CH, Moustakas A (2008). HMGA2 and Smads co-regulate SNAIL1 expression during induction of epithelial-to-mesenchymal transition. *J Biol Chem*. **283**, 33437-33446.

Thuault S, Valcourt U, Petersen M, Manfioletti G, Heldin CH, Moustakas A (2006). Transforming growth factor-beta employs HMGA2 to elicit epithelial-mesenchymal transition. *J Cell Biol*. **174**, 175-183.

Tiscornia G, Singer O, Verma IM (2006). Production and purification of lentiviral vectors. *Nat Protoc*. **1**, 241-245.

Uchida N, Buck DW, He D, Reitsma MJ, Masek M, Phan TV, Tsukamoto AS, Gage FH, Weissman IL (2000). Direct isolation of human central nervous system stem cells. *Proc Natl Acad Sci USA*. **97**, 14720–14725.

Utikal J, Polo JM, Stadtfeld M, Maherali N, Kulalert W, Walsh RM, Khalil A, Rheinwald JG, Hochedlinger K (2009). Immortalization eliminates a roadblock during cellular reprogramming into iPS cells. *Nature*. **460**, 1145-1148.

van der Flier LG, van Gijn ME, Hatzis P, Kujala P, Haegebarth A, Stange DE, Begthel H, van den Born M, Guryev V, Oving I, van Es JH, Barker N, Peters PJ, van de Wetering M, Clevers H (2009). Transcription factor achaete scute-like 2 controls intestinal stem cell fate. *Cell.* **136**, 903-912.

van de Wetering M, Sancho E, Verweij C, de Lau W, Oving I, Hurlstone A, van der Horn K, Batlle E, Coudreuse D, Haramis AP, Tjon-Pon-Fong M, Moerer P, van den Born M, Soete G, Pals S, Eilers M, Medema R, Clevers H (2002). The b-catenin/TCF-4 complex imposes a crypt progenitor phenotype on colorectal cancer cells. *Cell*. **111**, 241–250.

Vandewalle C, Comijn J, De Craene B, Vermassen P, Bruyneel E, Andersen H, Tulchinsky E, Van Roy F, Berx G (2005). SIP1/ZEB2 induces EMT by repressing genes of different epithelial cell-cell junctions. *Nucleic Acids Res.* **33**, 6566-6578.

Velasco-Velázquez MA, Popov VM, Lisanti MP, Pestell RG (2011). The role of breast cancer stem cells in metastasis and therapeutic implications. *Am J Pathol*. **179**, 2-11.

Vermeulen L, Sprick MR, Kemper K, Stassi G, Medema JP (2008). Cancer stem cells--old concepts, new insights. *Cell Death Differ*. **15**, 947-958.

Vincan E, Barker N (2008). The upstream components of the Wnt signalling pathway in the dynamic EMT and MET associated with colorectal cancer progression. *Clin Exp Metastasis*. **25**, 657-663.

Visvanathan KV, Pocock RD, Summerhayes IC (1988). Preferential and novel activation of H-ras in human bladder carcinomas. *Oncogene Res*. **3**, 77-86.

Wakefield LM, Roberts AB (2002). TGF-beta signaling: positive and negative effects on tumorigenesis. *Curr Opin Genet Dev.* **12**, 22-29.

Wang CQ, Jacob B, Nah GS, Osato M (2010). Runx family genes, niche, and stem cell quiescence. *Blood Cells Mol Dis.* **44**, 275-286.

Wang J, Guo LP, Chen LZ, Zeng YX, Lu SH (2007). Identification of cancer stem cell-like side population cells in human nasopharyngeal carcinoma cell line. *Cancer Res*. **67**, 3716-3724.

Wang Q, Stacy T, Miller JD, Lewis AF, Gu TL, Huang X, Bushweller JH, Bories JC, Alt FW, Ryan G, Liu PP, Wynshaw−βoris A, Binder M, Marin-Padilla M, Sharpe AH, Speck NA (1996). The CBFbeta subunit is essential for CBFalpha2 (AML1) function in vivo. *Cell.* **87**, 697-708.

Watabe T, Miyazono K (2009). Roles of TGF-beta family signaling in stem cell renewal and differentiation. *Cell Res*. **19**, 103-115.

Weber K, Bartsch U, Stocking C, Fehse B (2008). A multicolor panel of novel lentiviral "gene ontology" (LeGO) vectors for functional gene analysis. *Mol Ther.* **16**, 698-706.

Wei D, Gong W, Oh SC, Li Q, Kim WD, Wang L, Le X, Yao J, Wu TT, Huang S, Xie K (2005). Loss of RUNX3 expression significantly affects the clinical outcome of gastric cancer patients and its restoration causes drastic suppression of tumor growth and metastasis. *Cancer Res*. **65**, 4809-4816.

Weinberg RA (2007). *The biology of cancer*. (1st edition).

Weiss S, Reynolds BA, Vescovi AL, Morshead C, Craig CG, van der Kooy D (1996). Is there a neural stem cell in the mammalian forebrain? *Trends Neurosci*. **19**, 387-393.

Wheeler JC, VanderZwan C, Xu X, Swantek D, Tracey WD, Gergen JP (2002). Distinct in vivo requirements for establishment versus maintenance of transcriptional repression. *Nat Genet*. **32**, 206-210.

Whiteman EL, Liu CJ, Fearon ER, Margolis B (2008). The transcription factor snail represses Crumbs3 expression and disrupts apico-basal polarity complexes. *Oncogene*. **27**, 3875-3879.

Willert K, Brown JD, Danenberg E, Duncan AW, Weissman IL, Reya T, Yates JR 3rd, Nusse R (2003). Wnt proteins are lipid-modified and can act as stem cell growth factors. *Nature*. **423**, 448-52.

Woolf E, Xiao C, Fainaru O, Lotem J, Rosen D, Negreanu V, Bernstein Y, Goldenberg D, Brenner O, Berke G, Levanon D and Groner Y (2003). Runx3 and Runx1 are required for CD8 T cell development during thymopoiesis. *Proc Natl Acad Sci USA*. **100**, 7731-7736.

Wotton D, Ghysdael J, Wang S, Speck NA, Owen MJ (1994). Cooperative binding of Ets-1 and core binding factor to DNA. *Mol Cell Biol*. **14**, 840–850.

Wright SJ, Centonze VE, Stricker SA, DeVries PJ, Paddock SW, Schatten G (1993). Introduction to confocal microscopy and three-dimensional reconstruction. *Methods Cell Biol*. **38**, 1-45.

Wu C, Alman BA (2008). Side population cells in human cancers. *Cancer Lett*. **268**, 1-9.

Xu X, Brodie SG, Yang X, Im YH, Parks WT, Chen L, Zhou YX, Weinstein M, Kim SJ, Deng CX (2000). Haploid loss of the tumor suppressor Smad4/Dpc4 initiates gastric polyposis and cancer in mice. *Oncogene*. **19**, 1868−1874.

Xu J, Lamouille S, Derynck R (2009). TGF−βeta-induced epithelial to mesenchymal transition. *Cell Res*. **19**, 156-172.

Xuan D, Li S, Zhang X, Hu F, Lin L, Wang C, Zhang J (2008). Mutations in the RUNX2 gene in Chinese patients with cleidocranial dysplasia. *Ann Clin Lab Sci.* **38**, 15-24.

Yamashita T, Ji J, Budhu A, Forgues M, Yang W, Wang HY, Jia H, Ye Q, Qin LX, Wauthier E, Reid LM, Minato H, Honda M, Kaneko S, Tang ZY, Wang XW (2009). EpCAM-positive hepatocellular carcinoma cells are tumor-initiating cells with stem/progenitor cell features. *Gastroenterology*. **136**, 1012-1024.

Yang J, Mani SA, Donaher JL, Ramaswamy S, Itzykson RA, Come C, Savagner P, Gitelman I, Richardson A, Weinberg RA (2004). Twist, a master regulator of morphogenesis, plays an essential role in tumor metastasis. *Cell.* **117**, 927-939.

Yano T, Ito K, Fukamachi H, Chi XZ, Wee HJ, Inoue K, Ida H, Bouillet P, Strasser A, Bae SC, Ito Y (2006). The RUNX3 tumor suppressor upregulates Bim in gastric epithelial cells undergoing TGF-beta-induced apoptosis. *Mol Cell Biol*. **26**, 4474–4488.

Yin AH, Miraglia S, Zanjani ED, Almeida-Porada G, Ogawa M, Leary AG, Olweus J, Kearney J, Buck DW (1997). AC133, a novel marker for human hematopoietic stem and progenitor cells. *Blood.* **90**, 5002–5012.

Yokomizo T, Ogawa M, Osato M, Kanno T, Yoshida H, Fujimoto T, Fraser S, Nishikawa S, Okada H, Satake M, Noda T, Nishikawa S, Ito Y (2001). Requirement of Runx1/AML1/PEBP2alphaB for the generation of haematopoietic cells from endothelial cells. *Genes Cells*. **6**, 13-23.

Zaiman AL, Lenz J (1996). Transcriptional activation of a retrovirus enhancer by CBF (AML1) requires a second factor: evidence for cooperativity with c-Myb. *J Virol.* **70**, 5618–5629.

Zhang DE, Hetherington CJ, Meyers S, Rhoades KL, Larson CJ, Chen HM, Hiebert SW, Tenen DG (1996). CCAAT enhancer-binding protein (C/EBP) and AML1 (CBFa2) synergistically activate the macrophage colony-stimulating factor receptor. *Mol Cell Biol.* **16**, 1231–1240.

Zhang YW, Yasui N, Ito K, Huang G, Fujii M, Hanai J, Nogami H, Ochi T, Miyazono K, Ito Y (2000). A RUNX2/PEBP2alpha A/CBFA1 mutation displaying impaired transactivation and Smad interaction in cleidocranial dysplasia. *Proc Natl Acad Sci USA*. **97**, 10549-54.

Zhou BB, Zhang H, Damelin M, Geles KG, Grindley JC, Dirks PB (2009). Tumour-initiating cells: challenges and opportunities for anticancer drug discovery. *Nat Rev Drug Discov*. **8**, 806-823.

Zhou S, Schuetz JD, Bunting KD, Colapietro AM, Sampath J, Morris JJ, Lagutina I, Grosveld GC, Osawa M, Nakauchi H, Sorrentino BP (2001). The ABC transporter Bcrp1/ABCG2 is expressed in a wide variety of stem cells and is a molecular determinant of the side-population phenotype. *Nat Med*. **7,** 1028-1034.